Studies on platelet cytoskeletal dynamics and receptor regulation in genetically modified mice

Untersuchungen zur Zytoskelettdynamik und Rezeptorregulation in Blutplättchen genetisch modifizierter Mäuse

Doctoral thesis for a doctoral degree
at the Graduate School of Life Sciences,
Julius-Maximilians-Universität Würzburg,
Section Biomedicine

submitted by

Markus Bender
from
Würzburg

Würzburg, 2009

Submitted on: ……

Office stamp

Members of the *Promotionskomitee*:

Chairperson: ……..

Primary Supervisor: Prof. Dr. Bernhard Nieswandt

Supervisor (Second): Prof. Dr. Dr. Manfred Schartl

Supervisor (Third): Prof. Dr. Dr. Stefan Engelhardt

Date of Public Defence: ……

Date of Receipt of Certificates: ……...

Summary

Platelets are produced by bone marrow megakaryocytes in a process involving actin dynamics. Actin-depolymerizing factor (ADF) and cofilin are actin-binding proteins that act as key regulators in actin turnover by promoting filament severing and depolymerization. The overall significance of ADF/cofilin function and actin turnover in platelet formation is presently unclear. In the first part of this thesis, platelet formation and function were studied in mice constitutively lacking ADF and/or mice with a conditional deficiency (Cre/loxP) in n-cofilin. To delete cofilin exclusively in megakaryocytes and platelets, *cofilin*$^{fl/fl}$ mice were crossed with *PF4 (platelet factor 4)-Cre* mice. While a single-deficiency in ADF or n-cofilin resulted in no or only a minor platelet formation defect, respectively, a double-deficiency in ADF and n-cofilin led to an almost complete loss of platelets. Bone marrow megakaryocytes of ADF/n-cofilin-deficient mice showed defective platelet zone formation. Interestingly, *in vitro* and *ex vivo* megakaryocyte differentiation revealed reduced proplatelet formation and absence of platelet-forming swellings. These data establish that ADF and n-cofilin have redundant but essential roles in the terminal step of platelet formation *in vitro* and *in vivo*.

In the second part of the thesis, mechanisms underlying cellular regulation of the major platelet collagen receptor, glycoprotein VI (GPVI), were studied. GPVI mediates platelet activation on exposed subendothelial collagens at sites of vascular injury, and thereby contributes to normal hemostasis but also to occlusion of diseased vessels in the setting of myocardial infarction or stroke. Thus, GPVI is an attractive target for anti-thrombotic therapy, particularly because previous studies have shown that anti-GPVI antibodies induce irreversible down-regulation of the receptor in circulating platelets by internalization and ectodomain shedding. Metalloproteinases of the ADAM (a disintegrin and metalloproteinase domain) family are suspected to mediate this ectodomain shedding, but *in vivo* evidence for this is lacking. To study the mechanism of GPVI regulation *in vivo*, two mouse lines, *Gp6* knock-out and *Adam10*$^{fl/fl,\ PF4\text{-}Cre}$ mice, were generated and in addition low TACE (TNFα converting enzyme) mice were analyzed. It was shown that GPVI can be cleaved *in vitro* by ADAM10 or TACE depending on the shedding-inducing signaling pathway. Moreover, GPVI was down-regulated *in vivo* upon antibody injection in ADAM10-deficient and low TACE mice suggesting that either both or an additional metalloproteinase is involved in GPVI regulation *in vivo*.

Zusammenfassung

Blutplättchen werden von Megakaryozyten im Knochenmark in einem Prozess produziert, an dem Aktin beteiligt ist. Aktin-Depolymerisierungsfaktor (ADF) und Cofilin sind Aktin-bindende Proteine, die als entscheidende Regulatoren im Aktinumsatz agieren, indem sie das Schneiden und Depolymerisieren von Filamenten unterstützen. Die Bedeutung von ADF/Cofilin und des Aktinumsatzes in der Bildung von Blutplättchen ist gegenwärtig nicht bekannt. In der vorliegenden Arbeit wurden Mäuse untersucht, die eine konstitutive ADF-Defizienz und/oder die eine konditionale n-Cofilin Defizienz (Cre/loxP) aufweisen. Um Cofilin nur in Megakaryozyten und Blutplättchen auszuschalten, wurden *Cofilin$^{fl/fl}$* Mäuse mit *PF4-Cre* Mäusen verpaart. ADF- oder n-Cofilin-defiziente Mäuse hatten keinen oder nur einen geringen Phänotyp in Blutplättchen. Eine Defizienz von ADF und n-Cofilin führte hingegen zu einem beinahe kompletten Verlust der Blutplättchen, was mit Defekten in der Bildung von Plättchenzonen in Knochenmark-Megakaryozyten einherging. Weitere Untersuchungen an *in vitro* und *ex vivo* kultivierten Megakaryozyten zeigten eine Reduzierung der Bildung von Proplättchen und das Fehlen der typischen Verdickungen der Proplättchen. Diese Daten zeigen redundante aber essentielle Funktionen von ADF und n-Cofilin im terminalen Schritt der Plättchenbildung *in vitro* und *in vivo*, und belegen erstmals eine wichtige Rolle des Aktinumsatzes in diesem Prozess.

Im zweiten Teil dieser Dissertation wurden die Mechanismen untersucht, die für die zelluläre Regulierung des Hauptkollagenrezeptors auf Blutplättchen, Glykoprotein VI (GPVI), verantwortlich sind. Nach einer Gefäßwandverletzung wird subendotheliales Kollagen freigelegt, wodurch GPVI die Aktivierung von Blutplättchen vermittelt, und damit zur Blutstillung (Hämostase), aber auch zum Verschluss eines verletzten Gefäßes beitragen kann, was letztendlich zu einem Myokardinfarkt oder einem Schlaganfall führen kann. Deshalb ist GPVI ein attraktives Zielprotein für eine anti-thrombotische Therapie, insbesondere weil frühere Studien gezeigt haben, dass anti-GPVI Antikörper eine irreversible Herunterregulierung des Rezeptors auf zirkulierenden Blutplättchen mittels Internalisierung und Abspaltung induzieren. Es wird vermutet, dass Metalloproteinasen der ADAM (*a disintegrin and metalloproteinase domain*) - Familie das Abspalten vermitteln, jedoch fehlt *in vivo* der Beweis dafür. Um die Mechanismen des Abspaltungsprozesses des GPVI Rezeptors *in vivo* besser verstehen zu können, wurden zwei Mauslinien, GPVI- und konditionale

ADAM10-defiziente Mäuse, generiert und zusätzlich sogenannte „low TACE (*TNFα converting enzyme*)“ Mäuse analysiert. Es konnte gezeigt werden, dass GPVI *in vitro* von ADAM10 oder TACE in Abhängigkeit der Signalwege, die zum Abspalten des Rezeptors führen, geschnitten werden kann. Darüberhinaus wurde GPVI *in vivo* nach Antikörperverabreichung in ADAM10-defizienten Mäusen und „low TACE“ Mäusen herunterreguliert, was vermuten lässt, dass entweder beide Metalloproteinasen an diesem Prozess beteiligt sind oder noch eine zusätzliche Metalloproteinase für die GPVI Regulation *in vivo* verantwortlich ist.

Table of contents

A. Introduction

Platelets are an important component of the blood system because they play a pivotal role in two processes: primary hemostasis and thrombosis. When the endothelium of a blood vessel is disrupted, platelets are able to interact with the exposed subendothelium, start reactions to seal smaller lesions and thereby prevent further blood loss. On the other hand, under pathological conditions such as a rupture of an atherosclerotic plaque in a diseased vessel, platelets are able to essentially contribute to uncontrolled thrombus formation that leads to complete occlusion of the vessel and consequently results in stroke or myocardial infarction. These two events are the main causes of death in industrialized countries[1].

A.1. Platelet morphology and structure

Platelets display a discoid shape and are the smallest cells of the blood system, with a diameter of 1-2 µm in mice and 3-4 µm in humans. The number of platelets in human blood is about 150,000-300,000/µL, whereas the platelet count in mice is approximately 1,000,000/µL. Platelets have only a short lifespan of about five and ten days in mice and humans, respectively, before they are removed from the circulation in the spleen. Platelets are anucleated cell fragments and thus are not able to synthesize proteins *de novo*. But they can rapidly change their discoid shape to a spherical shape with pseudopodia formation upon activation with different ligands. A non-activated platelet contains several components in the cytoplasm like an opened and closed cannalicular system, mitochondria, peroxisomes, glycogen stores, lysosomal granules, dense granules and α-granules. α-granules contain adhesion proteins (fibrinogen, vWF), growth factors (PDGF) or coagulation factors (FV, FXIII), whereas dense granules contain mostly small anorganic molecules including ADP, serotonin and Ca^{2+}.

A.2. Thrombus formation

After injury of the vessel wall, the response of platelets is a primary event in thrombus formation[2]. The formation of a thrombus can be divided into three distinct processes, (I) adhesion, (II) activation and (III) aggregation of platelets (Fig. 1). The platelet membrane receptors GPIb-V-IX, GPVI, GPIa/IIa and GPIIb/IIIa are centrally involved in these processes.

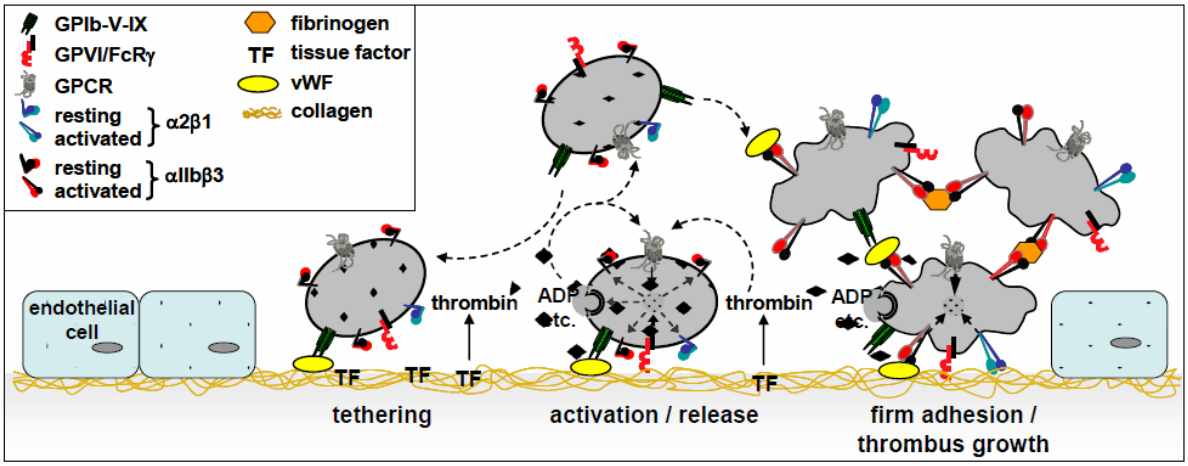

Fig. 1: Model of thrombus formation (Varga-Szabo *et al.*)[3].
At sites of vascular injury, the extracellular matrix becomes exposed and allows platelet adhesion and aggregation. Under high shear flow conditions, the initial contact is mediated by the immobilized von-Willebrand factor on collagen and GPIb. Then, GPVI-collagen interactions lead to platelet activation with a shift of integrins to a higher-affinity state and release of second-wave mediators (ADP, thromboxane A2). In parallel, tissue factor triggers thrombin generation that contributes to cellular activation. Finally, integrins in a higher-affinity state mediate firm adhesion of platelets.

Following rupture of the endothelial barrier, the subendothelium containing adhesive molecules like laminin, collagen and fibronectin is exposed to the blood stream. Collagen, one of the major subendothelial matrix components, which is also found in atherosclerotic plaques of diseased vessels, stimulates thrombus formation via platelet activation[4]. In the beginning of the process, von Willebrand factor (vWF) circulating in the plasma is immobilized on exposed collagen. Under high shear conditions as it is found in arterioles and small arteries the reversible interactions between the platelet adhesion receptor complex GPIb-V-IX and the immobilized vWF cause the deceleration and the rolling of the flowing platelets along the vessel wall[5;6], a process termed “tethering”. The rolling of the platelets enables them to stay in close contact with the exposed extracellular matrix components. Finally, the platelet receptor GPVI binds directly to exposed collagen[7;8] and platelets become activated and release secondary mediators like ADP and thromboxane A_2 which in turn mediate thrombus growth by activating additional platelets. In parallel, generation of thrombin contributes to cellular activation. Additionally, a shift of integrins from a low-affinity to a high-affinity state takes place[9;10]. The conformational change of the integrins $\alpha 2\beta 1$ (GPIa/IIa) and $\alpha IIb\beta 3$ (GPIIb/IIIa) mediated by activation of platelets through the collagen receptor GPVI induces firm adhesion of platelets. Activated

GPIa/IIa and GPIIb/IIIa bind to collagen and vWF, respectively. Following this, platelet-platelet interaction is mediated by binding of activated αIIbβ3 (GPIIb/IIIa) to plasma fibrinogen.

A.3. Megakaryocytes and platelet production

Platelets are cell fragments originating from megakaryocytes (MKs) in the bone marrow (BM) (Fig. 2). MKs evolve from hematopoietic stem cells and develop to become the largest cells of the BM (up to 100 µm in diameter). Within the bone marrow, megakaryocyte maturation is regulated by a variety of cytokines including IL-3, IL-6, IL-11 and mainly thrombopoietin (TPO)[11] that binds to its receptor (c-Mpl) and plays a primary role in this process. Endomitosis is a TPO-driven unique process in MKs, that is characterized by DNA replication without cell division, resulting in a polyploid and multilobed nucleus with a DNA content ranging from 4N to 128N[12]. Thus, endomitosis of MKs is an abortive mitosis that fails to complete especially in the late stage phases of the process by cleavage furrow regression[13-15]. For platelet biogenesis, maturation of the MK cytoplasm is a prerequisite. Platelet secretory granules are assembled in the MK body and the production of the demarcation membrane system (DMS) occurs that subdivides the cytoplasm into fields, associates with the actin cytoskeleton and serves as a membrane reservoir for proplatelet elaboration[16]. It has been reported that extension of cytoplasmic protrusions (proplatelets) is mechanically driven by tubulin sliding and assembly, while proplatelet shaft bifurcation is based on actin-dependent processes. This is supported by the observation that actin filaments are highly abundant in the swellings of the proplatelet shaft[17]. According to the current model, the tip of these protrusions extends into the lumen of a vessel and seems to be sheared by blood shear forces. However, the released proplatelets in the circulation are larger in size than normal platelets since beaded proplatelets and barbell-shaped platelet pairs were observed in the blood leading to speculations that finalization of platelets may occur in the circulation[18]. Disorders in the process of platelet formation can influence platelet count and size. Patients with congenital macrothrombocytopenia have been described with defects in the GPIb/V/IX complex, in transcription factors e.g. GATA-1 or in the *Myh9* gene encoding the nonmuscle myosin heavy chain-A[19;20]. However, in many cases the reason for congenital macrothrombocytopenia is unknown. In

addition, many aspects of the complex process of platelet biogenesis are controversial and currently unclear.

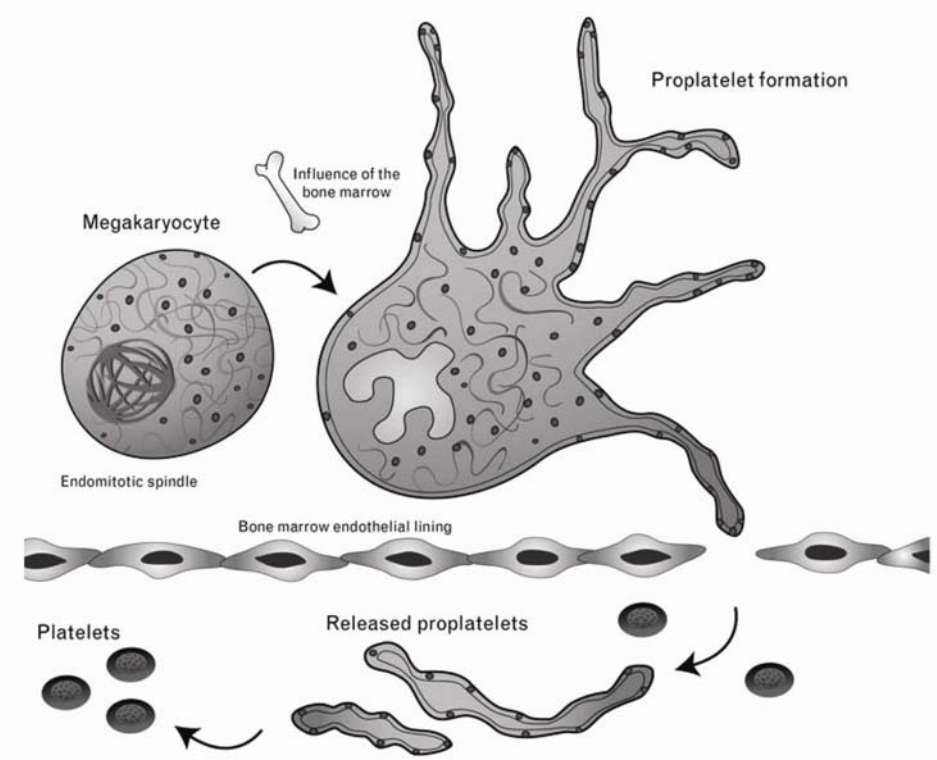

Fig. 2: Model of platelet formation (Battinelli *et al.*)[16].
Platelets are originated from bone marrow megakaryocytes (MKs). MKs undergo proplatelet formation, initiated by development of pseudopods and followed by proplatelet elongation and branching. Tips of these protrusions extend into the lumen of a vessel and are sheared by blood shear forces resulting in released platelets.

A.4. Actin-depolymerizing factor (ADF) and cofilin

A.4.1. Structure, location and expression of ADF and cofilin

The first members of the ADF/cofilin (AC) family were identified in the early 1980s. Whereas the first observation for the actin-depolymerizing factor (ADF) was that it rapidly reduces the viscosity of F-actin in solution, cofilin was primarily found to bind to F-actin, hence the name cofilamentous structures with actin. ADF and cofilin are actin-binding proteins of a molecular mass of about 15-21 kD (113-168 amino acids) and share a high sequence identity of about 70%. ADF and cofilin are composed of a single fold ADF homology domain which is similarly found in other actin-binding proteins like gelsolin. The most highly conserved regions between the species is the actin binding site and a phosphorylation site (Ser 3)[21;22]. In mammals, three isoforms of the ADF/cofilin family on different chromosomes exist that have arisen from two

sequential gene duplications, namely *Adf* (actin-depolymerizing factor/destrin), *cofilin-1 (n-cofilin)* and *cofilin-2 (m-cofilin)*. ADF and non-muscle cofilin (n-cofilin) are expressed in most tissues, but only n-cofilin shows high expression levels during embryonic development. Muscle cofilin (m-cofilin) is found only in muscle cells[23-25].

A.4.2. Cellular function of ADF and n-cofilin

The cytoskeleton of a cell is composed of several proteins among which actin is of particular importance. Actin monomers (G-actin) can assemble to each other to form a polar filamentous actin structure (F-actin). Due to this property actin is not only an important structural protein but its highly dynamic assembly and disassembly is also essential for a variety of cellular processes including cytokinesis, cell polarization and morphological changes.

The rate of actin turnover *in vivo* is significantly higher than *in vitro*[26-28] which is based on the presence of actin-binding proteins that are known to accelerate actin remodeling[29]Among them, members of the ADF/cofilin family play a pivotal role in spatially and temporally regulating actin turnover[21;30-32]. Upon dephosphorylation, ADF and n-cofilin preferentially bind in a cooperative manner to ADP-bound F-actin[22;29;33;34]. Older filaments are marked for turnover by containing more ADP-actin monomers. Upon binding to actin, ADF and n-cofilin have the unique property to induce a twist in the actin filament (5° rotation per subunit) and with this, to weaken the lateral binding. Following this, actin turnover is enhanced by dissociation of actin monomers from the minus (pointed) end and by filament severing[33-37]. These two processes (Fig. 3) enhance actin turnover since other proteins transfer dissociated monomers to the plus (barbed ends) or severed filaments provide new plus ends for addition of actin monomers to the growing filament.

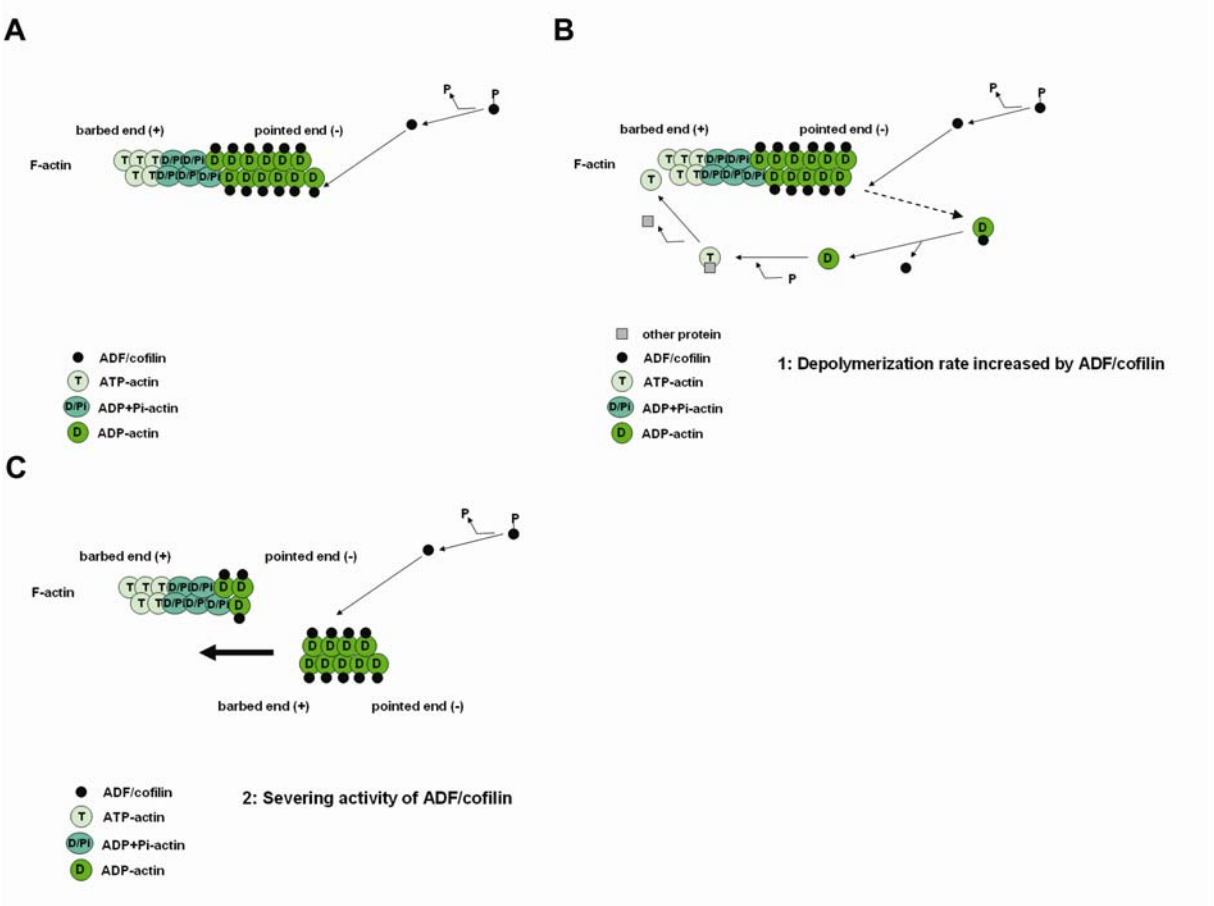

Fig. 3: Model of cellular function of ADF and n-cofilin
(A) After dephosphorylation ADF/n-cofilin bind to the ADP-bound actin filament at the minus end. **(B)** Dissociation of an actin monomer mediated by ADF/n-cofilin. Transfer of an actin monomer to the barbed end via other proteins. **(C)** The severing activity of ADF and n-cofilin leads to an actin filament strand break followed by an increase of barbed ends.

A.4.3. Regulation of ADF/n-cofilin activity

The activity of ADF/n-cofilin is regulated by several mechanisms, including the isoform expression pattern, the compartmentalization, competitive binding with other proteins like tropomyosin, pH value and phosphatidylinositol (4,5) biphosphate (PIP_2) binding[21]. However, the main and best studied regulatory mechanism is (de-) phosphorylation of ADF/n-cofilin. ADF and n-cofilin are tightly regulated via (de-) phosphorylation at the highly conserved amino acid serine 3[38]. LIM kinase (LIMK) and testicular protein kinase (TESK) phosphorylate and inactivate ADF/n-cofilin activity, whereas dephosphorylation and consequently activation of ADF/n-cofilin is mediated by phosphatases such as PP1, PP2A, slingshot and chronophin[39-43]. Activation of phosphorylated ADF/n-cofilin is a rapid process in response to different stimuli in many cell types[35]. In platelets, approximately 90% of n-cofilin at position

serine 3 is phosphorylated in resting state, suggesting a slow actin turnover. After stimulation with thrombin, maximal n-cofilin dephosphorylation (75%) occurs within 1-2 minutes[44].

A.4.4. *In vivo* functions of ADF/n-cofilin

Studies on different model organisms have revealed an essential role for ADF/cofilin during development. Deficiency of the single isoform of ADF/cofilin in *yeast* or *drosophila* resulted in lethality[45-47]. The same was found in *C. elegans* when both isoforms UNC-60A and UNC-60B were affected[48;49]. In mice, n-cofilin deficiency led to defects in neural crest cell migration, neural tube closure and embryonic lethality[50]. Furthermore, conditional gene targeting in mice revealed an association of n-cofilin with cell cycle control in the cerebral cortex and disorders in neuronal migration[51]. In contrast, mice constitutively lacking ADF are viable and display no obvious defect in brain development[51]. However, in the cornea, where ADF (destrin) is the predominant isoform, *corneal disease-1 (corn1)* mice with a spontaneous mutation in the *Adf* gene show an increased proliferation of epithelial cells and consequently thickening of the cornea[52].

A.5. Glycoprotein VI (GPVI)

A.5.1. Structure, location and expression of the *GP6* gene

The mouse and the human *GP6* gene consists of eight exons which span over 23 kbp. Exon 1 and 2 encode for the signal peptide, whereas exon 3 and 4 encode for one immunoglobulin domain each. The mucin-like sequence is encoded by exons 5-7. The transmembrane and cytoplasmic domains of GPVI are represented by exon 8[53]. Human and mouse *GP6* have been mapped on chromosome 19 and 7, respectively[53-55].

Furthermore, splice variants of *GP6* have been described. Compared to GPVI-1, GPVI-2 lacks 18 amino acids between the immunoglobulin domains and the transmembrane domain without a frameshift. The splice variant GPVI-3 contains an insertion of four amino acids encoded in exon 7. In consequence of the frameshift, this splice variant is elongated of 361 amino acids with no apparent transmembrane domain[53] (Fig. 4).

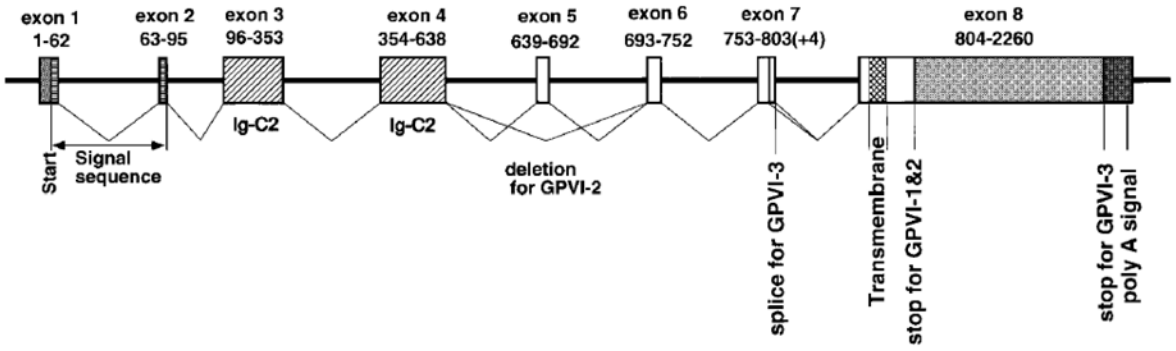

Fig. 4: Genomic structure of the human *GP6* gene with alternative splice variants[53].
The eight exons of *GP6* are shown as boxes. The numbers above the boxes are nucleotides. The splice variants are labeled.

It was demonstrated that GPVI is expressed only in megakaryocytes and platelets. Furthermore, it was shown that the expression of GPVI increased together with the expression of the FcRγ-chain in the terminal phase of megakaryocyte differentiation. That is why GPVI can function as a marker of late-stage megakaryocyte differentiation[56].

A.5.2. Protein structure of GPVI

SDS gel electrophoresis showed that the apparent molecular weight of GPVI is approximately 62 kD. The first cloning study revealed that GPVI is a member of the immunoglobulin (Ig) receptor superfamily and closely related to the natural killer cell receptor and to FcαR[54]. Human GPVI is composed of 339 amino acids, whereas mouse GPVI is composed of 319 amino acids. Interestingly, the cytoplasmic part of GPVI is not closely related to other receptors indicating an unique function of this receptor in different signaling processes[57].

The extracellular part of GPVI consists of two immunoglobulin (Ig)-like domains that protrude from the platelet surface (Fig. 5). These Ig-like domains contain a collagen binding site and two N-linked glycosylation sites (N92 and S94 in human and N93 and N244 in mouse GPVI). Closer to the platelet surface, there is a mucin-like stalk with a serine/threonine-rich region bearing many O-glycosylation sites[8;57].

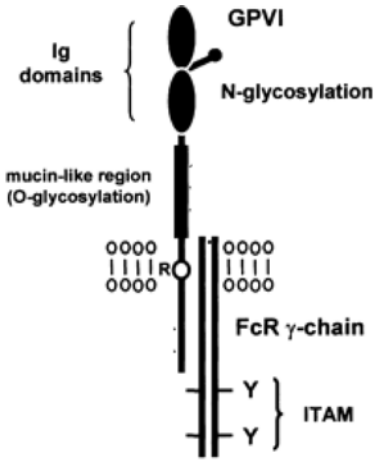

Fig. 5: Structure of GPVI associated with FcRγ-chain; modified from Nieswandt and Watson[8].

The transmembrane region is crucial for the stabilization of GPVI into the lipid membrane and for the association of GPVI to the FcRγ-chain. GPVI binds to the FcRγ-chain non-covalently through Arg252[8;57;58]. The association is mediated by forming a salt bridge between the positively-charged arginine and a negatively-charged aspartic acid in the transmembrane region of the FcRγ-chain. The FcRγ-chain represents the signaling subunit of the receptor complex[59;60]. GPVI expression on the platelet surface is strictly dependent on the expression of the FcRγ-chain, as revealed by the analysis of FcRγ-chain-deficient mouse platelets which do not express GPVI[61].

The cytoplasmic tail of human GPVI is divided into four distinct but overlapping regions, namely (1) juxtamembrane-, (2) basic-, (3) proline-rich and (4) C-terminal-region (Fig. 6). The full length cytoplasmic tail in human consists of 51 amino acids. Interestingly, the cytoplasmic tail of mouse GPVI contains only 27 amino acids lacking the C-terminal region (Fig. 6)[62].

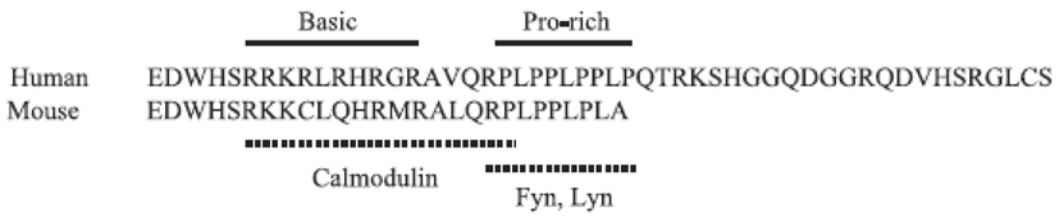

Fig. 6: Cytoplasmic tail of human and mouse GPVI[57].

The basic region is able to associate to calmodulin[63]. Disruption of calmodulin binding causes down-regulation of GPVI from the platelet surface by a yet undefined platelet-derived metalloproteinase[64].

The proline-rich sequence constitutively binds Src kinases like Fyn and Lyn[65]. The basic and juxtamembrane regions are important for the association of the FcRγ-chain to GPVI. This was shown by sequential deletion of the intracellular part of GPVI which leads to the dissociation of the FcRγ-chain from GPVI[66].

A.5.3. Extracellular ligands of GPVI

Collagen is the most important physiological ligand for GPVI. More than 20 isoforms of collagen exist in humans. The essential isoforms for platelet interaction are type I and III collagen. Monomeric collagens are cross-linked to form a fibrillar structure in the extracellular matrix. Collagen consists of many glycine (G), proline (P) and hydroxyproline (O) amino acid repeats (GPO). The proportion of GPO repeats in collagen I and III is about 10%. These amino acid repeats are essential for GPVI binding[8].

The synthetically produced collagen-related peptide (CRP) consists of many GPO repeats. CRP, with cross-linked N- and C-terminal cysteine or lysine residues to form a fibrillar structure, mimicks the physiological ligand collagen and is a powerful tool for GPVI analysis[8;66].

Furthermore, several snake venom toxins have been identified that specifically bind to GPVI and have significantly contributed to our understanding of platelet-collagen interaction. One example is convulxin, a C-type lectin from the venom of the rattlesnake *Crotalus durissus terrificus*, which strongly activates platelets through GPVI[67;68]. A few other C-type lectins have also been described like trimucytin[69], alboaggregin A[70;71]and alboluxin[72], all of which bind to GPVI.

The rat monoclonal antibody JAQ1 is a useful tool to detect mouse GPVI and to study the biological function of this receptor *in vitro* and *in vivo*. It was known that JAQ1 binds the collagen binding site on the Ig–like domain of GPVI and blocks aggregation induced by low concentrations of collagen[61]. However, when the concentration of collagen is increased, the inhibitory effect is overcome indicating the existence of a second activatory epitope within collagen[73]. JAQ1 alone is not able to induce platelet aggregation *in vitro* like other ligands. However, after cross-linking of JAQ1 with anti-rat IgG antibodies, aggregation takes place[61].

A.5.4. Intracellular ligands and signal transduction of GPVI

The exposure of platelets to collagen is believed to result in clustering of GPVI and these clusters mediate signals via the non-covalently associated FcRγ-chain. Ligand binding of GPVI induces tyrosine phosphorylation of the immunoreceptor tyrosine-based activation motif (ITAM) of the FcRγ-chain (Fig. 7)[60;61;74;75] via Fyn and Lyn Src kinases[76;77]. The phosphorylated ITAM serves as a binding site for the SH2-domains of Syk family kinases[78;79] leading to phosphorylation of Syk, which then serves as a binding partner for many adaptor proteins.

LAT (linker for activation of T-cell) is an adaptor protein which binds to the phosphorylated Syk kinases[80]. LAT contains many putative and mapped phosphorylation sites to recruit other proteins to the GPVI clusters, like phospholipase C γ2 (PLCγ2) and SLP-76[81]. PLCγ2 becomes activated upon binding to LAT. After activation, PLCγ2 liberates diacylglycerol (DAG) and inositol (1,4,5)-trisphosphate that are responsible for protein kinase C activation and Ca^{2+} mobilization, respectively (Fig. 7). Agonist-induced elevation of cytosolic Ca^{2+} is essential for many processes in platelets.

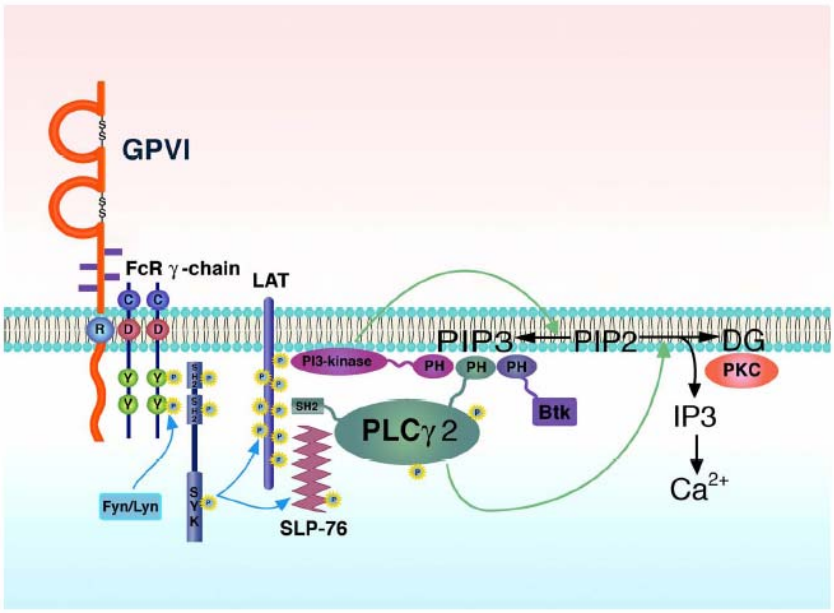

Fig. 7: GPVI signaling (Moroi, M. *et al.*)[57].
GPVI is non-covalently associated with the FcRγ-chain. Crosslinking of GPVI leads to phosphorylation of the immunoreceptor tyrosine-based activation motif (ITAM) of the FcRγ-chain by the Src kinases Fyn and Lyn. Binding and activation of Syk results in an activation cascade of adaptor and effector molecules including PLCγ2.

A.5.5. GPVI as an anti-thrombotic target

In vivo treatment of mice with the monoclonal anti-GPVI antibody JAQ1 induces down-regulation of the receptor GPVI in circulating platelets resulting in a prolonged "GPVI knock-out"–like phenotype[82] and profound anti-thrombotic protection in different thrombosis models[83;84]. Further, it was shown that both anti-mouse GPVI antibodies, JAQ2 and JAQ3, which bind to different epitopes, also induce down-regulation of GPVI. Thus, antibody-induced down-regulation of GPVI is independent of the binding site of the antibody to the epitope[85].

Antibody-induced loss of GPVI has also been reported in autoimmune patients who had developed anti-GPVI antibodies resulting also in down-regulation of the receptor[86;87]. Moreover, it has been demonstrated that GPVI can be cleared from human platelets by anti-GPVI antibodies *in vivo* in a nonobese diabetic severe combined immunodeficient (NOD/SCID) mouse model[88], confirming that GPVI is a powerful target for anti-thrombotic therapy. These data were confirmed by generated *Gp6* knock-out mice and patients with GPVI-related defects as described in detail in section A.5.7.

A.5.6. Cleavage and shedding processes of GPVI

Bergmeier *et al.* demonstrated in mice that GPVI is not down-regulated by stimulating the GPVI/FcRγ-chain or G protein-coupled receptor signaling pathways with CRP or thrombin, respectively. However, the authors showed that after activation of metalloproteinases using carbonyl cyanide m-chlorophenylhydrazone (CCCP) the GPVI/FcRγ-chain pathway is impaired in mouse and human platelets. This is caused by shedding of GPVI from the platelet surface by an unknown metalloproteinase-dependent cleavage mechanism[89].

As mentioned above, calmodulin binds the basic region of GPVI[63]. Metalloproteinase-mediated GPVI shedding was observed *in vitro* using the calmodulin inhibitor W7 which blocks the association between calmodulin and GPVI[64]. In this case, calmodulin indirectly regulates shedding of GPVI.

A.5.7. Phenotypic consequences of *GP6* mutations in mouse and human

As mentioned before, injection of JAQ1 antibody into wild-type mice causes a transient GPVI-deficiency accompanied by thrombocytopenia and a mild bleeding

defect[82]. Furthermore, FcRγ-chain knock-out mice do not express GPVI on the platelet surface[61].

Recently, a few reports described the function of GPVI using *Gp6* knock-out mice. Deletion of the *Gp6* gene neither has an impact on mice viability or development nor on fertility. Interestingly, the protein level of the FcRγ-chain is normal in these mice. Consistent with previous data, *Gp6* knock-out platelets show defective collagen- and convulxin-induced aggregation. Additionally, knock-out platelets lack spreading and thrombus formation on a collagen matrix *in vitro*. Contrary to JAQ1 antibody treated mice, the authors reported that an alteration of the tail bleeding time is not detectable and the primary adhesion process is also normal on the collagen-coated surface[90].

Another *Gp6* knock-out mouse model was published by Lockyer *et al.* where a different knock-out strategy was used to delete the *Gp6* gene. The knock-out phenotype was different suggesting an important role of GPVI in the process of primary adhesion of platelets to collagen[91].

To date, only few human individuals have been identified with defects associated with the receptor GPVI. In 1987, Sugiyama *et al.* reported a patient suffering from autoimmune thrombocytopenia caused by an autoantibody in her serum that was directed against a 60 kD platelet surface protein. This antigen was, however, absent in platelets of the patient. Furthermore, the patient´s platelets displayed defective aggregation in response to collagen[92]. These were the first indications that the 60 kD protein is a collagen receptor. In 1989, Moroi *et al.* described a patient deficient in GPVI. This individual also showed defective platelet aggregation in response to collagen but the response to other stimuli was normal. These results suggested that the identified 60 kD protein and GPVI are identical[87].

Over the last 20 years, a few patients have been reported with GPVI-related defects that can be categorized as follows: (1) an acquired deficiency, resulting from (a) anti-GPVI autoantibodies or (b) other causes; or (2) a congenital deficiency, where (c) GPVI is not expressed or (d) is expressed in a dysfunctional form[93]. These human individuals show primarily a mild bleeding phenotype and their platelets are unresponsive to collagen.

A.6. The metalloproteinases ADAM10 and ADAM17

A.6.1. ADAMs family

The ADAMs (a disintegrin and metalloproteinase domain) family is a group of 29 type I integral membrane-anchored proteins[94]. These multi-domain proteins are approximately 750 amino acids long (Fig. 8). The members contain a prodomain that is responsible for correct folding and inhibits the catalytic activity, and is followed by a metalloprotease domain. The disintegrin domain is supposed to be important for adhesion activity. The family name is derived from the existence of the last two mentioned domains. The cysteine-rich domain is also involved in adhesion, whereas the EGF-like domain is used for membrane fusion. The transmembrane domain anchors the protein in the membrane and the cytoplasmic part transfers signaling events[95].

Fig. 8: Modified scheme of the general domain structure of ADAM proteins[95].
N: N-terminus, S: signal peptide, Pro: prodomain, MP: metalloprotease, Dis: disintegrin, Cys: cysteine-rich, E: EGF-like, T: transmembrane, IC: (inner) cytoplasmic, C: C-terminus

ADAMs have been implicated in highly diverse processes, including fertilization, myogenesis, inflammatory responses, neurogenesis and shedding of various proteins. Fourteen ADAM members are expressed in somatic tissues, whereas the others are expressed specifically or predominantly in testis. Only 17 from 29 ADAM proteins have a protease active site, including ADAM10 and ADAM17[95]. Both, ADAM10 and ADAM17, are the best characterized metalloproteinases within the ADAMs family. Platelets express ADAM10 and ADAM17, but their role in platelet function is still poorly understood.

A.6.2. ADAM10

The *Adam10* gene was assigned to human chromosome 15 and to mouse chromosome 9, respectively[96;97]. The genomic region comprises 160 kbp with in total 16 exons (Fig. 9)[98].

Exon	Exon Size, bp	Intron	Intron Size, bp
1 with 5´UTR	80	I	24028
2	151	II	15253
3	119	III	3837
4	159	IV	18235
5	101	V	3629
6	153	VI	2233
7	93	VII	1757
8	184	VIII	5894
9	164	IX	7258
10	184	X	4317
11	151	XI	770
12	184	XII	754
13	109	XIII	875
14	221	XIV	7524
15	127	XV	1501
16 with 3´UTR	301		

Exon 1: 5´-untranslated region, signal peptide
Exon 2-5: prodomain
Exon 5-10: metalloproteinase domain
Exon 10-12: disintegrin domain
Exon 12-15: cysteine-rich domain
Exon 15-16: transmembrane domain
Exon 16: cytoplasmic region

Fig. 9: Modified scheme of the mouse *Adam10* gene with exon and intron sizes[98].
The mouse *Adam10* gene consists of 16 exons. The different domains of ADAM10 are indicated.

Mammalian ADAM10 is closely related to its homologous proteins Kuzbanian in *Drosophila* and SUP-17 in *C. elegans*, respectively. In these model organisms it was shown that ADAM10 controls proteolytic processing of Notch and that Notch is important for cell fate decision during embryonic development[99;100]. Fibroblast cell lines from ADAM10-deficient mice also revealed that ADAM10 is essential for the Notch signaling pathway and that this phenotype resembles the *Notch1* receptor knock-out phenotype. However, *Adam10*$^{-/-}$ mice die during embryogenesis at day 9.5 due to multiple defects mainly in the cardiovascular system, the central nervous system and the somites. Embryos display only a size of two-third of control embryos at this developmental stage[101]. Taken together, this demonstrates that ADAM10 and the Notch signaling pathway are crucial for embryonic development and ablation of one of the proteins results in an early embryonic abort. Recently, Tian and colleagues published the first mouse strain with a floxed *Adam10* gene. A mouse line carrying the *Lck-Cre* transgene was used to delete *Adam10* conditionally in T-cells. They showed that ADAM10 is essential in Notch1 activation during thymocyte development and confirmed with these observations previous results[102].

A.6.3. ADAM17

The *Adam17* gene was mapped to mouse chromosome 12 and human chromosome 2, respectively. The *Adam17* gene is approximately 50 kbp long and contains 19 exons (Fig. 10)[103].

Exon	Exon size (bp)	Splice donor	Intron	Splice acceptor	Intron size (kb)	Amino acid interupted
1	>97	ACTTGgtaaag	I	ttacctttatttcagAGAAG	11.1	G/lu (33)
2	133	AAAAGgtaatt	II	gcattctttcctcagGCATT	5.3	Ar/g (77)
3	131	GGTTGgtgagt	III	ttcttttccccaagGTGAG	2.1	G/ly (121)
4	89	TAGAGgtaagt	IV	tgtttccctttttagCCACT	1.5	Glu/ (160)
5	169	TGAAGgtaaga	V	tacaaattcatatagAGTTT	2.3	G/lu (217)
6	134	ACTTAgtaagt	VI	cttttctatccacagATAGA	1.6	Leu/ (261)
7	90	AGCAGgtactc	VII	ctctcttaagtatagATTCG	2.9	Qln/ (291)
8	114	TAGAGgtaggt	VIII	tccttctttttaaagCAATT	2.1	Glu/ (329)
9	145	GAAAGgtaagt	IX	tccttattcttttagCTTAT	0.113	Al/a (378)
10	89	CAAAGgtatgt	X	tccctgatccttaaagGAAGC	4.1	Lys/ (407)
11	153	ATAAGgtctgt	XI	ctgttttcttttaagATGTT	2.5	Lys/ (459)
12	200	TGCAGgtgaga	XII	tctgctcttccatagTGATA	1.3	Se/r (525)
13	104	CACAGgtatgc	XIII	ggtgtttgcctccagGGAAT	0.359	G/ly (560)
14	135	CATTGgtgagt	XIV	atgcttctctttcagGACAC	1.8	A/sp (605)
15	131	ATGAATgtaagt	XV	cttttctccttatagGGCAA	0.9	Asn/ (648)
			XV*	tgctgtttggcatagTGCGA	0.9	Asn/ (648)
16	79	TTTTGgtaagt	XVI	ttgaattattcacagGGAAG	0.88	G/ly (675)
16*	101					
17	89	GTGTGgtaagt	XVII	tcctatgctttctagGATAA	1.8	Val/ (714)
18	51	ACAGTgtaagt	XVIII	cctcgtccttcccagAACAT	0.515	Ser/ (721)
19	>348	3′ Noncoding				

*indicates junction found in the alternative spliced variant in λ5.

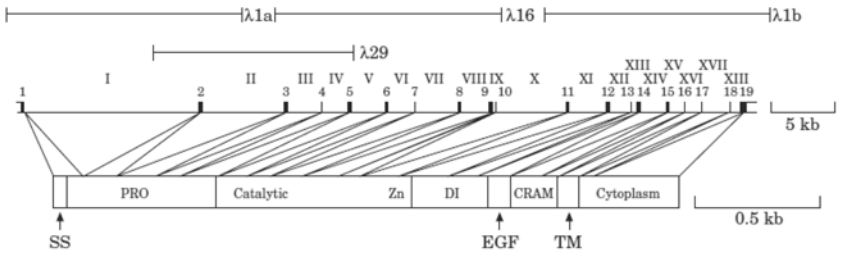

Fig. 10: Table of the mouse *Adam17* gene with exon-intron junctions (upper panel) and scheme of the genomic structure of the mouse *Adam17*; taken from Cerretti *et al.*[103]
The mouse *Adam17* gene consists of 19 exons. The different domains of ADAM17 are indicated. SS: signal sequence, Pro: prodomain, Catalytic: catalytic domain with the active site, Zn: zinc-binding motif, Di: disintegrin, EGF: EGF-like, TM: transmembrane

ADAM17 was identified as the major enzyme cleaving TNF (tumor necrosis factor) α and hence was termed TNFα converting enzyme (TACE). T cells showed a severe defect of TNFα cleavage when the Zn^{2+} binding domain of TACE (*TACE*$^{\Delta Zn/\Delta Zn}$) was disrupted by replacing the zinc-binding domain with a PGK-neo cassette[104]. *TACE*$^{\Delta Zn/\Delta Zn}$ mice die in the late stage of development between embryonic day 17.5 and the first day of birth. The lethality was surprising as mice that lack either TNFα or the TNF receptors p55 TNFR and p75 TNFR are viable and appear to develop normally[105-107]. As perinatal lethality of *TACE*$^{\Delta Zn/\Delta Zn}$ mice has prevented analysis of

TACE function for many cell types in the adult animal, conditional *TACE* knock-out mice (loxP) were recently generated. *Mx1-Cre* mice for temporal deletion and *LysM-Cre* mice for deletion in myeloid cells were used to analyze endotoxin shock. It was demonstrated that mice deficient in TACE are protected from endotoxin shock due to lower TNF levels[108]. Furthermore, mutant mice were generated with deletion of TACE using the Cre recombinase driven by a *Sox*9 promoter. These studies revealed that the mutant mice have a reduced life span to approximately 9-10 months with infertility and defects in the hematopoietic system, skeleton and skin[108].

A.6.4. ADAM10 and ADAM17 substrates

The ADAM proteins have emerged as the major proteinases involved in ectodomain shedding. The current understanding of ADAMs-mediated shedding is mainly based on the two members ADAM10 and ADAM17. Many studies have shown that ectodomain shedding regulates receptor function. 2-4% of receptor proteins are believed to be regulated by shedding[109]. In the last decade, many reviews contained comprehensive lists of substrates cleaved by ADAM10 and ADAM17. Whereas ADAM10 is the sheddase for example of EGF, Delta, CXCL-16 and others, TACE cleaves the proteins TNF receptor I and II, ErbB4, L-selectin and other proteins[110-115]. In some cases, however, a substrate is cleaved by more than one sheddase such as CX3CL-1 and the IL-6 receptor. These proteins are processed by both metalloproteinases, ADAM10 and ADAM17[116-118].

A.6.5. Shedding of platelet receptors by ADAM10 and ADAM17

To date, it has only been shown for a few platelet receptors that their surface expression is regulated by proteolytic cleavage. This key regulatory mechanism was demonstrated for the following adhesion receptors: P-selectin, CD40 ligand, GPIbα and GPV[119-122]. GPIbα is constitutively shed by ADAM17 (TACE) as soluble GPIbα (glycocalicin) levels were decreased in plasma of *TACE*$^{\Delta Zn/\Delta Zn}$ mice and increased levels GPIbα were detected on circulating platelets. It was demonstrated that TACE plays also a role in GPV shedding, however, only when shedding was induced[122]. A recent publication implicated a role of ADAM10, besides ADAM17, for GPV shedding[123]. However, not only adhesion receptors are subjected to ectodomain shedding, but also the platelet-activating receptor GPVI was identified to be regulated by proteolytic cleavage. The authors were able to show for the first time using a

mitochondrial injury model that GPVI is down-regulated from murine platelets by a metalloproteinase-dependent mechanism. Since GPVI plays a critical role in platelet activation and subsequent thrombus formation, it is important to understand the underlying mechanisms of GPVI regulation. ADAM10 and ADAM17 are believed to be candidate sheddases of GPVI. Cleavage studies on GPVI-based synthetic peptides indicated that ADAM10 is probably the GPVI sheddase under these special conditions[123]. However, the identity of the *in vivo* sheddase of GPVI remains elusive.

A.7. Aim of the study

The aim of this study was to investigate two different regulatory mechanisms in platelets:

Actin-depolymerizing factor (ADF) and non-muscle cofilin are both actin-binding proteins and play an important role in cytoskeletal dynamics. However, their role in platelets, that are highly dynamic cells, was only poorly investigated. The first aim of this study was to investigate the effect of ADF and/or cofilin deficiency and consequently altered actin turnover on platelet formation and function.

GPVI is the activatory receptor on the platelet surface. GPVI down-regulation can be induced *in vivo* by antibody treatment resulting in long-term anti-thrombotic protection without bleeding complications. It is essential to understand the mechanisms underlying this process, as this is crucial for the development of anti-GPVI based therapeutics. Therefore, the second aim of the study was to investigate the regulation of GPVI using genetically modified mouse lines.

B. Materials and methods

B.1. Materials

B.1.1. Chemicals

Acetic acid	Roth (Karlsruhe, Germany)
ADP	Sigma (Deisenhofen, Germany)
AEC solution	EUROPA (Cambridge, UK)
Agar	Roth (Karlsruhe, Germany)
Agarose	Roth (Karlsruhe, Germany)
Ampicillin	Roth (Karlsruhe, Germany)
Apyrase (grade III)	Sigma (Deisenhofen, Germany)
Bovine serum albumin (BSA)	AppliChem (Darmstadt, Germany), Sigma (Deisenhofen, Germany)
Cacodylate	AppliChem (Darmstadt, Germany)
Calcium chloride	Roth (Karlsruhe, Germany)
Canamycin sulfate	Roth (Karlsruhe, Germany)
Carbonyl cyanide m-chlorophenylhydrazone (CCCP)	Sigma (Deisenhofen, Germany)
Chloramphenicol	Roth (Karlsruhe, Germany)
Convulxin	Axxora (Lörrach, Germany)
DAPI	Invitrogen (Karlsruhe, Germany)
Disodiumhydrogenphosphate	Roth (Karlsruhe, Germany)
EDTA	AppliChem (Darmstadt, Germany)
Enhanced chemoluminiscence (ECL) detection substrate	MoBiTec (Göttingen, Germany)
Eosin	Roth (Karlsruhe, Germany)
Ethanol	Roth (Karlsruhe, Germany)
Ethidium bromide	Roth (Karlsruhe, Germany)
EZ-Link sulfo-NHS-LC-biotin	Pierce (Rockford, IL,USA)
Ficoll	Sigma (Deisenhofen, Germany)
Fibrillar type I collagen (Horm)	Nycomed (Munich, Germany)
Glucose	Roth (Karlsruhe, Germany)
Glutaraldehyde	Merck (Darmstadt, Germany)
Glycerol	Roth (Karlsruhe, Germany)

GM6001	Calbiochem (Bad Soden, Germany)
Hematoxylin	Sigma (Deisenhofen, Germany)
Hexamethyldisilazan	Merck (Darmstadt, Germany)
Hering sperm DNA	Sigma (Deisenhofen, Germany)
High molecular weight heparin	Sigma (Deisenhofen, Germany)
Human fibrinogen	Sigma (Deisenhofen, Germany)
Isopropanol	Roth (Karlsruhe, Germany)
Low melting agarose	Euromedex (Mundolsheim, France)
Magnesium sulfate	Roth (Karlsruhe, Germany)
Manganese chloride	Roth (Karlsruhe, Germany)
Milk powder	AppliChem (Darmstadt, Germany)
MOPS	AppliChem (Darmstadt, Germany)
NEM	Calbiochem (Bad Soden, Germany)
Nonidet P-40 (NP-40)	Roche Diagnostics (Mannheim, Germany)
Osmium tetraoxide	Merck (Darmstadt, Germany)
Paraformaldehyde	Applichem (Darmstadt, Germany)
Penicillin/streptomycin	PAN (Aidenbach, Germany)
Peptone (pancreatic digested)	Roth (Karlsruhe, Germany)
Phorbol 12-myristate 13-acetate (PMA)	Sigma (Deisenhofen, Germany)
Poly-L-Lysine	Sigma (Deisenhofen, Germany)
Potassium acetate	Roth (Karlsruhe, Germany)
Potassium chloride	Roth (Karlsruhe, Germany)
Prolong Antifade	Invitrogen (Karlsruhe, Germany)
Propidium iodide	Invitrogen (Karlsruhe, Germany)
Propylen oxide	Merck (Darmstadt, Germany)
Prostacyclin	Calbiochem (Bad Soden, Germany)
Protein G sepharose	GE Healthcare (Uppsala, Sweden)
Rubidium chloride	Roth (Karlsruhe, Germany)
Sodium chloride	AppliChem (Darmstadt, Germany)
Sodium citrate	AppliChem (Darmstadt, Germany)
Sodiumdihydrogenphosphate	Roth (Karlsruhe, Germany)
Sodium hydroxide	AppliChem (Darmstadt, Germany)
Tannic acid	Merck (Darmstadt, Germany)

Thrombin	Roche Diagnostics (Mannheim, Germany)
Thrombopoietin	Biosource (Solingen, Germany)
3,3,5,5-tetramethylbenzidine (TMB)	EUROPA (Cambridge, UK)
TRIS ultra	Roth (Karlsruhe, Germany)
Trizol	Invitrogen (Karlsruhe, Germany)
U46619	Alexis Biochemicals (San Diego, USA)
W7	Calbiochem (Bad Soden, Germany)
X-gal	AppliChem (Darmstadt, Germany)
Yeast extract	AppliChem (Darmstadt, Germany)

All enzymes were purchased from Fermentas (St. Leon-Rot, Germany) or obtained from Invitrogen (Karlsruhe, Germany).
Collagen related peptide (CRP) was kindly provided by S.P Watson (University of Birmingham, UK).

All other chemicals were obtained from Sigma (Deisenhofen, Germany) or Roth (Karlsruhe, Germany).

B.1.2. Kits

- Ligation:

Fast-Link DNA Ligation Kit	Eppicentre (Hess. Oldendorf, Germany)
Ready-to-go T4 DNA Ligase	Amersham Biosciences (Freiburg, Germany)
T4 DNA Ligase	Invitrogen (Karlsruhe, Germany)

- PCR:

GeneAmp XL PCR Kit	Applied Biosystems (New Jersey, USA)
Triple Master PCR System	Eppendorf (Hamburg, Germany)

- Cloning:

TOPO TA Cloning Kit	Invitrogen (Karlsruhe, Germany)
TOPO XL PCR Cloning Kit	Invitrogen (Karlsruhe, Germany)
Zero Blunt TOPO PCR Cloning Kit	Invitrogen (Karlsruhe, Germany)

- Site-directed mutagenesis:

QuickChange-XL	Stratagene (Amsterdam, The Netherlands)

- DNA Purification Kits:

Plasmid DNA Maxi/Midi Purification	Qiagen (Hilden, Germany)
Nucleo Spin Extract II Kit	Macherery-Nagel (Düren, Germany)
Nucleo Spin Plasmid Kit	Macherery-Nagel (Düren, Germany)
BACMAX DNA Purification Kit	Eppicentre (Hess. Oldendorf, Germany)

B.1.3. Cell culture material

Beta-mercaptoethanol	Roth (Karlsruhe, Germany)
DMEM	Gibco (Karlsruhe, Germany)
Fetal calf serum	Perbio (Bonn, Germany)
Geneticin	Gibco (Karlsruhe, Germany)
LIF (Leukemia Inhibitory Factor)	Chemicon (Hampshire, United Kingdom)
Kryo-tubes	Roth (Karlsruhe, Germany)
Nonessential amino acids	Gibco (Karlsruhe, Germany)
PBS	Gibco (Karlsruhe, Germany)
Penicillin/streptomycin	Gibco (Karlsruhe, Germany)
Stem cells	kindly provided by Nagy A.[124]
Tissue culture dishes (100/20 mm)	Greiner (Frickenhausen, Germany)
Tissue culture flasks (25 or 175 cm^2)	Greiner (Frickenhausen, Germany)
Trypsin	Gibco (Karlsruhe, Germany)
Well plates	Greiner (Frickenhausen, Germany)

B.1.4. Isotope lab material

Probequant G 50 Microcolumns	Amersham Biosciences (Freiburg, Germany)
Rediprime DNA Labeling Kit	Amersham Biosciences (Freiburg, Germany)
Redivue-α ^{32}P-dCTP; 250 µCi	Amersham Biosciences (Freiburg, Germany)

B.1.5. Buffers and media

All buffers were prepared and diluted using aqua $_{bidest}$.

- Blotting buffer A

Tris, pH 10.4	0.3 M
Methanol	20%

- Blotting buffer B

Tris, pH 10.4	25 mM
Methanol	20%

- Blotting buffer C

ε-amino-n-caproic acid	4 mM
Methanol	20%

- CATCH buffer

HEPES	25 mM
EDTA	3 mM
BSA	3.5%
PBS	

- Church buffer for southern blot

Phosphate buffer (0.5 M; pH 7.2)	50%
SDS (20%)	33%
EDTA (0.5 M)	0.1%
Hering sperm DNA	1%
BSA	10 g/L

- Church wash buffer for southern blot

Phosphate buffer (0.5 M; pH 7.2)	4%
SDS (20%)	5%

- Coating buffer, pH 9.0

$NaHCO_3$	50 mM

- Coomassie Stain

Acetic acid	10%
Methanol	40%
Brilliant blue	1 g
in H_2O	

- Coupling buffer 2x, pH 9.0

$NaHCO_3$	14 g/L
Na_2CO_3	8.5 g/L

- Decalcification buffer

EDTA	10%
PBS	
pH 7.4	

- Denaturation buffer for southern blot

NaCl	1.5 M
NaOH	0.5 M

- Destaining solution

Acetic acid	10%
H_2O	50%
Methanol	40%

- EF-Medium

DMEM	
FCS	10%

- ES-Medium

DMEM	
FCS	20%
Nonessential amino acids	1%
β-mercaptoethanol	3.5 µL
LIF	1,000 units/mL

- ES+G418 Medium

ES-Medium	
Geneticin	400 µg/mL

- Freezing-Medium

DMEM	
FCS	50%
DMSO	10%

- IP buffer

Tris/HCl (pH 8.0)	15 mM
NaCl	155 mM
EDTA	1 mM
NaN_3	0.005%

- Karnovsky fixation buffer

Paraformaldehyde	2%
Glutardialdehyde	2.5%
Cacodylate	0.1 M
pH 7.2	

- Laemmli buffer

Tris	40 mM
Glycin	0.95 M
SDS	0.5%

- LB-Medium

(solution)	
Peptone (pancreatic digested)	10 g/L
Yeast extract	5 g/L
NaCl	10 g/L
(agar)	
Agar	15 g/L

- Lysis buffer

TRIS base	100 mM
EDTA (0.5 M)	5 mM
NaCl	200 mM

SDS	0.2%
added Proteinase K (20 mg/mL)	100 µg/mL

- MK medium

IMEM	
FCS	10%
Penicillin/streptomycin	1%
Thrombopoietin	50 ng/mL

- Neutralisation buffer for southern blot

NaCl	1.5 M
TRIS base	0.5 M
HCl (37%) until pH 7.2	

- PHEM

PIPES	18.14 g/L
HEPES	5.96 g/L
EGTA	3.8 g/L
$AcMg^{2+}$	0.214 g/L
H_2O	
pH 6.9	

- Phosphate-buffered saline (PBS), pH 7.14

NaCl	137 mM
KCl	2.7 mM
KH_2PO_4	1.5 mM
$Na_2HPO_4 \times 2H_2O$	8 mM

- PBS/EDTA

PBS	
EDTA	5 mM

- Phosphate buffer (0.5%; pH 7.2)

Solution A (1 M)	

Na_2HPO_4 x 2 H_20	68.4%
Solution B (1 M)	
NaH_2PO_4 x 2 H_20	31.6%

- SDS sample buffer, 2x

β-mercaptoethanol (for red. conditions)	10%
Tris buffer (1.25 M), pH 6.8	10%
Glycerin	20%
SDS	4%
Bromophenolblue	0.02%

- Solution I for Mini DNA purification

Glucose	50 mM
TRIS base	25 mM
EDTA	10 mM

- Solution II for Mini DNA purification

NaOH	0.2 M
SDS	1%

- Solution III for Mini DNA purification pH 5.5

Potassium acetate	3 M

- 10x SSC for southern blot

NaCl	1.5 M
Na-citrate	0.25 M

- Storage buffer, pH 7.0

Tris	20 mM
NaCl	0.9%
BSA	0.5%
NaN_3	0.09%

- 50x TAE

TRIS base	0.2 M
Acetic acid	5.7%
EDTA (0.5 M)	10%

- TE buffer

TRIS base	10 mM
EDTA	1 mM

- TFB I solution for competent cells

Potassium acetate	30 mM
$MnCl_2$	5 mM
RbCl	100 mM
$CaCl_2$	100 mM
Glycerol	15%
Acetic acid (0.2 M) until pH 5.8	

- TFB II solution for competent cells

MOPS	10 mM
$CaCl_2$	75 mM
$RbCl_2$	10 mM
Glycerol	15%

- Tris-buffered saline (TBS), pH 7.3

NaCl	137 mM
Tris/HCl	20 mM

- Tyrode’s buffer, pH 7.3

NaCl	137 mM
KCl	2.7 mM
$NaHCO_3$	12 mM
NaH_2PO_4	0.43 mM
Glucose	0.1%
Hepes	5 mM

BSA	0.35%
$CaCl_2$	2 mM
$MgCl_2$	1 mM

- Washing buffer
  PBS
  Tween 20 0.1%

B.2. Methods

B.2.1. Molecular biology

B.2.1.1. BAC screening

For BAC screening, a BAC internal probe was labeled with the radioactive substance ^{32}P and then High Density Filters (CHORI, Oakland, USA) were hybridized with the BAC internal probe. Details of the labeling and hybridization steps are exactly explained in B.2.2.8. “Analysis of stem cell DNA (Southern Blot)”. Subsequently, a film was placed on top of the filters in a cassette. The film was developed after four hours exposure at RT. The signals were interpreted due to the supplied protocol to determine the position and thereby the labeling of positive clones. Positive clones were ordered at www.chori.org

B.2.1.2. General PCR schemes for amplification of construct flanking sites and probes

- Triple Master PCR (Eppendorf)
  PCR cycler: Mastercycler gradient (Eppendorf)

0.2 µg	Primer forward
0.2 µg	Primer reverse
10 ng	DNA template
5 µL	10x Triplemix buffer
1 µL	10 mM dNTP
0.5 µL	Triplemix enzyme (5 u/µL)

H_2O was added to a final volume of 50 µL.

Program 1: (product < 2kb)

96°C	2 min	
94°C	30 sec	35 cycles
x°C	30 sec	
72°C	30 sec	

Program 2: (product > 2kb)

96°C	3 min	
94°C	30 sec	35 cycles
x°C	30 sec	
68°C	5 min	

x°C : The PCR reaction was performed with different annealing temperatures per sample :
1: 50°C; 2: 50.3°C; 3: 51.4°C; 4: 53.2°C; 5: 55.5°C; 6: 58°C; 7: 60.8°C; 8: 63.5°C

- GeneAmp XL PCR (Appl. Biosystems);
  PCR cycler: GeneAmp PCR System 9700 (Appl. Biosystems)

0.2 µL	rTth polymerase (2 u/µL)
6 µL	3.3x XL buffer
100 ng	DNA template
1 mM	$Mg(OAc)_2$
1.6 µL	10 mM dNTP
100 ng	Primer forward
100 ng	Primer reverse

H_2O was added to a final volume of 20 µL.

Program:

94°C	1 min	
94°C	30 sec	35 cycles
58°C	20 sec	
68°C	2.15 min + 2 sec/cycle	
72°C	5 min	

- PCR using Taq-Polymerase (Fermentas)
  PCR cycler: GeneAmp PCR System 9700 (Appl. Biosystems)

100 ng forward primer
100 ng reverse primer
1 µL 10 mM dNTP
5 µL 10x Taq – buffer (+ KCl, - $MgCl_2$)
1 µL DNA template
0.4 µL Taq-Polymerase (5 u/µL)
2 µL 25 mM $MgCl_2$
H_2O was added to a final volume of 50 µL.

Program:
96°C 5 min
94°C 30 sec
60°C 30 sec } 35 cycles
72°C 30 sec
72°C 10 min

B.2.1.3. Agarose gel

1 g agarose was added to 100 mL 1x TAE buffer for a small 1% agarose gel. The agarose in TAE buffer was heated up in a microwave for 3 minutes. When the temperature was decreased to about 60°C again, 5 µL ethidium bromide were added and the fluid was poured into a slide with a comb. The slight was laid in a chamber filled with 1x TAE buffer. The samples were diluted in 10x loading buffer and loaded into the slots of the gel. The samples were run at about 120 V. In parallel, a 1 kb ladder was separated to determine the size of the DNA bands under UV light.
4 g agarose in 400 mL 1x TAE buffer were used for a big 1% agarose gel. Finally, 20 µL ethidium bromide were added to the solved agarose in 1x TAE buffer.
Additionally, 0.7% and 2% agarose gels were done to separate DNA bands.

B.2.1.4. DNA-Extraction from an agarose gel

A DNA band was excised from an agarose gel under UV light. 700 µL NT buffer (Macherey-Nagel) were added to the isolated agarose piece and shaken at 55°C for several minutes until the gel was completely dissolved. After 1-2 minutes incubation on ice, the DNA was applied to the column and centrifuged at 11,000 rpm for 30 seconds. Then the column was washed twice with 750 µL NT3 buffer with ethanol at 11,000 rpm for 1 minute. A drying step followed by centrifugation the empty column at 11,000 rpm for 2 minutes and the rest of ethanol was removed by air-drying the tube with opened lid for 3-5 minutes. Finally, 30 µL H_2O were added and incubated for 2-4 minutes. The DNA was eluted by centrifugation at 11,000 rpm for 2 minutes.

B.2.1.5. Treatment of insert and vector

- The pBluescript II KS vector was treated two times with 1 µL CIP (Calf Intestine Phosphatase) at 37°C for 30 minutes in order to prevent religation of the vector.
- The insert was treated with Klenow-Fragment and T4 Polynucleotide kinase to ligate the insert into a blunt end cut vector as follows:

  27 µL DNA insert
  5 u Klenow-Fragment
  2 µL 10 mM dNTP
  5 u T4 Polynucleotide kinase
  4 µL 10x Polynucleotide kinase buffer A (forward reaction)
  1 µL 10 mM ATP

  H_2O was added to a final volume of 40 µL. The sample was incubated at 37°C for 30 minutes.
- The insert was incubated with Taq polymerase to ligate the insert into a vector with T-overhangs as follows:

  47 µL DNA insert (PCR product)
  5 u Taq polmerase (Invitrogen)
  2 µL 10 mM dATP

  The incubation was performed at 72°C for 30 minutes.

B.2.1.6. Repurification of DNA

The repurification step is necessary to remove proteins from the DNA. Therefore, 500 µL NT buffer (Nucleo Spin Extract II Kit; Macherery-Nagel) were added to a sample

of 50 µL volume. The sample was immediately loaded on the column without a heating step. The remaining procedure is the same like in “DNA-Extraction from an agarose gel”.
Alternatively, another method was used to repurify DNA. One tenth 3 M sodium acetate (pH 5.2) and five times more 100% ethanol of the volume with DNA were added to the sample, mixed and incubated at –20°C for at least 30 minutes. After centrifugation at 14,000 rpm for 10 minutes at 4°C, the pellet was washed with 500 µL 70% ethanol and centrifuged again. The pellet was dried and dissolved in 30-50 µL H_2O.

B.2.1.7. Ligations

The amount of insert and vector DNA was estimated after running on a 1% gel.

- Fast-Link DNA Ligation Kit (Eppicentre)

1.5 µL 10x Fast-Link Ligation Buffer
1.5 µL 10 mM ATP
Insert DNA : Vector DNA 2:1
1 µL Fast-Link DNA Ligase
H_2O was added to a final volume of 15 µL; Incubation for one hour at 16°C.

- Ready-to-go T4 DNA Ligase (Amersham Biosciences)

Insert DNA : Vector DNA 2 : 1
H_2O was added to a final volume of 20 µL; Incubation for one hour at 16°C.

- T4 DNA Ligase (Invitrogen)

Insert DNA : Vector DNA 2 : 1
4 µL 5x Ligase Buffer
1 µL T4 Ligase
H_2O was added to a final volume of 20 µL; Incubation over night at 16°C.

B.2.1.8. Cloning with TOPO kits (Invitrogen)

- TOPO TA or Zero Blunt TOPO

1 µL PCR product (dilution depends on amount of DNA)
1 µL Salt Solution
1 µL TOPO vector

3 µL Sterile Water

The incubation time ranged from 5 – 20 minutes at room temperature.

- TOPO XL

For TOPO XL Cloning reaction a special preparation of the PCR product was necessary. Hence, the PCR product was run on an agarose gel, but this gel was stained with Crystal Violet and purified with a special supplied gel-purifying kit according to the manual.

4 µL Gel-purified PCR product

1 µL pCR-XL-TOPO vector

The incubation time ranged from 5 – 20 minutes at room temperature (RT) and the reaction was stopped with 1 µL 6x TOPO Cloning Stop.

All the following transformations were performed either with own competent cells (procedure explained in B.2.1.10. “Transformation”) or with competent cells supplied with the kit. Therefore, 2 µL of the TOPO Cloning reaction were added to one vial of chemically competent *E. coli* cells and incubated on ice for 30 minutes. The cells were heat-shocked at 42°C for 30 seconds. The tubes were transferred on ice for 2 minutes. Following addition of 250 µL S.O.C. medium, the samples were shaken at 37°C for one hour. 150 µL were spread on a LB plate containing 50 µg/mL canamycin. The plate was incubated at 37°C over night. When blue/white colony selection was necessary, 1.6 mg X-gal were added to one plate before plating the cells.

B.2.1.9. Transformation

5-7 µL of the ligation reaction or 1 µL of a ligated product were added to 100 µL chemically competent cells (DH5α, DH10Bα or XL10Gold) and incubated on ice for 45 minutes. The transformation was performed for 90 seconds at 42°C and then put on ice for 2 minutes. 1 mL LB-medium without antibiotics was added to the cells and incubated for 30 minutes at 37°C. Either all cells, after centrifugation for 3 minutes at 5,000 rpm, or 100 µL of the cells (retransformation of a vector) were plated on a LB plate containing 50 µg/mL ampicillin or canamycin. The plate was incubated over night at 37°C.

When blue/white colony selection was necessary, 1.6 mg X-gal were added to one plate before plating the cells.

B.2.1.10. Mini DNA purification

3 mL LB medium containing the selective antibiotic (50 µg/mL ampicillin or canamycin) and a picked single colony were shaken for 12-16 hours at 37°C. The cells were spun down at 11,000 rpm for 30 seconds and the pellet was resuspended in 200 µL solution I. 300 µL of solution II were used to lyse the cells for about 5 minutes at RT. Then, 300 µL of solution III were added and the sample was incubated for 5 minutes at RT. Subsequently, the tube was centrifuged at 11,000 rpm for 5 minutes. The supernatant was transferred into a new tube and mixed with 700 µL isopropanol and incubated on ice for 5 minutes. After centrifugation at 14,000 rpm for 10 minutes at 4°C, the pellet was washed with 500 µL 70% ethanol and incubated for 8 minutes at RT. The sample was centrifuged at 14,000 rpm for 8 minutes at 4°C and finally the dried DNA pellet was dissolved in 30 µL TE buffer with 0.1 µg/µL RNaseA.

B.2.1.11. Mini DNA purification (Macherey-Nagel)

This Mini DNA Plasmid Purification Kit was used in order to get clean DNA for sequencing.

Therefore, 3 mL LB medium containing the selective antibiotic (50 µg/mL ampicillin or canamycin) and a picked single colony were shaken for 12-16 hours at 37°C. The cells were centrifuged at 11,000 rpm for 30 seconds and the pellet was resuspended in 250 µL A1 buffer. Additional 250 µL of A2 buffer were used to lyse the cells for 5 minutes at RT. Next, 300 µL of A3 buffer were added and the sample was centrifuged at 11,000 rpm for 5 minutes. The supernatant was transferred to a column and centrifuged at 11,000 rpm for 1 minute. 600 µL of washing buffer AW with ethanol were applied to the column and centrifuged at 11,000 rpm for 1 minute. Following one minute incubation with 50 µL TE buffer, DNA was eluted by centrifugation at 11,000 rpm for 1 minute.

B.2.1.12. Sequencing of plasmid DNA

The sequencing of plasmid DNA was performed by the company MWG Biotech in Ebersberg (Germany). Therefore, 3 µg plasmid DNA diluted in TE buffer to a final volume of 20 µL were sent to MWG Biotech/eurofins. Either standard primers from the company were chosen or own primers were sent. For that, 1 µg primer was diluted in TE buffer in a final volume of 12 µL.

Two alignment programmes were used to analyze the sequencing results:
http://www.ncbi.nlm.nih.gov/blast/bl2seq/wblast2.cgi
http://searchlauncher.bcm.tmc.edu/multi-align/multi-align.html

B.2.1.13. Midi (Maxi) DNA Purification

150 mL (250 mL) LB medium containing the selective antibiotic (50 µg/mL ampicillin or canamycin) and a picked single colony were shaken for 12-16 hours at 37°C. The bacterial cells were harvested by centrifugation at 6,000 rpm for 15 minutes. The bacterial pellet was resuspended in 4 mL (10 mL) resuspension buffer. Then 4 mL (10 mL) lysis buffer were added and the tube was inverted 4-6 times and incubated for 5 minutes at RT. 4 mL (10 mL) neutralization buffer were poured to the sample and chilled for 15 minutes on ice. Next, the sample was centrifuged at 20,000 rpm for 30 minutes at 4°C and the supernatant was centrifuged for 20 minutes again. The supernatant containing the plasmid DNA was transferred to a Qiagen-tip 100 (Qiagen-tip 500), after the column was equilibrated by applying 4 mL (10 mL) equilibration buffer. Then 2 x 10 mL (2 x 30 mL) washing buffer were loaded to the column and subsequently, plasmid DNA was eluted by applying 5 mL (15 mL) elution buffer. 3.5 mL (10.5 mL) isopropanol were added to the eluted DNA and centrifuged at 15,000 rpm for 30 minutes at 4°C. The DNA pellet was washed with 2 mL (5 mL) 70% ethanol and centrifuged at 15,000 rpm for 10 minutes. Then, the pellet was dried, 200 µL (500 µL) TE buffer were added and the DNA concentration was measured at 260 nm.

B.2.1.14. BAC DNA purification

150 mL LB medium containing 12.5 µg/mL chloramphenicol and a piece of agar with BAC DNA in bacterial cells were shaken for 12-16 hours at 37°C. The cells were pelleted by centrifugation at 5,000 rpm for 8 minutes. The pellet was resuspended in 6 mL BACMAX Solution 1. Then 6 mL BACMAX Solution 2 were added and the tube was inverted for 2-3 times. After 5 minutes incubation, 4.5 mL BACMAX Solution 3 were poured to the sample and chilled for 15 minutes on ice. Next, the sample was centrifuged at 15,000 rpm for 15 minutes at 4°C and 0.6 volumes isopropanol were added to the removed supernatant. The mixed sample was centrifuged at 15,000 rpm for 15 minutes at 4°C and the pellet was dried before adding 500 µL TE buffer. After addition of 20 µL RiboShredder RNase Blend with incubation for 30 minutes at 37°C,

500 µL TE buffer and 1 mL of chilled BACMAX Solution 4 with incubation for 15 minutes on ice, the tube was centrifuged at 15,000 rpm for 15 minutes at 4°C. The recovered supernatant was mixed with 4 mL ethanol and centrifuged under the same conditions as before. The pellet was dried, dissolved in 200 µL TE buffer and the DNA concentration was measured at 260 nm.

B.2.1.15. Digestion of plasmid DNA

All samples were usually digested for at least 45 minutes at 37°C. Only when special enzymes were used, the incubation was performed at the appropriate temperature.

2-10 u	enzyme per sample
2 µL	10x enzyme buffer
0.5-2 µg	DNA

H_2O was added to a final volume of 20 µL.

Additional 2-10 units of the other enzyme were added for a double digestion if the reaction was possible under the same buffer and temperature conditions.
If a double digestion was not possible under same conditions, then at first a digestion with one enzyme was performed and after this the enzyme was inactivated for 10 minutes at 68°C. Subsequently, the sample was chilled for two minutes on ice and then the double volume was added that contained the second enzyme, 10x buffer and H_2O. Then, the incubation was performed at the temperature for the second enzyme.

B.2.1.16. Generation of competent cells

5 mL LB medium with a piece of cells (DH5α, DH10B or XL10 Gold) from a frozen glycerol stock were incubated at 37°C and 220 rpm over night. 1 mL from the over night culture was added to 150 mL LB medium supplemented with sterilely filtrated 10 mM KCl and 20 mM $MgSO_4$. The cells were allowed to grow at 37°C and 220 rpm until an OD_{600} = 0.4. Afterwards, the cells were centrifuged at 6,000 rpm for 10 minutes and the pellet was resuspended in 75 mL TFB I buffer. After 10 minutes incubation on ice, the cells were centrifuged again and the pellet was resuspended in 6 mL TFB II buffer. 100 µL were distributed in each tube and immediately stored at –80°C.

B.2.1.17. Site-directed mutagenesis

The site-directed mutagenesis comprised three different steps:

- PCR (PCR cycler: GeneAmp PCR System 9700; Appl. Biosystems)

125 ng	Primer forward
125 ng	Primer reverse
50-100 ng	dsDNA template
5 µL	10x reaction buffer
1 µL	dNTP mix
3 µL	Quick solution
1 µL	Pfu Turbo polymerase (2.5 u/µL)

H_2O was added to a final volume of 50 µL.

Program:

95°C	5 min	
95°C	30 sec	18 cycles
60°C	30 sec	
68°C	1 min/kb plasmid	
68°C	7 min	

- Digestion

Half volume of the PCR product was used as a transformation control later. The other half of the PCR product was treated with 1 µL Dpn I and incubated for 1 hour at 37°C.

- Transformation

Two tubes with 45 µL competent cells from the kit were put on ice. 2 µL β-mercaptoethanol were added to each tube and incubated on ice for 10 minutes. The tubes were gently shaken every second minute. Then 5 µL from the control and the digested sample were added to different tubes with competent cells and incubated for 30 minutes on ice. The heat shock step was performed for 30 seconds at 42°C and then the samples were immediately put for two minutes on ice. 500 µL prewarmed LB medium were added to each tube and shaken at 300 rpm and 37°C for 1 hour. Finally, 250 µL were plated on a plate with the appropriate selective

antibiotic (50 µg/mL ampicillin or canamycin) and incubated at 37°C over night. On the next day, the numbers of colonies on both plates were compared and colonies of the digested sample were picked.

B.2.2. Stem cell work

B.2.2.1. Preparation of feeder cells

A mouse strain containing a neomycin cassette in the genome was used for the preparation of feeder cells. For this, fertile collagen IX knock-out mice were time-mated. At day 14.5 mice embryos were excised of the pregnant mouse. Then, the embryos were washed in PBS and subsequently, skeleton muscles and skin of the embryos were homogenized in a final volume of 10 mL EF-Medium (for a number of 7-9 embryos) with 10% trypsin and incubated in a 37°C waterbath for at least 5 minutes. This step was repeated once. One mL of the homogenized embryos in medium was added to 9 mL EF-Medium in a 10 cm tissue culture dish. After one day of incubation at 37°C and 5% CO_2, the EF-Medium was changed and when the cells were grown confluently, one 10 cm tissue culture dish was split into two 175 cm^2 tissue culture flasks. The densely grown cells were trypsinized, collected and spun down (all cell culture centrifugation steps: 5 minutes with 900 rpm in a Multifuge 3 S-R from Heraeus). The cells were collected in a final volume of 15 mL EF-Medium. Subsequently, the cells were irradiated with 40 Gray (1.031 Gray/min; at MSZ Würzburg). After spinning down, Freezing-Medium was added to the pellet and the cells in Freezing-Medium were stored as 1 mL aliquots (cells of an 175 cm^2 tissue culture are frozen in 3 mL freezing medium) in 2 mL Kryo-Tubes at –80°C. One Kryo-Tube with cells was used for checking contamination and efficiency of irradiation. Therefore, one tube with feeder cells was added to a 10 cm tissue culture dish with EF-Medium and was checked under the microscope every day for one week.

B.2.2.2. Electroporation

Before electroporation, wild-type stem cells (R1 clone, passage number 13)[124] were cultured. Therefore, 1/6 of a vial feeder cells and one vial stem cells were diluted in ES-Medium and used for one six-well (growth at 37°C and 5% CO_2). Next day, stem cells were transferred into a 75 cm^2 flask. New feeder cells were necessary for this step. 1.5 mL feeder cells were spun down and the pellet was diluted in ES-Medium. Feeder cells and trypsinized stem cells in ES-Medium were transferred in the 75 cm^2

flask and diluted with additional ES-Medium. Next day, the medium was changed and the following day the cells were transferred into two 175 cm^2 flasks. After reaching a certain density, usually the cells of one flask were used for electroporation of two constructs. Before electroporation, cells were checked for mycoplasm contamination.
100 µg DNA of the final construct were digested (2 hours, 37°C) to linearize the vector for electroporation:

100 µg DNA
10x enzyme buffer
200 units enzyme
ad H_2O

The linearization of the vector was confirmed by comparing same amounts of DNA of the digested and the undigested vector on a 0.7% gel. To precipitate the digested DNA, phenol/chloroform was added to the sample in the ratio 1:1 and shaken. After centrifugation at 14,000 rpm for 8 minutes, the upper layer was transferred into a new 1.5 mL tube. Then, after addition of chloroform (ratio 1:1), the sample was shaken and centrifuged again. The supernatant was supplemented with 10% 3 M sodiumacetate pH 5.2 and three times more 100% ethanol. The precipitated DNA was washed twice in a sterile tube with 800 µL 70% ethanol. After spinning down, DNA was dried under sterile conditions for several minutes and then resuspended in 700 µL PBS and well vortexed.
The stem cells in the 175 cm^2 tissue culture flask were trypsinized and diluted in ES-Medium. Subsequently, cells were spun down and washed three times in PBS. The number of cells was approximately 4 x 10^7/mL. Cells were centrifuged again and the supernatant was removed. The DNA in 700 µL PBS was transferred to the stem cells and then electroporated in a cuvette (Cat. No.: 165-2088; 0.4 cm electrode gap, Biorad, Munich, Germany) with 0.8 kV and 3 µF (Gene Pulser II from Bio-Rad). The electroporated stem cells were diluted with 7 mL ES-Medium and distributed to seven beforehand prepared 10 cm tissue culture dishes. Therefore, one vial feeder cells diluted in ES-medium was added per dish.

B.2.2.3. Selection of stem cells

First day after electroporation, the selection was started by treatment with the antibiotic Geneticin (G418) which is structurally similar to neomycin. Thus, the ES-

Medium was removed and 10 mL ES-Medium with 400 µg/mL Geneticin (ES+G418 Medium) were added. The selection was performed for at least 7 days. Every day each tissue culture dish was checked for contamination with bacteria or yeast. Before cell picking the cells were checked once for contamination with mycoplasm.

B.2.2.4. Picking of neomycin-resistant stem cell clones

1 vial feeder cells was used for one 24-well plate. Therefore, ES+G418 Medium was added to the feeder cells and spun down. Afterwards, the pellet of feeder cells was diluted with 24 mL ES+G418 Medium and evenly distributed to each well of a 24 well plate and incubated at 37°C until use.

Picking with a 200 µL pipette was performed under a LEICA MS5 microscope (setting: 0.63x magnification). Clones that had survived the Geneticin treatment were picked when they had the appropriate shape, color and size. Cells looking differentiated or necrotic were not picked. Each picked clone was transferred into one well of a 96 well plate containing two drops of trypsin (~ 100 µL) in order to solve the cell clone into single cells. After incubation for 5 minutes at 37°C and 5% CO_2, each clone was resuspended in the well with trypsin and added to one well of the beforehand prepared 24 well plate. The cells were incubated at 37°C over night and then the ES+G418 Medium was changed. After this, the cells grew 2 days without changing medium. Every day each well plate was checked for contamination with bacteria or yeast. Before freezing, cells were checked once for contamination with mycoplasm.

B.2.2.5. Freezing of picked stem cell clones

Cells in a 24-well plate were trypsinized and then 1 mL Freezing-Medium was added to each well. After resuspension, 600 µL of the sample were transferred to a labeled Kryo-tube and immediately stored at –80°C. Each well was labeled with the same number according to the Kryo-tube. The remaining 400 µL were filled up with ES+G418 Medium and incubated over night at 37°C. After this, the medium was replaced by 1 mL new ES+G418 Medium.

B.2.2.6. Lysis of stem cells

After the color of the medium had become yellow which was usually after 3-4 days, the supernatant was removed and the cells were lysed with lysis buffer

supplemented with 100 µg/mL proteinkinase K. Half mL lysis buffer was added to one well. The cells were lysed for at least 1 day at 37°C and 5% CO_2.

B.2.2.7. Precipitation of stem cell DNA

Following the lysis, DNA of the stem cells was precipitated with 0.5 mL isopropanol per well. Therefore, sterile conditions were not necessary. The samples were agitated on a shaker between 4-6 hours at room temperature. In the meantime, 1.5 mL tubes were labeled with the corresponding numbers and filled with 150 µL TE buffer. The precipitated DNA fibers were transferred with a stick into the corresponding 1.5 mL tube. After shaking the samples for a few minutes at 55°C with open lid to remove traces of isopropanol, DNA was incubated with closed lid in a 55°C incubator over night. Afterwards, the samples were shortly vortexed and ready for analysis.

B.2.2.8. Analysis of stem cell DNA

- Digestion of stem cell DNA

Each stem cell DNA was digested in order to distinguish a positive clone that integrated the electroporated DNA via homologous recombination and a negative clone that could not integrate the electroporated DNA via homologous recombination. The genomic stem cell DNA was digested over night at 37°C:

20 µL stem cell DNA
4 µL 10x enzyme buffer
25 u enzyme
H_2O was added to a final volume of 40 µL.

- Southern blot

The digested DNA samples were run on a 1% agarose gel for at least 3-4 hours at 140 V. Then, a photo was taken from the gel with a ruler to estimate the size of the bands after development. The gel was incubated with denaturation buffer for 20 minutes twice and subsequently with neutralization buffer for 20 minutes twice. Afterwards, DNA was blotted from the agarose gel on a nitrocellulose membrane (Hybond XL, Amersham Biosciences, Freiburg, Germany) over night at RT.

After blotting, gel slots were labeled on the membrane. Then, DNA was crosslinked with the membrane (120,000 µJ/cm^2; HL-2000 HybriLinker from UVP). For probe labeling and hybridization, the following steps were performed in an isotope lab:
The external probe (10 - 100 ng) was diluted in 35 µL TE buffer and incubated for 3 minutes at 96°C. When the DNA was resuspended in the Rediprime DNA Labeling Kit, 5 µL radioactive substance ^{32}P was added to one sample and incubated for 20 minutes at 37°C. In the meantime, the buffer of the Probequant G 50 Microcolumns was removed via centrifugation and the membrane was briefly preincubated in Church wash buffer. The DNA with the radioactive substance was loaded on the column and centrifuged for 1 minute at 2,000 rpm (Biofuge A from Heraeus). The flow-through containing the radioactively labeled DNA was incubated for 3 minutes at 96°C and then added to the membrane in Church buffer. The membrane was shaken in Church buffer over night at 68°C. Then, the membrane was washed twice with Church wash buffer for 20 minutes at 68°C. Subsequently, a film was put on the top of the membrane and stored at –80°C. The film was developed after 3-5 days depending on the signal.

B.2.2.9. Reculturing of positive stem cells

Frozen tubes of those clones that had been identified as positive were thawn and added to one well of a six well plate containing feeder cells and ES-Medium+G418. After growing at 37°C and 5% CO_2 to a certain density, cells were trypsinized and cultured in a 25 cm^2 flask. Two days later, cells were trypsinized again and added to a 75 cm^2 tissue culturing flask. Finally, cells were trypsinized and a small amount of cells were transferred to one well of a 24 well plate to check again for homologous recombination via Southern Blot. The majority of cells were frozen into four aliquots. Three Kryo-tubes were stored at –80°C and one tube with ES cells was used for the generation of chimeric mice. Therefore, this tube was sent on dried ice to Michael Bösl (MPI, Munich) who injected these cells into blastocysts and sent obtained the chimeric mice.

B.2.3. Genotyping of mice

B.2.3.1. Genomic DNA isolation from mouse ear/tail

A small piece of the ear/tail was cut and dissolved in 700 µL lysis buffer by over night incubation at 56°C under shaking conditions (1,000 rpm). 250 µL of saturated NaCl

(6 M) solution was added to the samples and then centrifuged at 14,000 rpm for 10 min. 750 µL supernatant was transferred, 500 µL isopropanol was added and samples were shaken for 2 min. After centrifugation at 14,000 rpm for 10 min, the DNA pellet was washed twice with ice cold 70% ethanol. The DNA pellet was left to dry and finally resuspended in 50 µL H_2O.

B.2.3.2. PCR-Genotyping

- Mx-Cre

2 µL	DNA Template
5 µL	10x Taq buffer (+KCl, -$MgCl_2$)
5 µL	$MgCl_2$ (25 mM)
2 µL	dNTPs (10 mM)
2 µL	primer forward (1:10 in H_2O, stock: 1 µg/µL)
2 µL	primer reverse (1:10 in H_2O, stock: 1 µg/µL)
0.5 µL	Taq Polymerase (5 u/µL, native, without BSA)
31.5 µL	H_2O
---	
50 µL	

PCR program:

95°C	3 min	
95°C	30 sec	
63°C	30 sec	
-1°C		
R=3.0°C/sec		10x
G=0.0°C		
72°C	30 sec	
95°C	30 sec	
53°C	30 sec	35x
72°C	30 sec	
4°C	∞	

Primer:

MxCre1_for 5´ AAC ATG CTT CAT CGT CGG 3´

MxCre2_rev 5´ TTC GGA TCA TCA GCT ACA CC 3´

Expected band size: 450 bp

- PF4-Cre

2 µL	DNA Template
5 µL	10x Taq buffer (+KCl, -$MgCl_2$)
5 µL	$MgCl_2$ (25 mM)
2 µL	dNTPs (10 mM)
2 µL	primer forward (1:10 in H_2O, stock: 1 µg/µL)
2 µL	primer reverse (1:10 in H_2O, stock: 1 µg/µL)
0.5 µL	Taq Polymerase (5 u/µL, native, without BSA)
31.5 µL	H_2O
---	
50 µL	

PCR program:

96°C	3 min	
94°C	30 sec	} 35x
58°C	30 sec	
72°C	45 sec	
72°C	3 min	

Primer:

PF4-Cre_for: 5´ CCC ATA CAG CAC ACC TT TG 3´

PF4-Cre_rev: 5´ TGC ACA GTC AGC AGG TT 3´

Expected band size: 450 bp

- Adam10

2 µL	DNA Template
2 µL	10x Taq buffer (+KCl, -$MgCl_2$)
1.2 µL	$MgCl_2$ (25 mM)
0.4 µL	dNTPs (10 mM)
0.1 µL	primer loxP_f (stock: 1 µg/µL)

0.1 µL	primer AD10e2_f2 (stock: 1 µg/µL)
0.3 µL	primer A10_3fsc_r (stock: 1 µg/µL)
0.125 µL	Taq Polymerase (5 u/µL, native, without BSA)
13.775 µL	H_2O
---	
20 µL	

PCR program:

96°C	5 min	
94°C	30 sec	35x
51.4°C	30 sec	
72°C	1 min	
72°C	10 min	

Primer:

loxP-f: 5´ CGT ATA ATG TAT GCT ATA CG 3´

A10e2_f2: 5´ CTT CTA GAT TTC CAT GCT CA 3´

A10_3fsc_r: 5´ CTG TAT GTT ACT GAT TAA AT 3´

Expected band size: approx.: wt: 380 bp, floxed: 480 bp; deleted: 100 bp

- Low TACE

2 µL	DNA Template
5 µL	10x Taq buffer (+KCl, -$MgCl_2$)
4 µL	$MgCl_2$ (25 mM)
1 µL	dNTPs (10 mM)
0.5 µL	primer forward (diluted 1:10 in H_2O; stock: 1 µg/µL)
0.5 µL	primer reverse (diluted 1:10 in H_2O; stock: 1 µg/µL)
0.5 µL	Taq Polymerase (5 u/µL, native, without BSA)
36.5 µL	H_2O
---	
50 µL	

PCR program:

95°C	5 min	
95°C	1 min	40x
52°C	1 min	
72°C	1 min	
72°C	5 min	

Primer:

flox_A17_f: 5´ CTT ATT ATT CTC GTG GTC ACC 3`

flox_A17_r: 5´ TAT GTG ATA GGT GTA ATG 3´

Expected band size: wt: 281 bp; ex: 451 bp

- ADF

1 µL	DNA Template
2 µL	10x Taq buffer (+KCl, -$MgCl_2$)
1.2 µL	$MgCl_2$ (25 mM)
0.4 µL	dNTPs (10 mM)
0.5 µL	primer A (diluted 1:10 in H_2O; stock: 1 µg/µL)
1.5 µL	primer B (diluted 1:10 in H_2O; stock: 1 µg/µL)
0.5 µL	primer C (diluted 1:10 in H_2O; stock: 1 µg/µL)
0.125 µL	Taq Polymerase (5 u/µL, native, without BSA)
12.775 µL	H_2O
---	
20 µL	

PCR program:

94°C	2 min	
94°C	30 sec	35x
58°C	30 sec	
68°C	40 sec	
68°C	5 min	

Primer:

Primer A: 5´ GAT TAA GTT GGG TAA CGC C 3`

Primer B: 5´ GAA GAA GGC AAA GAG ATC TT 3´

Primer C: 5´ CTA CCT AAA GGG CAT CCT TTC 3´
Expected band size: wt: 420 bp; ko: 180 bp

- n-cofilin

1 µL	DNA Template
2 µL	10x Taq buffer (+KCl, -$MgCl_2$)
1.2 µL	$MgCl_2$ (25 mM)
0.4 µL	dNTPs (10 mM)
0.5 µL	primer A (diluted 1:10 in H_2O; stock: 1 µg/µL)
1.5 µL	primer B (diluted 1:10 in H_2O; stock: 1 µg/µL)
0.5 µL	primer C (diluted 1:10 in H_2O; stock: 1 µg/µL)
0.125 µL	Taq Polymerase (5 u/µL, native, without BSA)
12.775 µL	H_2O
---	
20 µL	

PCR program:

94°C	2 min	
94°C	30 sec	} 35x
58°C	30 sec	
68°C	40 sec	
68°C	5 min	

Primer:
Primer A: 5´ CGC TGG ACC AGA GCA CGC GGC ATC 3`
Primer B: 5´ CTG GAA GGG TTG TTA CAA CCC TGG 3´
Primer C: 5´ CAT GAA GGT TCG CAA GTC CTC AAC 3´
Expected band size: wt: 380 bp; fl: 420 bp; deleted: 170 bp

B.2.3.3. RT-PCR

Two mice were bled in heparin (20 u/mL) in TBS. Platelets were washed with PBS/EDTA and pellet was resuspended in 200 µL IP buffer with 1% NP-40. Following addition of 800 µL Trizol reagent, the sample was incubated for 60 min at 4°C. After shaking, 200 µL chloroform was added and incubated for 15 min at 4°C. Sample was centrifuged at 10,000 rpm for 10 minutes and upper phase was

incubated with 3x vol of 70% ethanol and with 10% sodium acetate pH 5.2 for one hour at -20°C. After centrifugation at 14,000 rpm for 15 min, the pellet was washed with 70% ethanol, then centrifuged again and pellet was dried. 30 µL of RNase free water was added and concentration was determined.

Generation of cDNA was performed as follows:

Mastermix 1:

1 µg	mRNA
2 µL	Oligo dT (0.5 µg/µL)
x µL	H_2O
total 20 µL	denaturation at 70°C for 10 min, then incubation on ice

Mastermix 2:

4 µL	5x first strand buffer
2 µL	DTT (0.1 M)
1 µL	dNTP (10 mM)
0.1 µL	RNase inhibitor (5 u/µL)

Mix 2 was added to mix 1 and then 1 µL Super Script RT (200 u/µL) was added and sample was incubated at 42°C for 1 hour and inactivated at 70°C for 10 minutes;

A gradient PCR was performed afterwards with Taq polymerase as described. Following this, a PCR with the appropriate annealing temperature was performed.

B.2.4. Animals

B.2.4.1. Genetically modified mice

Mice were either self-generated as described or obtained from the following collaboration groups: *Adf* knock-out and *cofilin*$^{fl/fl}$ mice from W. Witke (Bonn, Germany)[50;51], low TACE mice from S. Rose-John (Kiel, Germany), *PF4-Cre* mice from R. Skoda (Basel, Switzerland)[125] and *Mx-Cre* mice from C. Brakebusch (Copenhagen, Denmark)[126].

B.2.4.2. Bone marrow chimeras

Recipient C57BL/6 mice of an age between 5-6 weeks were lethally irradiated with 10 Gray. Femur and tibia of donator mice were prepared. Bone marrow was flushed with a 22G needle into prewarmed DMEM with 10% FCS and 1% antibiotics. Ten µL of cells was diluted 1:100 and counted in a Neubauer chamber under 10x

magnification. Four million cells diluted in 150 µL DMEM were intravenously injected into one recipient mouse. Animals received 2 g/L neomycin in water for 6 weeks.

B.2.5. Antibodies

B.2.5.1. Monoclonal antibodies (mAbs)

All mAbs (see list below) used for experiments were generated and modified in our laboratory.

antibody	clone	isotype	antigen	described in
JAQ1	98A3	IgG2a	GPVI	82
JAQ2	21G10	IgG2a	GPVI	85
JAQ3	0E3	IgG2a	GPVI	85
DOM1	89F12	IgG2a	GPV	127
DOM2	89H11	IgG2a	GPV	127
WUG 1.9	5C8	IgG1	P-selectin	unpublished
p0p6	56F8	IgG2b	GPIX	127
JON1	6C10	IgG2b	αIIbβ3	127
MWReg30	5D7	IgG1	αIIbβ3	128
JON/A	4H5	IgG2b	αIIbβ3	129
INU1	11E9	IgG1	CLEC-2	130
p0p3	7A9	IgG2a	GPIbα	128
p0p4	15E2	IgG2b	GPIbα	127
p0p/B	57E12	IgG2b	GPIbα	84
p0p1	3G6	IgG1	GPIbβ	128
ULF1	96H10	IgG2a	CD9	127
EDL-1	57B10	IgG2a	β3	127
	12C6		α2	unpublished

Anti-ADF and anti-cofilin 1 antibody were kindly provided by Walter Witke. Anti-tubulin antibody was purchased from Molecular Probes (Invitrogen, Karlsruhe, Germany).

B.2.5.2. Polyclonal antibodies (pAbs)/secondary reagents

Rabbit anti-rat IgG (-FITC, -HRP), streptavidin-HRP and goat anti-rabbit IgG–HRP were purchased from DAKO (Hamburg, Germany). Anti-ADAM10 (Calbiochem, Bad Soden, Germany), Alexa-conjugated secondary antibodies (Molecular Probes, Invitrogen, Karlsruhe, Germany) and anti-actin (Sigma, Deisenhofen, Germany) were purchased.

Alexa-conjugated phalloidin, a high affinity probe for F-actin, was purchased from Molecular Probes (Invitrogen, Karlsruhe, Germany).

B.2.5.3. Biotinylation of antibodies

Antibody (3 mg) was dialyzed against coupling buffer over night at 4°C. After that EZ-link sulfo-NHS-LC-biotin was added to a final concentration of 300 µg/mL for 30 minutes at RT with rotation. Reaction was stopped by addition of 100 µL of 1 M NH_4Cl and the antibody was finally dialyzed against PBS over night at 4°C.

To check the efficacy of the biotinylation, washed platelets were incubated with the biotinylated antibody (2, 5 and 10 µg/mL) for 10 min at RT, then centrifuged (2,800 rpm, 5 min) to remove unbound antibody, and subsequently incubated with FITC-labeled streptavidin (1.5 µg/mL; 10 min, RT). Reaction was stopped by addition of 500 µL PBS, and samples were analyzed immediately by flow cytometric analysis.

B.2.6. Platelet handling

B.2.6.1. Platelet preparation and washing

Mice were bled under isofluran anesthesia from the retroorbital plexus. Blood was collected into a tube contaning 20 u/mL heparin in TBS, pH 7.3 (300 µL). Blood was centrifuged at 800 rpm (Eppendorf 5415*C*) for 5 min. Supernatant was taken and centrifuged at 800 rpm for 6 min at RT to obtain platelet rich plasma (prp). To wash platelets, prp was centrifuged at 2,800 rpm for 5 min in the presence of prostacyclin (PGI_2) (0.1 µg/mL) and apyrase (0.02 u/mL) and the pellet was resuspended in Tyrode's buffer without Ca^{2+} containing PGI_2 (0.1 µg/mL) and apyrase (0.02 u/mL) and left to incubate at 37°C for 5 min. After a second centrifugation step, platelets were resuspended in the same buffer and incubated at 37°C for 5 min. Platelets were finally centrifuged as above, resuspended in Tyrode's buffer with 2 mM Ca^{2+} containing apyrase (0.02 u/mL) and left to incubate for at least 30 min at 37 °C before analysis.

B.2.6.2. Platelet isolation with ficoll

Platelet isolation with ficoll was performed when mice had less than 10% platelet count of control mice. One volume of ficoll containing 3 µL/mL heparin and 0.5 µL/mL PGI_2 (stock: 10^{-3} M) was added to two volumes blood (bled in ACD) and centrifuged at 250 rpm (37°C) for 10 minutes (always with slow stop). Upper layer was incubated with 3 mL Tyrode`s containing 0.1 M $Ca^{2+}$, heparin and $PGI_2$ for 10 min at 37°C and subsequently centrifuged at 2,200 rpm (37°C) for 3 min. The pellet was resuspended twice in Tyrode`s, incubated and centrifuged at 1,900 rpm (37°C) for 2.5 min. Finally, the platelets were resuspended in Tyrode`s with 2 mM Ca^{2+} and left to incubate for 30 min at 37 °C before analysis.

B.2.6.3. Platelet counting

For determination of platelet counts, blood (50 µL) was obtained from the retroorbital plexus of anesthetized mice using siliconized microcapillaries and diluted 1:20 in PBS and analyzed in a Sysmex cell counter.

B.2.6.4. Platelet surface biotinylation

To biotinylate platelet surface molecules, washed platelets (in PBS/EDTA) were resuspended in PBS/EDTA at a concentration of 2 x 10^9 platelets/mL. EZ-link sulfo-NHS-LC-biotin was then added at a final concentration of 25 µg/mL and left to incubate for 10 min at RT with rotation. Reaction was stopped by addition of Tris buffer (final concentration 10 µM). The sample was centrifuged at 2,200 rpm for 5 min. The final platelet pellet was resuspended in Tyrode's buffer with 2 mM Ca^{2+} containing apyrase (0.02 u/mL) and PGI_2 (0.1 µg/mL). To check the efficacy of the biotinylation, a sample (1:20 diluted in PBS; 50 µL) was incubated with FITC-labeled streptavidin (1.5 µg/mL; 10 min, RT), reaction was stopped by the addition of 500 µL PBS and samples were analyzed immediately by flow cytometry.

B.2.6.5. Platelet life span

Five µg (2 µg in mice with less than 10% platelet count) of an anti-GPIX antibody conjugated with Dylight-488 were injected i.v. Percentage of positively labeled platelets were determined in a FACSCalibur at the indicated time points.

B.2.7. Immunoprecipitation and immunoblotting

B.2.7.1. Immunoprecipitation of cleaved surface receptors

For immunoprecipitation, 10 µg/mL antibody was added to biotinylated platelets (2 x 10^9) for 5 min at RT. If necessary, shedding was induced and samples were centrifuged after incubation time at 2,800 rpm for 5 min. Pellet was immediately prepared for immunoblotting and supernatant was treated with 25 µL G-sepharose (washed 3x in IP buffer). Samples were left to incubate over night at 4°C with rotation. Samples were then washed once with IP buffer containing 1% NP-40 and twice with IP buffer (14,000 rpm, 1 min).

B.2.7.2. Immunoblotting

For Western blot analysis, platelets were washed 2x in PBS/EDTA and finally solubilized in 80 µL IP buffer containing 1% NP-40. Samples were separated by 10, 12 or 15% SDS-PAGE and transferred onto a polyvinylidene difluoride membrane. To prevent non-specific antibody binding, the membrane was incubated in 10% fat-free milk (dissolved in washing buffer) for 1 h at RT. After that, the membrane was incubated with the required antibody (5 µg/mL) for 1 h at RT. For washing, the membrane was incubated 3x with washing buffer for 10 min at RT. After washing steps, HRP-labeled secondary reagent was added and left to incubate for 1 h at RT. After several washing steps, proteins were visualized by ECL.

B.2.8. *In vitro* analysis of platelet function

B.2.8.1. Flow cytometry

Platelets (1 x 10^6) were activated with the indicated agonists or reagents and stained for 15 min with saturating amounts of fluorophore-conjugated antibodies. Reaction was stopped by addition of 500 µL PBS, and sample was immediately analyzed on a FACSCalibur (Becton Dickinson).

B.2.8.2. Aggregometry

To determine platelet aggregation, light transmission was measured using washed platelets adjusted to a platelet concentration of 3 x 10^8 platelets/mL with Tyrode's buffer without calcium. Alternatively, heparinized prp was used for measurements with ADP. Agonists or reagents were added as 100-fold concentrates and light transmission was recorded over 10 min on an Apact 4-channel optical aggregation

system. Before starting the measurements, Tyrode's buffer (for washed platelets) or plasma (for prp) was set as 100% aggregation and washed platelet suspension (for washed platelets) or prp (for prp) was set as 0% aggregation. For activation with thrombin, platelets were diluted in Tyrode`s with 2 mM $Ca^{2+}$, for other agonists platelets were diluted in Tyrode`s with 2 mM Ca^{2+} and 70 µg/ml fibrinogen.

B.2.8.3. Induction of shedding of platelet receptors

Washed platelets resuspended at a concentration of ~1.5 x 10^9 platelets/mL in Tyrode's buffer containing calcium and apyrase (0.02 u/mL) were treated for 1 h (CCCP, W7) or 20 min (NEM, PMA) at 37°C with the indicated agents and immediately analyzed on a FACSCalibur. Alternatively, samples were preincubated with the indicated inhibitors for 30 minutes at 37°C.

B.2.8.4. GPVI shedding ELISA assay

Washed platelets with PBS/EDTA were resuspended in Tyrode's buffer without Ca^{2+} containing PGI_2 (0.1 µg/mL) and apyrase (0.02 u/mL). After incubation for 5 min at 37°C, biotinylated JAQ1 anitbody (10 µg/mL) was added and incubated for 5 min at RT. Then, volume was expanded to 1 mL and centrifuged (2,800 rpm, 5 min). Platelets were resuspended in Tyrode's buffer containing calcium and apyrase (0.02 u/mL). To induce GPVI shedding, the cells were then treated with CCCP (100 µM) or W7 (150 µM) for 1 h or with NEM (2 mM) for 20 min at 37°C. Platelets were centrifuged (2,800 rpm, 5 min) and supernatants were incubated on JAQ3-coated (10 µg/mL) ELISA plates for 1 h at 37°C. After extensive washing, plates were incubated with HRP-labeled streptavidin for 45 min at 37°C and after extensive washing, developed using 3,3,5,5-tetramethylbenzidine (TMB). The reaction was stopped by addition of 2 N H_2SO_4 and absorbance at 450 nm was recorded on a Multiskan (Thermo Scientific).

B.2.8.5. Adhesion under flow conditions

Blood was collected in 300 µL 20 u/mL heparin and finally diluted as follows: 2:1 in Tyrode`s buffer containing Ca^{2+}. Coverslips (24 x 60 mm) were coated with fibrillar (Horm) collagen (0.2 mg/mL, Nycomed, Munich, Germany) over night at 37°C and finally blocked for 1 h with 1% bovine serum albumin. Perfusion studies were performed as follows. Transparent flow chambers with a slit depth of 50 µm,

equipped with the coated coverslips, were connected to a syringe filled with the anti-coagulated blood. Perfusion was performed using a pulse-free pump under high shear stress equivalent to a wall shear rate of 1,000 s^{-1} (4 min). Thereafter, chambers were rinsed with Tyrode`s buffer at the same shear stress and phase-contrast images were recorded from at least five different microscope fields (40x objectives). Analysis was performed using MetaVue ® software.

B.2.8.6. Platelet spreading on fibrinogen

Thrombin (0.001 u/mL) was added to washed platelets and 60 µL platelets (300,000 plts/µL in Tyrode`s containing calcium) were immediately allowed to spread on a fibrinogen-coated (1 mg/mL, 1 hour at 37°C, blocked with 1% BSA for 1 hour at RT) rectangular coverslip (24 x 60 mm). Platelet spreading was monitored under 100x magnification with taken pictures every 5 seconds for 20 min. For statistical analysis, bound platelets were fixed with 4% PFA in Tyrode´s buffer at the indicated time points and counted. Alternatively, for analysis with STED (stimulated emission depletion microscopy) microscopy (Leica SP5), spread platelets on fibrinogen were stained with phalloidin-Atto 647.

B.2.8.7. F-actin assembly

150,000-200,000/µL of washed platelets were diluted 1:10 in Tyrode`s buffer containing calcium and were subsequently incubated with 10 µL anti-GPIX DyLight649 antibody for a sample of a volume of 100 µL for 3 minutes at 37°C and 400 rpm. Subsequently, the platelets were not stimulated or stimulated with 1 u/mL thrombin for 2 min at 37°C and 400 rpm. The platelets were fixed with 0.55 volume of 10% paraformaldehyde for 10 min at 37°C and 400 rpm and then centrifuged. The pellet was resuspended in 55 µL Tyrode`s containing calcium with 0.1 volume 1% Triton X-100. After this, the platelets were stained with 10 µM phalloidin-FITC for 30 min at RT, stopped with PBS, centrifuged at 2,800 rpm for 5 min, resuspended in 500 µL PBS and analyzed on a FACSCalibur from Becton Dickinson. Resting values were set to 1.

B.2.9. *In vivo* experiments

B.2.9.1. Measurement of cleaved GPVI in plasma

Isofluran anaesthetized mice were injected intravenously with biotinylated JAQ1 (100 µg) and blood (100 µL in 100 µL heparin) was collected. Blood was centrifuged at 2,800 rpm for 5 min and supernatant again at 14,000 rpm for 5 min. Plasma was collected and incubated on JAQ3-coated ELISA plates. ELISA was performed as described in B.2.8.4.

B.2.9.2. Measurement of cleaved GPIb and GPV in plasma

100 µL blood was collected in 100 µL 20 u/mL heparin in TBS and centrifuged at 2,800 rpm for 5 minutes and plasma was used for ELISA. Plates were coated with 30 µg/mL 7A9 (GPIb) or 89H11 (GPV) over night at 4°C and subsequently blocked with 5% BSA for 2 hours at 37°C. Plasma was added to the plates and diluted in log2 dilutions in 1% BSA in PBS for 1 hour at 37°C. After 3x washing, plates were incubated with 15E2-HRP (GPIb) 1:500 or 89F12-HRP (GPV) 1:1,000 for 1 hour at 37°C. After 3x washing, samples were developed using 3,3,5,5-tetramethylbenzidine (TMB). The reaction was stopped by addition of 2 N H_2SO_4 and absorbance at 450 nm was recorded on a Multiskan.

B.2.9.3. Measurement of thrombopoietin level in plasma

Experiment, preparations and dilutions were performed according to the manufacturer´s protocol (R&D Systems, Minneapolis, USA). Briefly, 50 µL assay diluent was added to each well and then either 50 µL of standard, control or mouse plasma was added and incubated for 2 hours. Each step was performed at RT. After 5x washing with wash buffer, 100 µL TPO conjugated was added for 2 hours. After washing, 100 µL substrate solution was added for 30 minutes under light protection and reaction was stopped with 100 µL stop solution. The absorbance was measured at 450 nm on a Multiskan.

B.2.9.4. Intravital microscopy of thrombus formation in $FeCl_3$-injured mesenteric arterioles

Mice of a weight between 15 - 18 g were anesthetized with 2.5% avertin and the mesentery was exteriorized through a midline abdominal incision. 35 – 60 µm diameter arterioles were visualized at 10x with an inverted microscope (Axiovert 200;

Carl Zeiss, Inc.) equipped with a 100-W HBO fluorescent lamp source and a camera (CoolSNAP-EZ; Visitron). Injury was induced by topical application of a 3-mm^2 filter paper saturated with 20% $FeCl_3$. Thrombus formation of fluorescently labeled platelets (DyLight 488–conjugated anti-GPIX Ig derivative) in arterioles was monitored for 40 min or until complete occlusion occurred (blood flow stopped for >1 min).

B.2.9.5. Aorta occlusion model

A longitudinal incision was performed to open the abdominal cavity of anesthetized mice and expose the abdominal aorta. An ultrasonic flow probe was placed around the vessel, and thrombosis was induced by a single firm compression with a forceps. Blood flow was monitored until complete occlusion occurred or 30 min had elapsed.

B.2.10. Bleeding time experiments

Mice were anesthetized by intraperitoneal injection of the substances dormitor, dormicum and fentanyl, and a 1 mm segment of the tail tip was cut off with a scalpel. Tail bleeding was monitored by gently absorbing the drop of blood with a filter paper without contacting the wound site. When no blood was observed on the paper after 20 second intervals, bleeding was determined to have ceased. The experiment was manually stopped after 20 minutes.

B.2.11. Electron microscopy of platelets

B.2.11.1. Sample preparation for transmission electron microscopy (TEM)

Fixed platelets (300,000/µL) with 2.5% glutaraldehyde (GA) were washed 3x with cacodylate buffer and centrifuged at 1,500x *g* for 5 min. Then, 1 mL 2% agarose (45°C) was added to the platelets and centrifuged at high speed for 5 min. The supernatant except 100 µL was discarded. After 10 min, the platelet pellet in agarose was cut into small pieces and transferred in cacodylate buffer. The pieces were incubated with 1% osmium for 1 hour at RT and then washed 2x with cacodylate buffer and 2x with H_2O. Then 2% uranyl acetate was added for 1 hour at 4°C. The samples were washed 3x with H_2O and dehydrated with ethanol (70% 4 x 5´, 95% 3 x 15´, 100% 3 x 15´). Next, samples were incubated with propylenoxide 2 x 10´ at RT and propylenoxide and epon in the ratio 1:1 for 1 hour at RT under rotation. Following this, epon was added over night at RT under rotation and next day again for 2 hours.

The samples were embedded in gelatine tubes filled with epon and incubated at 60°C for 48 hours. Then the sample preparation was finshed and could be used for cutting and analysis.

B.2.11.2. Sample preparation for scanning electron microscopy (SEM)

Fixed resting platelets (1,000x *g* for 5´, washed once in cacodylate buffer) were allowed to adhere for 20 minutes at RT on coverslips coated with 0.01% Poly-Lysin (coating for 10 minutes and then left to dry over night at RT or 2 hours at 60°C).
For the spreading of platelets, coverslips were coated with 100 µg/mL fibrinogen for 2 h at RT and blocked with 1% BSA. Platelets (30,000/µL) were preactivated with 0.1 u/mL thrombin and applied to the cover slip. The samples were stopped after the indicated time points with 2.5% GA for 1 hour at 37°C. Samples were washed once with cacodylate buffer and treated as follows:

ethanol:	70%	4x5´
	80%	1x5´
	95%	1x5´
	100%	2x30´

hexamethyldisilazan (HMDS) diluted in 100% ethanol:

25%	1x5´
50%	1x5´
75%	1x5´
100%	2x5´

Then, samples were fixed on specimen mount stubs and left to dry at RT. Following this, samples were coated with gold/palladium in a Sputter Coater and analyzed.
Alternatively for analysis of the cytoskeleton, spread platelets were treated with cytoskeleton buffer for 2 minutes and then fixed with 2% PFA in PHEM buffer. The samples were washed 3x in PHEM, 1x in H_2O and treated with 0.2% tannic acid for 30 min. After extensive washing with H_2O, samples were incubated with 0.5% OsO_4 for 5 min and washed 3x with H_2O. Then, dehydration was performed with ethanol (70% 4 x 5´, 80% 1 x 5´, 95% 1 x 5´ and 100% 2 x 30´) and then treated as described above with HMDS and sputtered.

B.2.12. Staining of histological sections

B.2.12.1. Paraffin sections

Spleen or bone marrow (femur at least 6 weeks in decalcification buffer) was cut after embedding in paraffin into 5 µm thin sections. Deparaffination was performed with xylol (2 x 3´) and then rehydrated with ethanol (100%, 96%, 90%, 80% and 70% each 2 min) and H_2O. Samples were stained with hematoxylin for 30 sec and after running under tab water for several minutes with 0.05% eosin for 3 min. Dehydration was performed in reversed order. The samples were mounted with a Xylol-based medium (Eukitt).

B.2.12.2. Cryo sections

Spleen was frozen in liquid nitrogen and cut into 5 µm thin sections. The samples were fixed in cold acetone for 20 min and washed in PBS. Peroxidase inhibition was done with 0.03% H_2O_2 at RT for 20 min. After washing in PBS, samples were blocked with 1% BSA in 0.3% rat serum for 60 min. Anti-GPIb (15E2/3G6) antibody conjugated with HRP (1:500) was added for 2 hours and then removed by washing with PBS. Then, samples were treated with AEC solution for approximately 30 min and then counterstained with hematoxylin for 30 sec. The samples were mounted with aquatex.

B.2.13. Analysis of megakaryocytes

B.2.13.1. *In vitro* differentiation of megakaryocytes

Fetal liver cells of embryos at day 13.5-14.5 were prepared and homogenized with a syringe and using 18G and 22G needles. The cells were centrifuged once with MK medium and cultured with MK medium containing 50 ng/mL thrombopoietin (TPO) in a 12 well plate at 37°C and 5% CO_2. On day 3, megakaryocytes were enriched by gradient density filtration with 1.5 and 3% BSA. Therefore, collected cells were gently overlayed on the prewarmed BSA gradient and incubated for 45 minutes at RT. The lowest phase of 500 µL contained the cells with the biggest size. These cells were centrifuged again and cultured with MK medium containing 50 ng/mL thrombopoietin (TPO) in a 12 well plate for one day at 37°C and 5% CO_2. On day 4, megakaryocytes were analyzed and counted for proplatelet formation under a light microscope. Visual fields containing at least 10 differentiated megakaryocytes without contact inhibition were counted for proplatelet formation.

B.2.13.2. Staining of *in vitro* differentiated megakaryocytes

For analysis under a confocal microscope, 250 µL of the cultured cells were centrifuged on an object slide at 800 rpm for 6 minutes, fixed in 4% paraformaldehyde, 0.05% GA and 0.05% triton-X for 12 minutes at RT. After 3x washing with 1x PHEM, samples were incubated with 0.1% $NaBH_4$ in PHEM 2x for 10 min. Cells were washed 3x in PBS and permeabilized with 0.5% triton-X in PBS and washed again. Then the samples were blocked with 3% BSA for 2 hours and stained with the indicated antibodies for 1 hour. Staining with DAPI was performed for 5 minutes. The samples were mounted with Prolong Antifade.

B.2.13.3. Determination of ploidy from bone marrow megakaryocytes

Femur from one mouse was flushed with CATCH buffer. 1/10 of the suspension was centrifuged at 1,200 rpm for 5 min and resuspended in 400 µL 1:1 mixture CATCH/PBS with 5% FCS. Unspecific binding sites were saturated with an anti-FcγR antibody (1/50 dilution; 2.4G2 antibody) for 15 min on ice and then stained either for control with an anti-rat IgG1-FITC antibody (1/5 dilution) or with an anti-GPIIb antibody (1/5 dilution; 5D7-FITC) for 20 minutes on ice. Finally, 1 mL CATCH/PBS with 5% FCS buffer was added, the sample centrifuged and after resuspension in 250 µL PBS/0.1% EDTA fixed with additional 250 µL PBS/1% PFA for 10 min on ice. Washing was performed with addition of 3 mL PBS and after centrifugation, permeabilization was done by resuspending the pellet in 500 µL PBS/0.1% Tween for 10 min on ice. After washing, samples were stained with 500 µL propidium iodide staining solution over night at 4°C and analyzed in a flow cytometer.

B.2.13.4. TEM analysis of bone marrow megakaryocytes

For transmission electron microscopy the femura of mice were cut with scissors in pieces, and then fixed for 3 hours or over night at 4°C with 0.1 M sodium cacodylate (pH 7.2) containing 2.5% glutaraldehyde and 2% formaldehyde. The bone was removed with forceps. The remaining bone marrow was washed with 50 mM sodium cacodylate (pH 7.2) and subsequently fixed for 2 hours at 4°C with 2% osmium tetroxide in 50 mM sodium cacodylate (pH 7.2). Samples washed with distilled water were stained over night with 0.5% aqueous uranyl acetate, dehydrated with ethanol and embedded in Epon 812. Ultrathin sections were stained with 2% uranyl acetate (in 100% ethanol) followed by lead citrate.

For immunolocalization pieces of femur containing bone marrow were fixed for 3 hours or over night at 4°C with PBS containing 4% formaldehyde. The bone marrow was then processed for embedding in LR-White resin exactly as described[131]. Ultrathin LR-White sections were incubated with actin antibody (1:20 dilution) followed by the incubation with a secondary antibody conjugated to 12 nm colloidal gold. LR-White sections were incubated with antibodies, washed and finally stained with uranyl acetate and lead citrate as described[131]. Sections were inspected with an EM900 electron microscope (Zeiss, Oberkochen, Germany). Negatives were digitalized by scanning and processed with Adobe Photoshop.

B.2.13.5. Analysis of bone marrow explants

Bone marrow was obtained by flushing femora with Tyrode's buffer. The bone marrow was cut in transverse sections of 0.5 mm and placed in an incubation chamber containing Tyrode's buffer supplemented with 5% mouse serum. Each chamber contained 12 fragments and was maintained at 37°C for 6 h. Megakaryocytes at the periphery of the tissue were observed under a phase contrast microscope (63x objective) coupled to a video camera. Images were acquired sequentially at 5 second intervals and processed with Metamorph software. Cells were classified according to their morphology.

B.2.14. Data analysis

The results shown are mean ± S.D. Statistical analysis was performed using Mann-Whitney-U-test with $P < 0.05$ taken as the level of significance (*) and $P < 0.001$ taken as the level of highly significance (***).

C. Results

C.1. ADF/cofilin-dependent actin turnover is essential for platelet formation

Adf$^{-/-}$ mice are viable, whereas mice lacking n-cofilin die during embryonic development[50;51]. To study n-cofilin (further on referred to as cofilin) function in megakaryocytes and platelets, mice carrying a floxed (loxP sites) *n-cofilin* gene were crossed with mice expressing Cre recombinase under the control of the megakaryocyte-specific platelet factor 4 (PF4) promoter (*cofilin*$^{fl/fl}$, *PF4-Cre*)[125]. Western blot analysis confirmed that both ADF and cofilin were strongly expressed in wild-type platelets (Fig. 11). The absence of the proteins in platelets from the respective knock-out mice was confirmed demonstrating that the recombination of the loxP sites mediated by the Cre recombinase under the PF4 promoter efficiently abrogated cofilin expression. Possible mutual up-regulation of one isoform in response to the loss of the other was not obvious, indicating that compensatory mechanisms were not active in the mutant megakaryocytes/platelets.

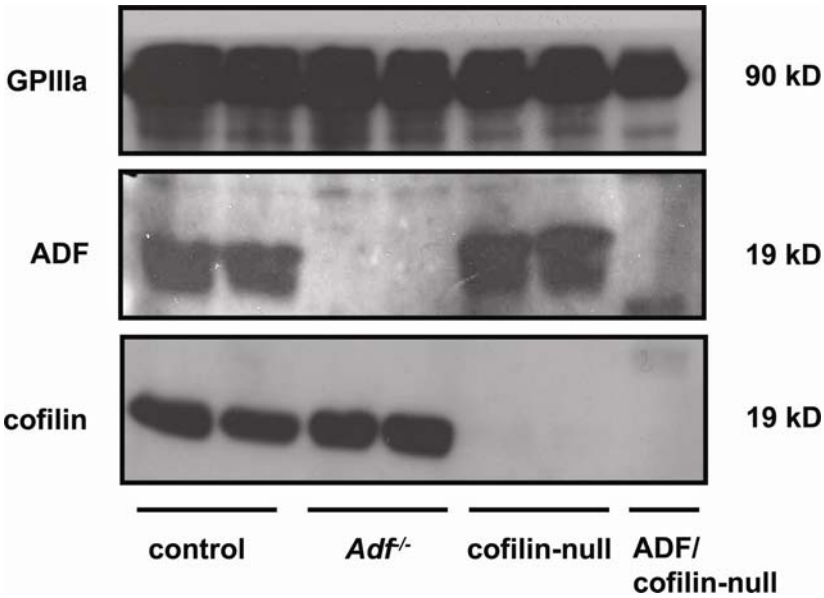

Fig. 11: Whole platelet proteins were separated by SDS-PAGE under reducing conditions and immunoblotted with anti-ADF (1:500), anti-cofilin (1:500) or anti-GPIIIa (1:1,000) antibodies.

C.1.1. Analysis of ADF-null and cofilin-null platelets

To study consequences of the lack of ADF or cofilin in platelet function and physiology, peripheral platelet counts and platelet size were determined. Mice constitutively lacking ADF had normal platelet counts (Fig. 12A) and size (not shown, see also Fig. 12C). In contrast, mice lacking cofilin displayed moderately reduced platelet counts varying from approximately 60 to 80% of control (Fig. 12A).

Remarkably, however, the size of these platelets was markedly increased compared to the control as revealed by determination of the forward scatter signal in flow cytometry (Fig. 12B) and transmission electron microscopy (Fig. 12C). In contrast to wild-type and *Adf*$^{-/-}$ platelets which appeared normal in size and displayed a discoid shape, platelets from cofilin-deficient mice were giant and displayed an ovoid shape.

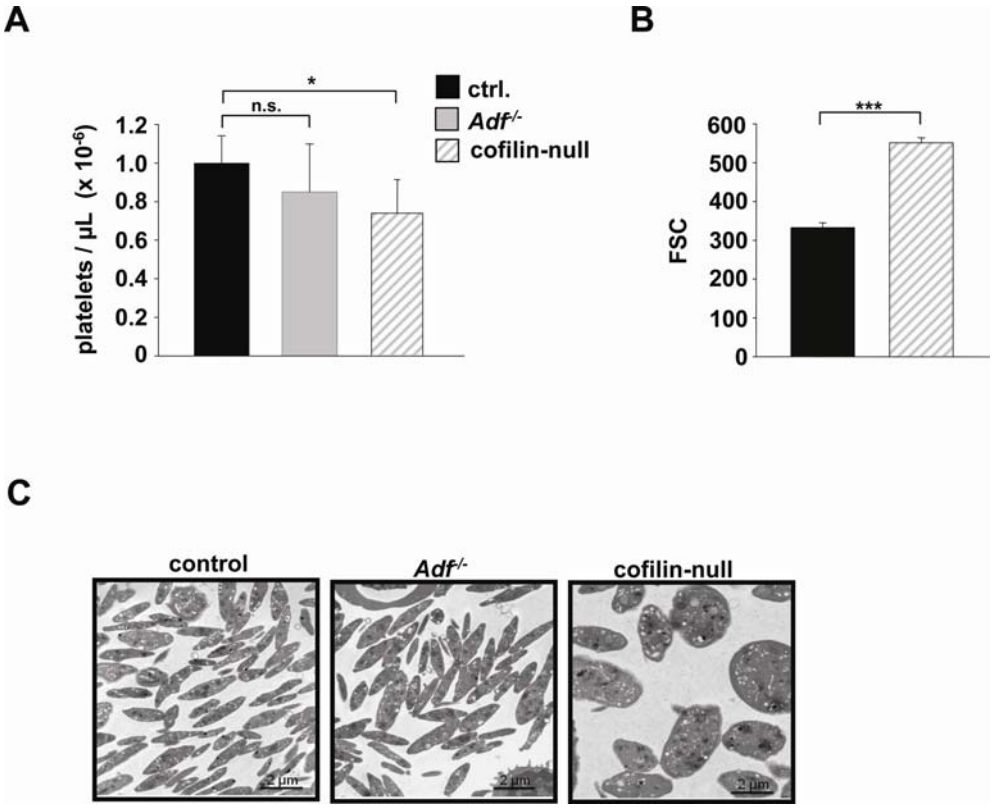

Fig. 12: Determination of platelet count, size and shape of single knock-out platelets.
Platelet count **(A)** and size **(B)** were determined by flow cytometry. Results are mean ± SD (*n* = 6 mice per group). *, $P < 0.05$; ***, $P < 0.001$. **(C)** Transmission electron microscopy analysis of resting platelets under 6,500x magnification.

Further analysis of *Adf* knock-out mice revealed no obvious phenotype. Briefly, *Adf* $^{-/-}$ platelets displayed normal expression of prominent platelet receptors (Fig. 13A), overall unaltered agonist-induced integrin activation and P-selectin exposure, a marker for α-granule release (Fig. 13B and C), and platelet aggregation (Fig. 13D) upon activation with all tested agonists and different concentrations (not shown).

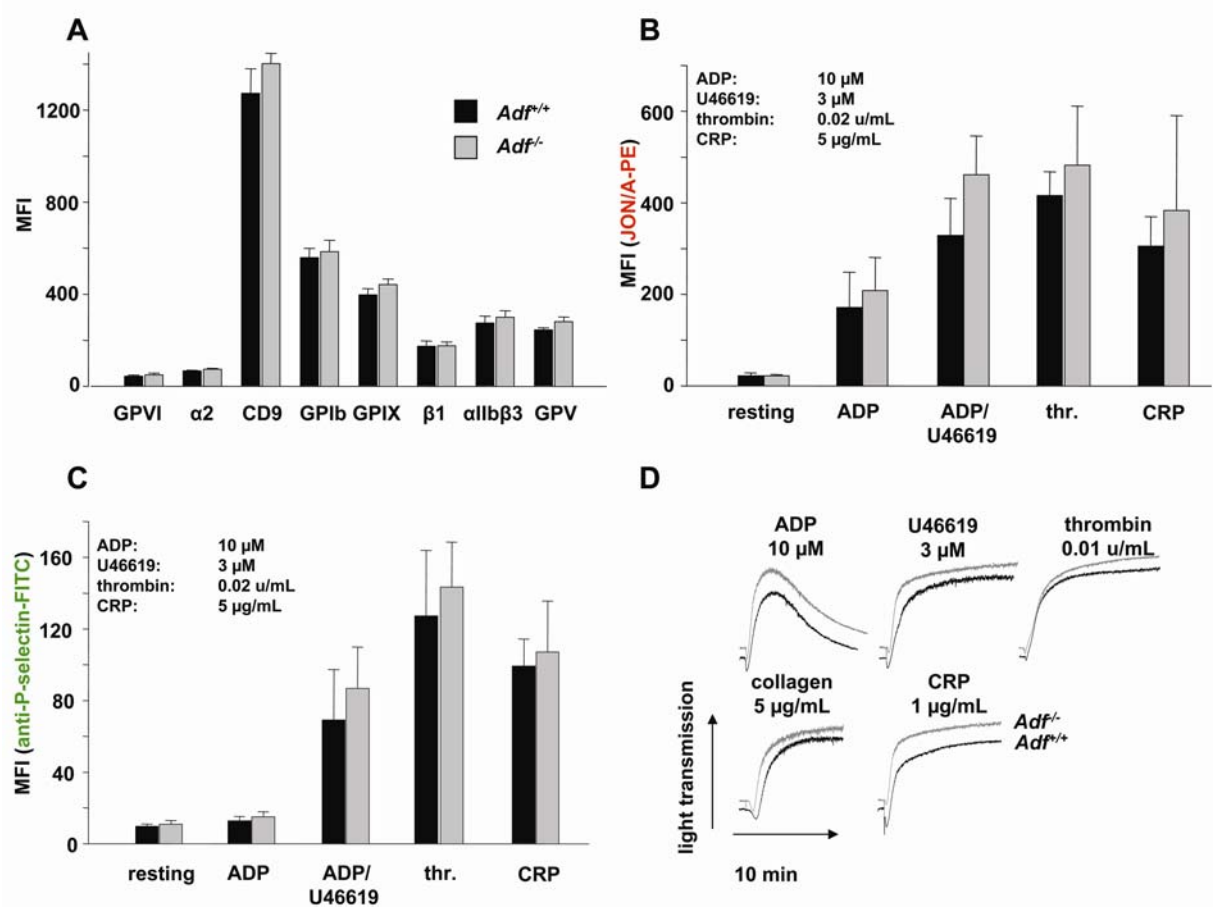

Fig. 13: Unaltered protein expression, platelet activation and aggregation of *Adf*$^{-/-}$ platelets.
(A) Flow cytometric analysis of glycoprotein expression. Platelets were stained with the indicated fluorophore-labeled antibodies for 15 minutes and directly analyzed. Results are mean ± SD (*n* = 6 mice per group). **(B+C)** Flow cytometric analysis of integrin αIIbβ3 activation (binding of JON/A-PE) and degranulation-dependent P-selectin exposure. Washed blood was incubated with the indicated agonists for 15 minutes and analyzed on a FACSCalibur. Results are mean ± SD (*n* = 6 mice per group). **(D)** Aggregation of *Adf*$^{-/-}$ platelets (gray lines) in response to indicated agonists (recording time = 10 min).

Next, hemostatic function of *Adf*$^{-/-}$ mice was tested in a tail bleeding assay. For this, 1 mm of the tail tip was cut with a scalpel and bleeding was determined as ceased when no blood drop was observed on a Whatman filter paper. *Adf* knock-out mice arrest bleeding within a similar time frame as control mice (Fig. 14A). ADF-deficient platelets were able to adhere and form thrombi in the *ex vivo* flow chamber system, in which anti-coagulated whole blood was perfused over a collagen-coated surface (Fig. 14B). Similarly, they formed normal thrombi in a $FeCl_3$-induced arterial thrombosis model *in vivo* (Fig. 14C) where injury is induced by applying a drop of 20% $FeCl_3$ on a mesenteric arteriole. Taken together, this demonstrates that ADF is dispensable for platelet production and function in mice.

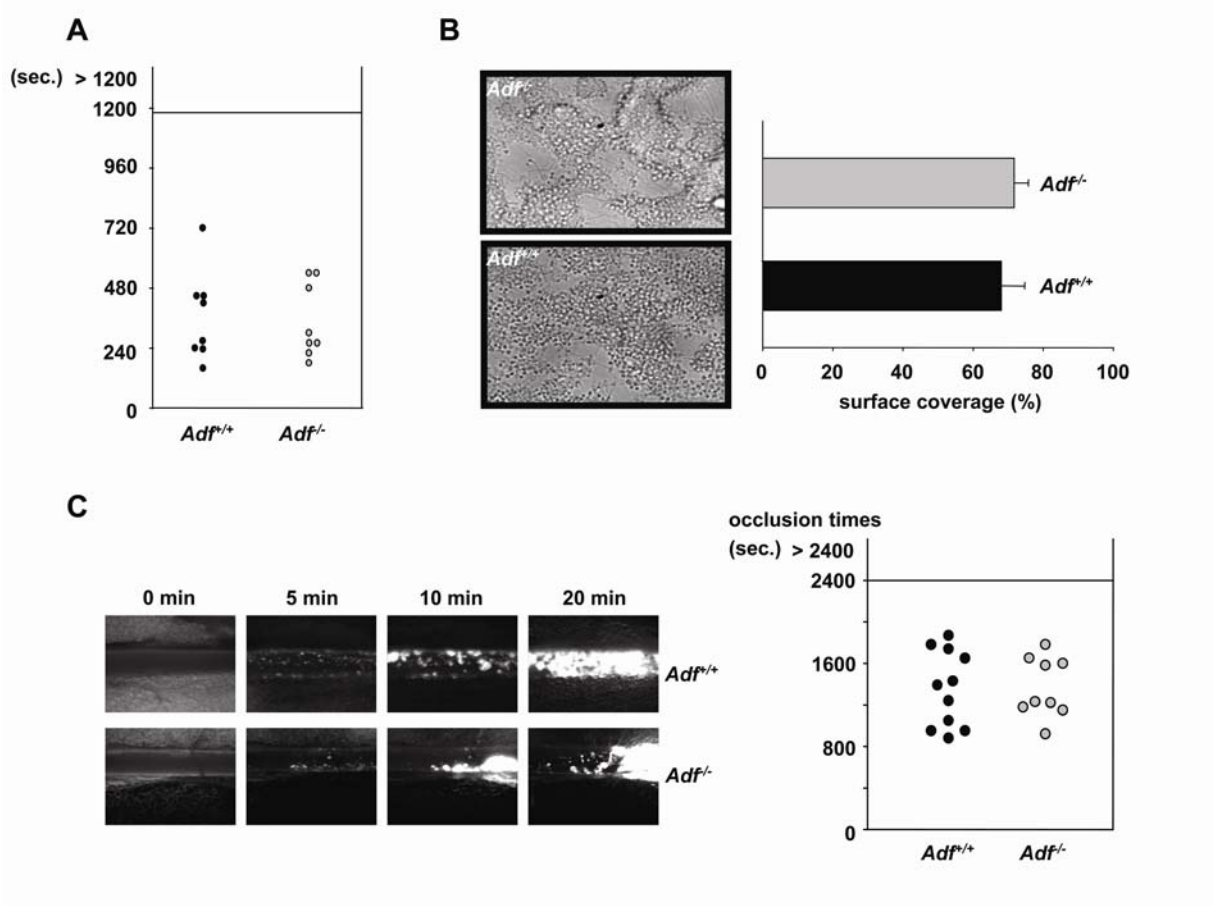

Fig. 14: Unaltered hemostatic function and thrombus formation in ADF-deficient mice.
(A) 1 mm of the tail tip was cut with a scalpel and bleeding was determined to have ceased when no blood drop was observed on a filter paper. **(B)** Whole blood in buffer (Tyrode´s with calcium) was perfused over 0.2 mg/mL collagen in a flow chamber with a shear rate of 1,000 s^{-1}. Representative pictures were taken (63x magnification). Mean surface coverage was measured with Metamorph. *n* = 8 mice **(C)** Mesenteric arterioles were treated with 20% $FeCl_3$, adhesion and thrombus formation of fluorescently labeled platelets were monitored by *in vivo* video microscopy. Representative images and statistical evaluation of time to occlusion are shown.

Due to their increased size, cofilin-deficient platelets showed increased levels of prominent surface receptors (Table 1). This finding again indicated that cofilin is of major importance in the regulation of platelet size.

The ultrastructure of cofilin-deficient giant platelets was not disordered, but according to their increased platelet size they contained more granules than control platelets. In line with this, these platelets exposed higher levels of α-granule-derived P-selectin in response to strong agonists, such as thrombin or collagen related peptide (CRP) as compared to control (Fig. 15A). Agonist-induced inside-out activation of αIIbβ3 was not affected (Fig. 15B). Cofilin-null platelets were also able to form aggregates after stimulation with various agonists (Fig. 15C) at different concentrations (not shown).

	control	cofilin-null
GPIb	387 ± 25	556 ± 69
GPIX	483 ± 10	621 ± 49
GPV	397 ± 7	471 ± 39
CD9	1461 ± 24	1612 ± 92
GPVI	59 ± 5	66 ± 7
α2	91 ± 3	118 ± 9
β1	181 ± 11	201 ± 12
αIIbβ3	296 ± 8	316 ± 24

Table 1: Flow cytometric analysis of surface protein expression. Platelets were stained with the indicated fluorophore-labeled antibodies for 15 minutes and directly analyzed. Results are mean ± SD (*n* = 6 mice per group).

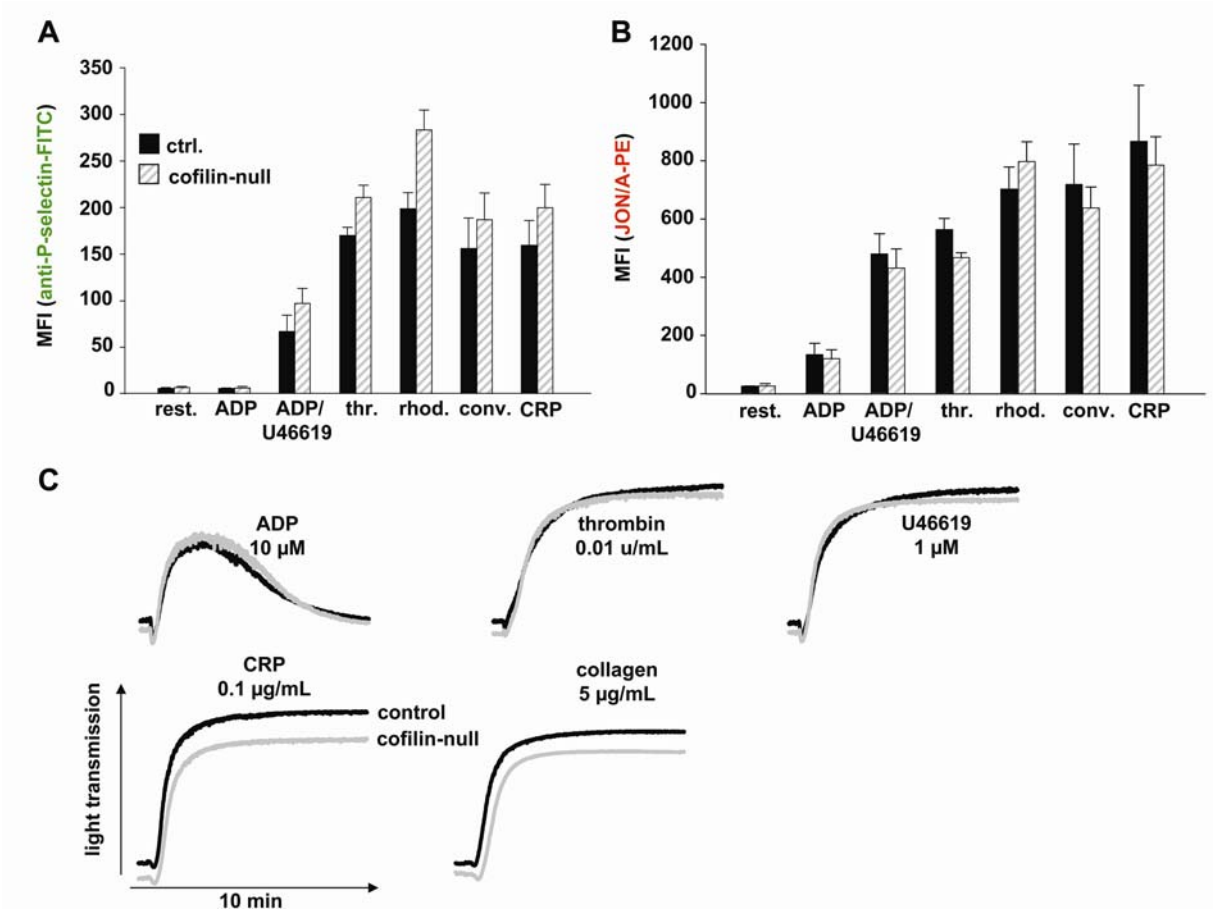

Fig. 15: Unaltered platelet activation and aggregation of cofilin-null platelets.
Flow cytometric analysis of degranulation-dependent P-selectin exposure **(A)** and integrin αIIbβ3 activation **(B)**. Washed blood was incubated with the indicated agonists for 15 minutes and analyzed on a FACSCalibur. Results are mean ± SD (*n* = 6 mice per group). **(C)** Aggregation of cofilin-null platelets (gray lines) in response to indicated agonists (recording time = 10 min). Agonists were added after 30 seconds.

Cofilin-null mice also displayed normal bleeding times (Fig. 16A) and normal thrombus formation in the *ex vivo* flow chamber system (Fig. 16B) and in the *in vivo* $FeCl_3$-induced arterial thrombosis model (Fig. 16C). This suggests that cofilin is not essential to arrest bleeding or to form stable thrombi.

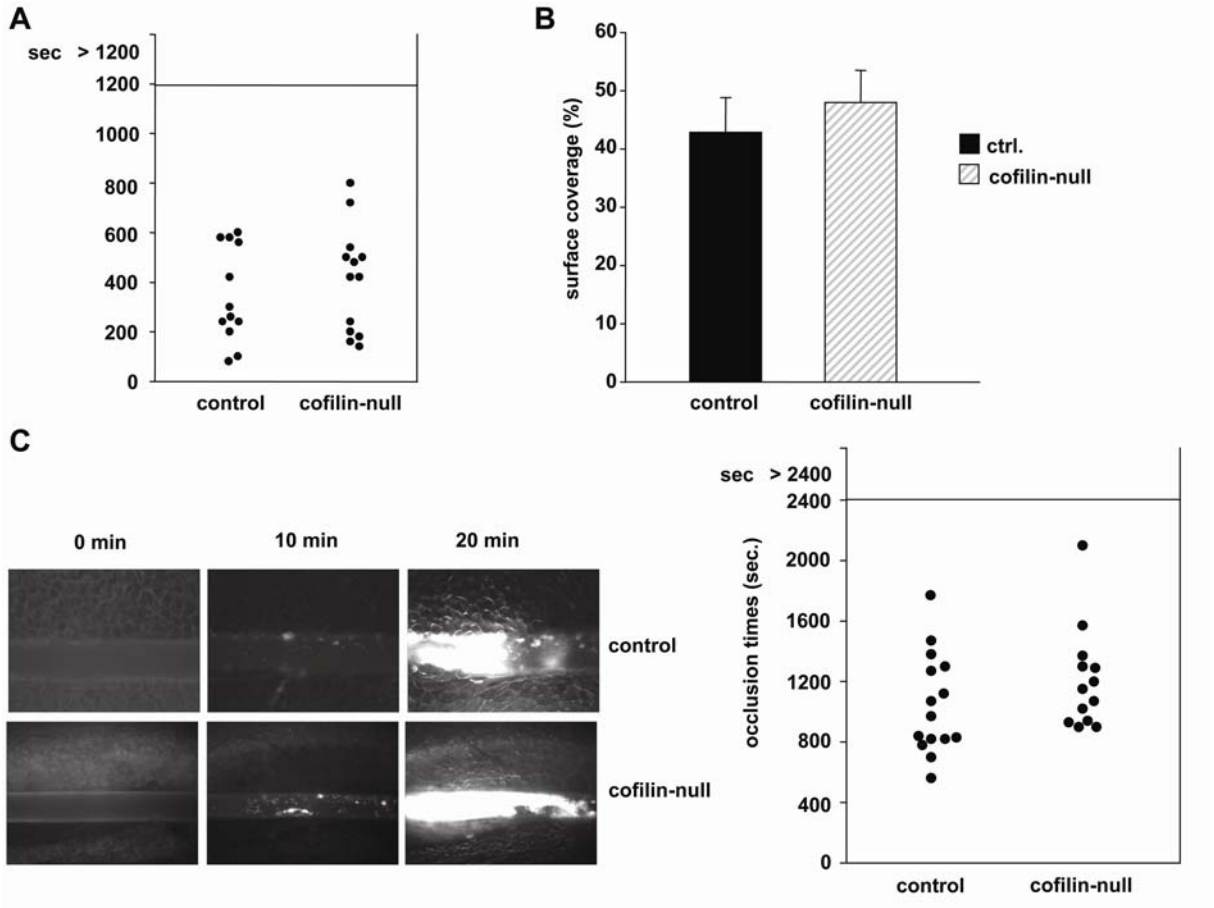

Fig. 16: Unaltered hemostatic function and thrombus formation in cofilin-null mice.
(A) 1 mm of the tail tip was cut with a scalpel and bleeding was determined as ceased when no blood drop was observed on a whatman paper. **(B)** Whole blood in buffer (Tyrode´s with calcium) was perfused over 0.2 mg/mL collagen in a flow chamber at a shear rate of 1,000 s^{-1}. Mean surface coverage was measured with Metamorph. *n* = 8 mice **(C)** Mesenteric arterioles were treated with 20% $FeCl_3$, adhesion and thrombus formation of fluorescently labeled platelets was monitored by *in vivo* video microscopy. Representative images and statistical evaluation of time to occlusion are shown.

To test the possibility that the increased platelet size and altered shape of cofilin-deficient platelets resulted from an increased turnover of the platelets, their *in vivo* life span was determined. Therefore, a fluorescently labeled non-cytotoxic platelet-specific antibody was intravenously injected into mice and the percentage of fluorescently labeled platelets was determined over time[132]. No differences were found in the turnover between wild-type, *Adf*$^{-/-}$ and cofilin-deficient mice with

continuous loss of the fluorescent platelet population over approximately 5 days (Fig. 17). These data suggested that the lack of cofilin directly affected the production of correctly sized and shaped platelets rather than indirectly by increasing platelet production due to a reduced platelet life span.

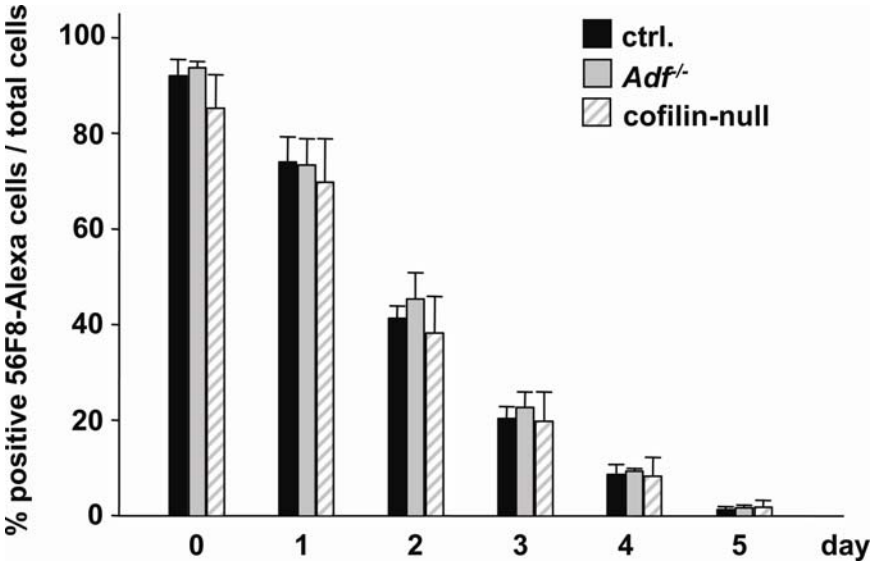

Fig. 17: Normal platelet life span of ADF- and cofilin-deficient platelets.
Anti-GPIX antibody was injected i.v. Percentage of positively-labeled platelets were determined in a FACSCalibur at the indicated time points.

Platelets are able to change their shape and spread on adhesive surfaces such as immobilized fibrinogen. This is a highly dynamic process that requires rapid reorganization of the actin cytoskeleton enabling filopodia and subsequent lamellipodia formation. To test a role of ADF or cofilin in this process, wild-type and mutant platelets were allowed to spread on immobilized fibrinogen for 60 min and analyzed at different time points (Fig. 18A). *Adf*$^{-/-}$ platelets were able to spread with the same kinetics as wild-type platelets with >90% of the cells having formed lamellipodia after 20 minutes. In contrast, while the adherence of cofilin-null platelets to the fibrinogen surface was normal, filopodia and subsequent lamellipodia formation were profoundly delayed. After 20 minutes, only approximately 40% of the cells had started lamellipodia formation. However, all cofilin-null platelets were principally able to form lamellipodia as shown after 60 minutes. This was also confirmed by electron and STED microscopy which revealed normal reorganization of the cytoskeleton in spread cofilin-deficient platelets at that time point (Fig. 18B+C). These results indicated that cofilin can functionally compensate the loss of ADF in

platelets and cofilin-mediated accelerated platelet actin dynamics are important in outside-in signaling through integrins but as shown before dispensable for initial agonist-induced activation[44].

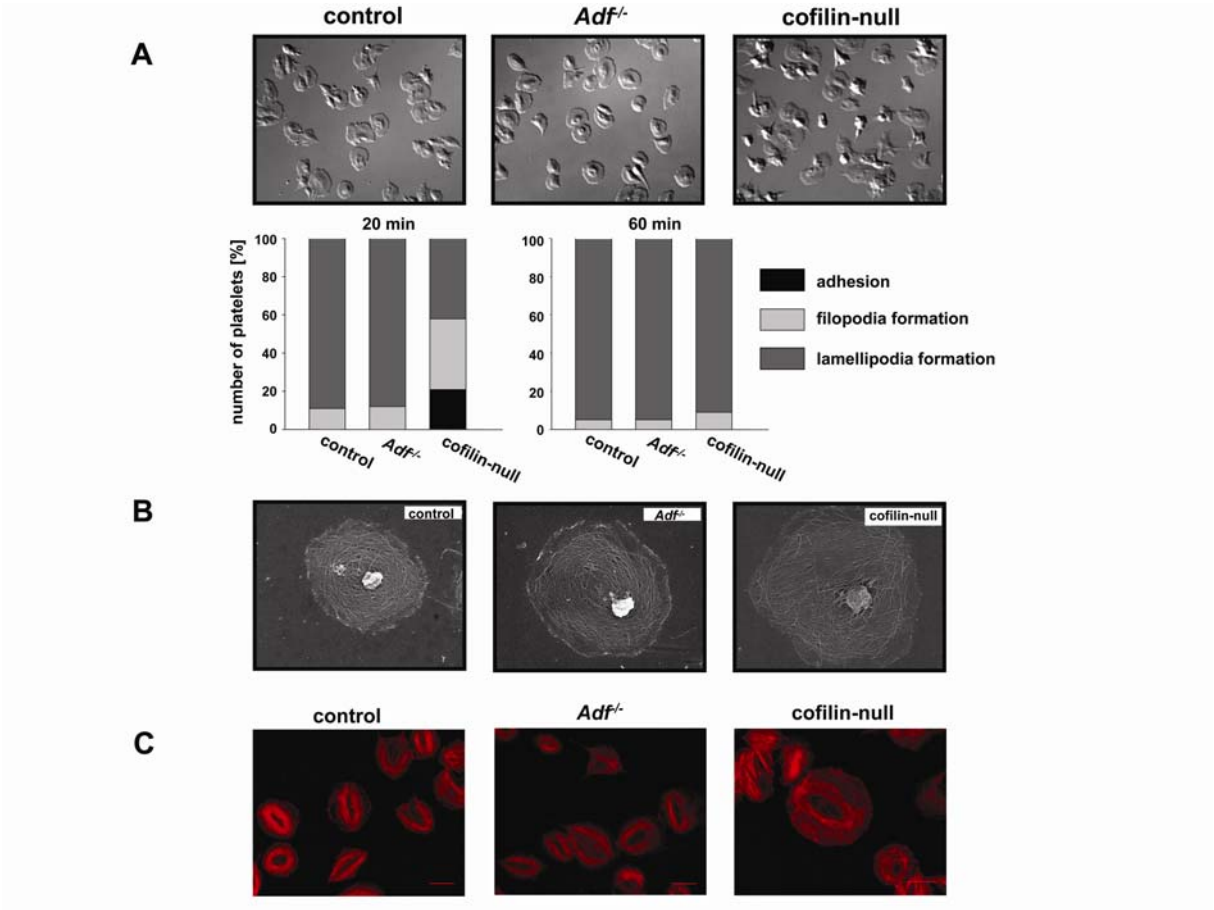

Fig. 18: Delayed spreading of cofilin-null, but not of ADF-null platelets on fibrinogen.
(A) Platelets were allowed to spread on a fibrinogen-coated surface. Platelets were fixed at different time points and counted. Pictures (upper panel; 100x magnification) were recorded after 20 minutes. **(B)** Scanning electron microscopy of spread platelets after plasma membrane denudation (pictures after 60 minutes; magnification 15,000x). **(C)** STED microscopy of spread platelets stained with phalloidin (pictures after 60 minutes; bar: 3 µm).

C.1.2. Analysis of ADF/cofilin double-deficient platelets

As described above, the lack of cofilin in megakaryocytes resulted in the formation of giant, non-discoid platelets. To further assess the role of ADF/cofilin in the process of platelet formation, mice were generated lacking both ADF and cofilin in megakaryocytes (*Adf*$^{-/-}$*/cofilin*$^{fl/fl}$*, PF4-Cre*). Remarkably, platelet counts in these double-mutant mice were dramatically reduced to < 5% of control mice (Fig. 19A), but the animals did not show any signs of spontaneous bleeding (data not shown). Transmission electron microscopy revealed that the few circulating platelets

displayed a marked variability in size and morphology (Fig. 19B). Giant platelets and microparticle-like platelets were observed and in most cases the ultrastructure was disordered. In contrast to single-deficient platelets, ADF/cofilin-deficient platelets contained accumulation of filaments in the cytoplasmic and the peripheral zone as shown by transmission electron microscopy of resting platelets (Fig. 19C). These findings demonstrate that combined lack of ADF and cofilin results in severely defective platelet production. Further functional analyses revealed marked functional deficits in the double-mutant platelets, including defective spreading as shown with scanning electron microscopy after denudation of the plasma membrane (Fig. 19D).

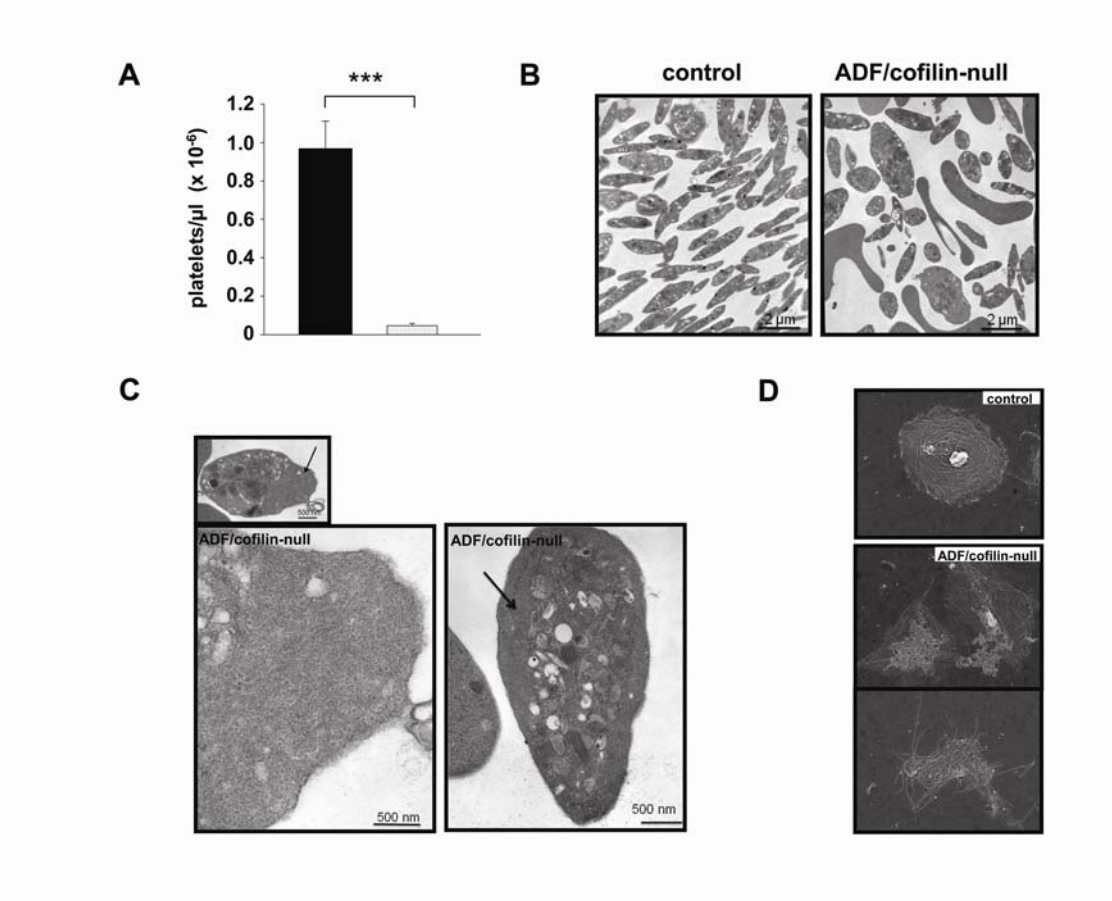

Fig. 19: Determination of platelet count, shape and ultrastructure of double knock-out platelets. **(A)** Platelet count was determined in a flow cytometry. Results are mean ± SD (*n* = 6 mice per group).*, *P* < 0.05; ***, *P* < 0.001. **(B+C)** Transmission electron microscopy analysis of resting platelets. **(D)** Scanning electron analysis of spread platelets (60 minutes) after denudation of the membrane (15,000x magnification).

ADF and cofilin are actin-binding proteins that enhance the depolymerization rate at the pointed end of filamentous actin, thereby promoting actin turnover and F-actin assembly. To test this directly, a F-actin assembly assay in platelets was performed using flow cytometry. The F-actin assembly ratio of thrombin-activated and resting

platelets was compared between all mouse lines. F-actin assembly in *Adf*$^{-/-}$ platelets was similar as observed in wild-type platelets (Fig. 20). A reduced ratio of F-actin assembly was measured in cofilin-null platelets. However, cofilin-null platelets were still able to polymerize actin. Strikingly, F-actin assembly was completely abolished in ADF/cofilin-deficient platelets. These results show that ADF along with cofilin are necessary for successful F-actin assembly, whereas absence of one of these proteins induces either no or a milder phenotype.

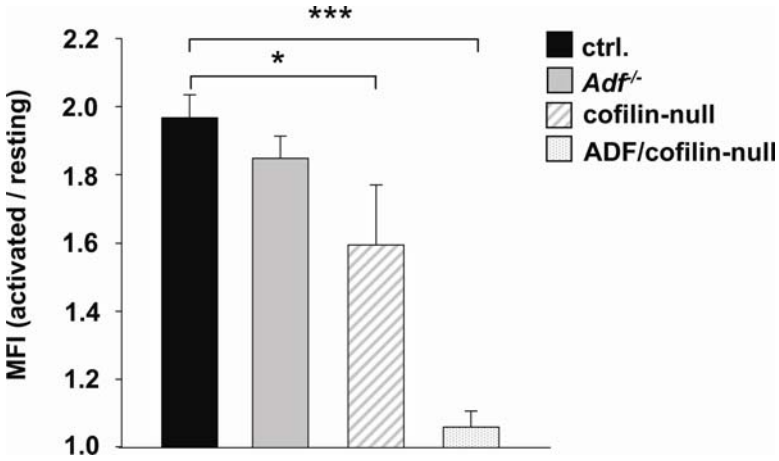

Fig. 20: F-actin assembly is abolished in ADF/cofilin-deficient platelets.
After activation with thrombin, platelets were fixed, permeabilized, stained with phalloidin-FITC and analyzed in a FACSCalibur. Resting wild-type value (mean fluorescence intensity) was set to 1 and ratio of activated platelets and resting platelets was determined.

C.1.3. *In vitro* and *in vivo* analysis of megakaryocytes

To assess the reason for the severe thrombocytopenia in ADF/cofilin-deficient mice, megakaryocytes (MK) were analyzed in spleen and bone marrow. ADF/cofilin-null mice displayed a severe splenomegaly (Fig. 21A). Interestingly, even at an early time point such as nine weeks the spleen/body weight ratio was significantly increased. After five months the splenomegaly was such profound that the spleen/body weight ratio was approximately six-fold increased compared to wild-type. Notably, in wild-type and single-deficient mice (*Adf*$^{-/-}$ mice not shown) the spleen/body weight ratio did not change over time. Histological sections of the spleen revealed that in contrast to single-deficient mice, in ADF/cofilin-deficient mice the number of megakaryocytes was strongly increased (visual field: 328 x 246 µm; wt: 1.93 ± 0.14; ADF/cofilin-null 12.8 ± 1.06) (Fig. 21B). This was confirmed by analysis of splenic cryo-sections stained with an anti-GPIb antibody specific for megakaryocytes and platelets (left

panel) and hematoxylin-eosin (HE)-stained paraffin sections (right panel). Apparently, a high number of anucleated megakaryocytes were observed in HE sections. However, sequential cuttings revealed that the same megakaryocyte that appeared to be anucleated on the one section contained a nucleus on one of the following sections (not shown). Together, these results demonstrated that the severe thrombocytopenia in ADF/cofilin-deficient mice was not caused by defective differentiation of megakaryocytes.

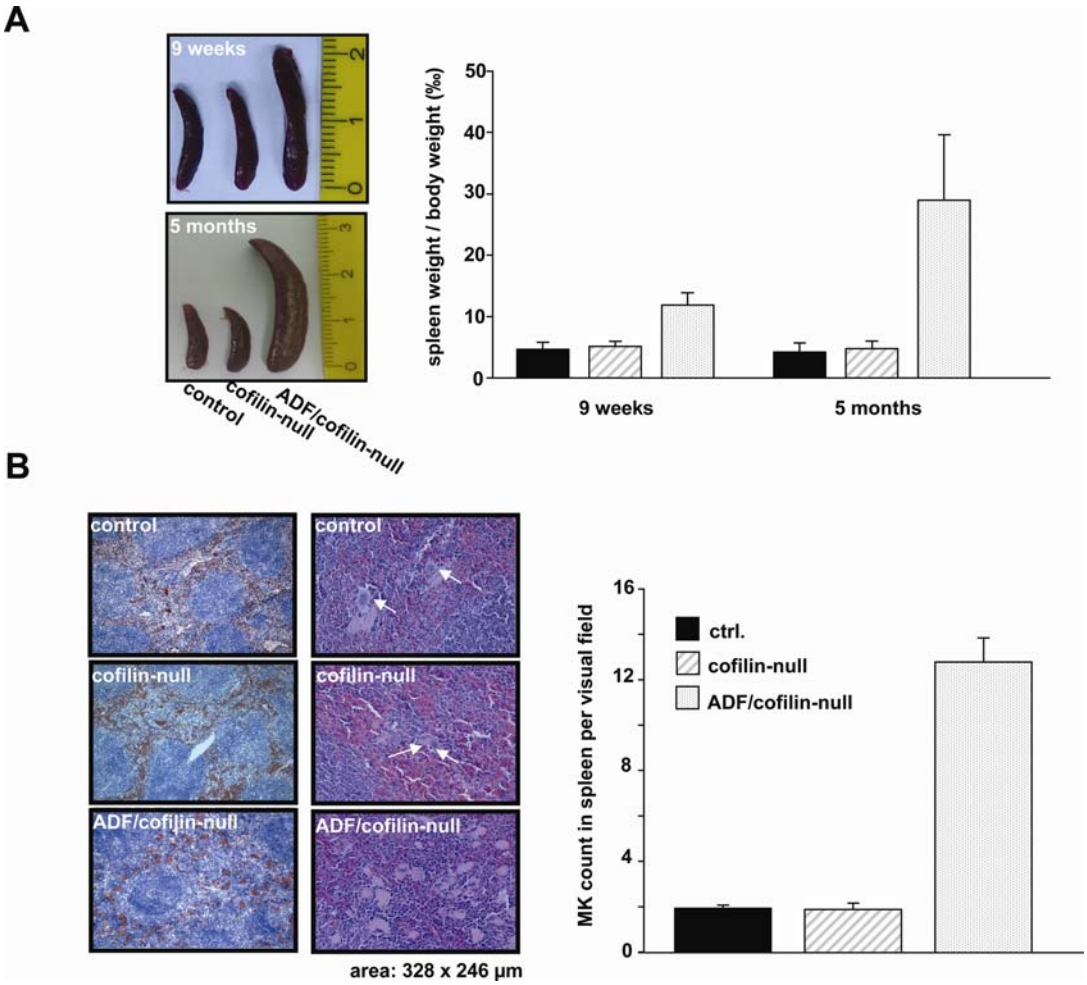

Fig. 21: Splenomegaly and elevated MK (megakaryocyte) numbers in ADF/cofilin knock-out mice. **(A)** Spleen and body weight was measured after 9 weeks and 5 months. **(B)** Cryo and paraffin-embedded sections (5 µm) were stained with anti-GPIb-HRP/hematoxylin and hematoxylin/eosin, respectively. Numbers of MKs per visual field (328 x 246 µm) were determined. White arrows indicate MK.

Prompted by the splenomegaly and the elevated MK numbers, plasma thrombopoietin levels were measured to determine a possible role of thrombopoietin (TPO) for the observed phenotype. However, no obvious differences of TPO level in

plasma were found in the knock-out mice, excluding a role of TPO for the strong spleen phenotype observed in ADF/cofilin knock-out mice (Fig. 22).

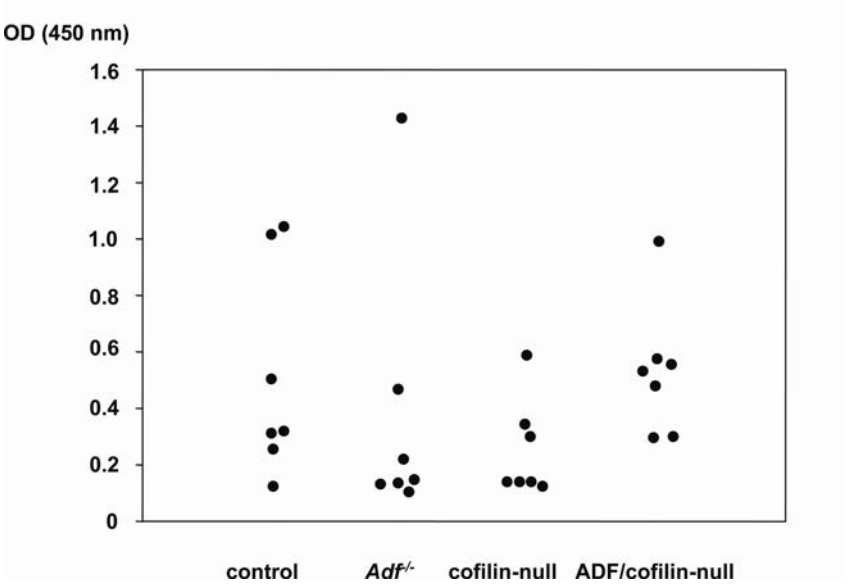

Fig. 22: Similar TPO plasma levels in the analyzed mice.
Plasma was collected from mice and investigated for TPO levels in a Multiskan photometer at 450 nm. Each symbol represents one mouse.

Similar to spleen, MK numbers in the bone marrow of ADF/cofilin-null mice were markedly increased compared to wild-type controls (visual field: 328 x 246 µm; wt: 8.46 ± 2.13; ADF/cofilin-null: 26.6 ± 5.6) (Fig. 23A), whereas no alterations were found in the single-mutant mice. The structure of the bone marrow was not obviously altered in any of the single- or double-mutant mice. However, transmission electron microscopy revealed marked morphological abnormalities in ADF/cofilin-null MKs. The typical highly organized structure of the cytoplasm was totally absent (Fig. 23B). Only remaining parts of the demarcation membrane system (DMS) were observed and granule distribution was severely defective. These results implicated that ADF/cofilin are crucial for the formation of platelet zones in MKs. The peripheral zone was enlarged due to enrichment of actin filaments and in addition, significant accumulation of actin filaments in the cytoplasm was frequently seen in ADF/cofilin-deficient MKs (Fig. 23B). Actin accumulation was also confirmed by actin immunlocalization (Fig. 23C). In summary, ADF/cofilin are highly important for the correct development and organization of the demarcation membrane system in the megakaryocyte cytoplasm which is required for normal platelet production.

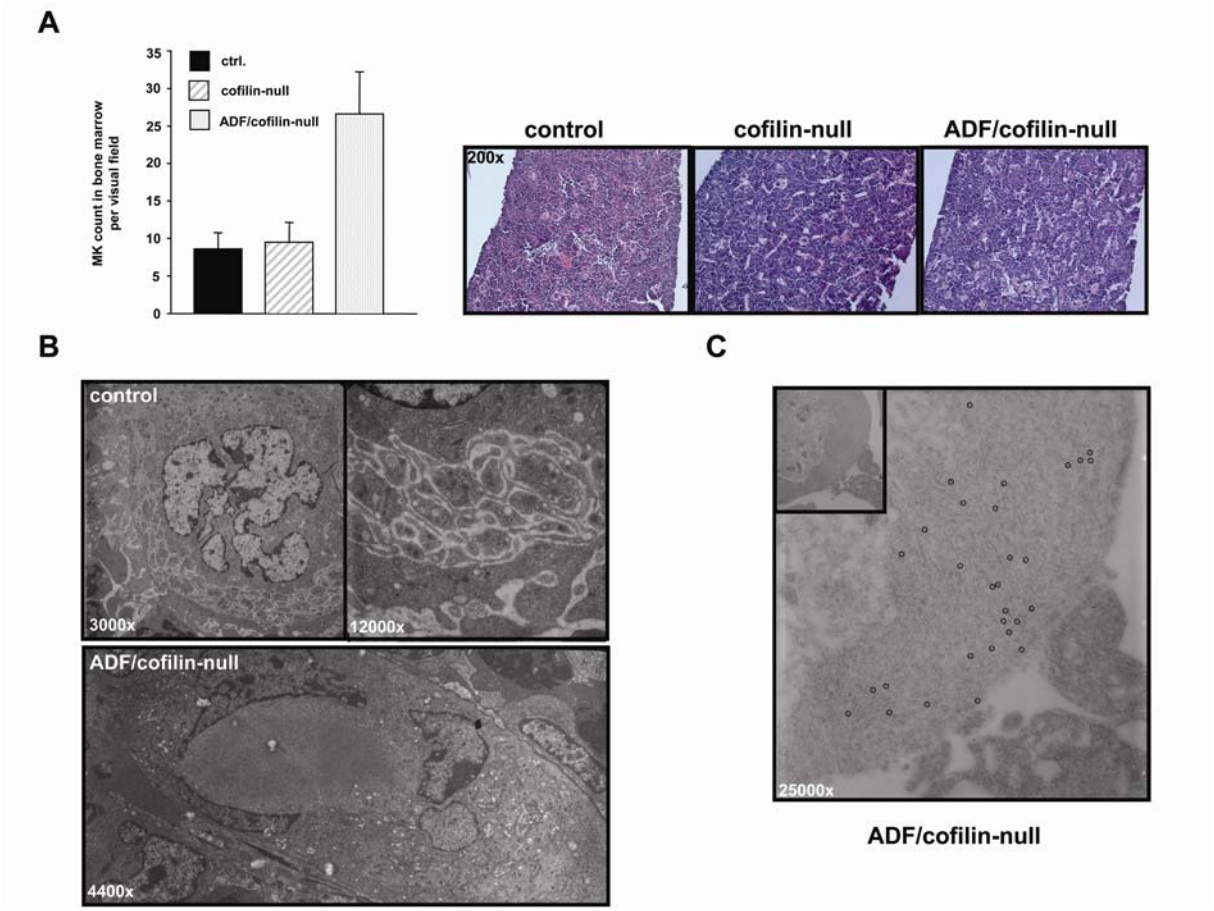

Fig. 23: Morphological abnormalities in bone marrow MKs of ADF/cofilin-null mice.
(A) Paraffin-embedded sections (5 µm) were stained with hematoxylin/eosin. Numbers of MKs per visual field (328 x 246 µm) were determined. **(B)** Transmission electron microscopy of bone marrow MKs. **(C)** Actin-immunlocalization in bone marrow MK of ADF/cofilin-null mice. Individual 12 nm gold particles are marked with a black circle.

To test whether the abnormal ultrastructure of bone marrow MKs is a consequence of a defect in early MK maturation, ploidy as a marker for endomitosis was investigated. Therefore, distribution of DNA content in bone marrow MKs was measured after harvesting the bone marrow. The frequency of distribution of MK DNA content was similar between all mouse lines (Fig. 24). Only a minor shift to higher ploidy was observed in ADF/cofilin-null MKs which is in agreement with reports on minor increase in ploidy in acute thrombocytopenia[133]. However, a defect in endomitosis and with this a defect in MK maturation was not observed. This suggested that the defect in development of the demarcation membrane system is a late stage defect.

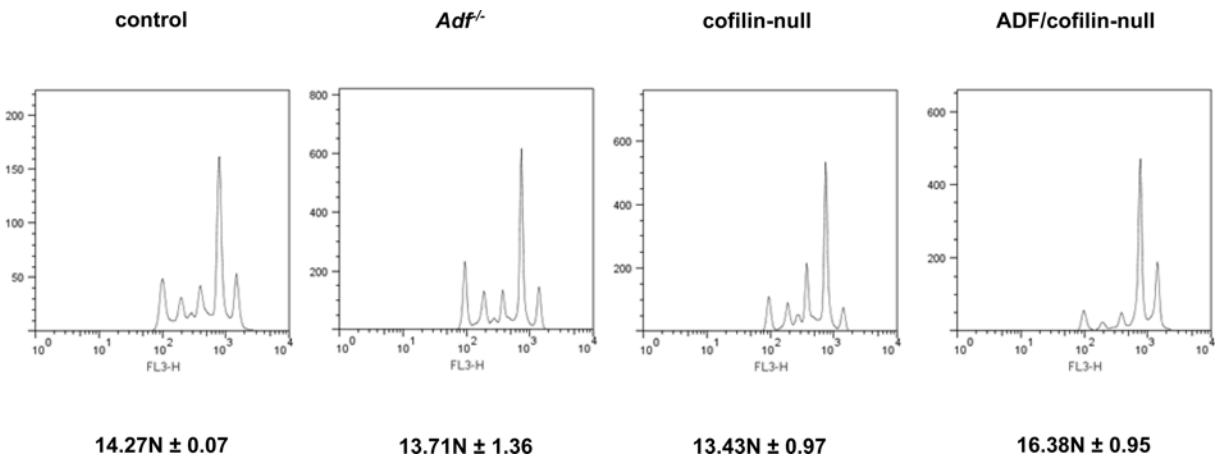

Fig. 24: Similar distribution of bone marrow MK DNA content
Bone marrow was harvested and MK DNA was stained with propidium iodide and DNA distribution was measured on a FACSCalibur. Representative histograms are depicted. Results are mean ± SD (*n* = 4 mice per group).

To further study platelet biogenesis in more detail, fetal liver cells of wild-type and mutant mice were cultured and allowed to differentiate into MKs for 4 days as described[134]. While in cultures of ADF- or cofilin-null mice proplatelet formation occurred to the same level as wild-type cultures, a significant ($P < 0.001$) reduction in the number of proplatelet forming MKs (wt: 33.46 ± 4.12%; ADF/cofilin-null: 16.98 ± 3.88%) was seen in the double-mutant cultures (Fig. 25A). Given the fact that ADF/cofilin-null mice show a severe thrombocytopenia (< 5% of wt) and bone marrow megakaryocytes are unable to form a normal demarcation membrane system *in vivo*, it was surprising that still a significant number of ADF/cofilin-null megakaryocytes were able to produce proplatelets. Therefore, the differentiated ADF/cofilin-deficient megakaryocytes were investigated in more detail. Again, it was observed that actin accumulates in the cell body as shown by phalloidin staining (Fig. 25B). Most strikingly, however, the typical periodical swellings located at the proplatelet shaft in wild-type MKs[12] were absent (Fig. 25C). This finding strongly suggests that ADF/cofilin are crucially involved in the formation of proplatelet swellings *in vitro*. This lead to the hypothesis that the formation of proplatelet swellings *in vitro* rather than the formation of proplatelets is the more likely correlate to the formation of platelet zones in bone marrow megakaryocytes *in vivo*. Further, explantation of wild-type and ADF/cofilin-null bone marrow was performed and MK differentiation observed and analyzed. During preparation it was generally observed that double knock-out bone marrow was less compact and more transluctant. To analyze MK differentiation, MKs

were classified into four categories: small MKs, spherical MKs, MKs with large pseudopodia and MKs with proplatelets. Fig. 25D shows that the number of small MKs is 2-3x increased in double knock-out bone marrow but they are less capable to form proplatelets.

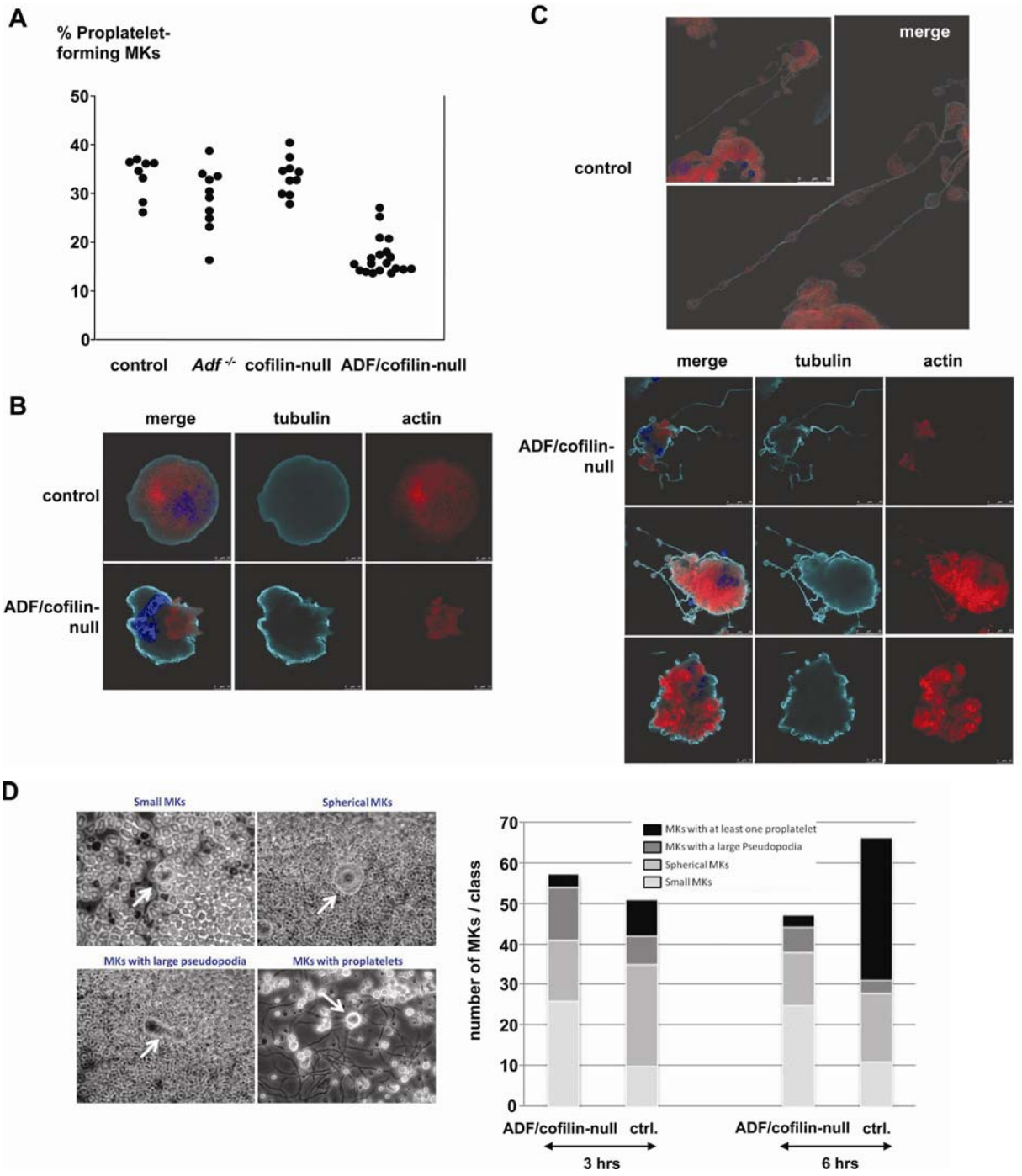

Fig. 25: Reduced proplatelet and absent swelling formation of ADF/cofilin-null MKs.
(A) Fetal liver cells were cultured for 4 days and MKs were analyzed for proplatelet formation. **(B+C)** *In vitro* MKs (**(B)** without proplatelets; **(C)** with proplatelets) were analyzed with confocal microscopy after staining for the nucleus (blue), tubulin (magenta) and actin (red). **(D)** MKs from bone marrow explants were cultured for the indicated time points and classified into different stages. Left pictures depict different stages of wild-type MK differentiation. MKs are marked with white arrows.

Detailed observation showed that the cytoplasm and nucleus of ADF/cofilin-deficient MKs are not clearly delineated and the contour appeared to be more irregular (Fig. 26B). The few proplatelet-like extensions that were formed by double-deficient MKs appeared to be thinner, without swellings and shorter (Fig. 26A). Interestingly, after the 6 hours observation period many thin extensions of double-deficient MKs were found loosely in the chamber (Fig. 26C). This possibly indicates that proplatelet swellings contribute to the stabilization of proplatelets. The results shown in figure 26 support previous findings that ADF/cofilin-null MKs form significantly less proplatelets and that formed proplatelet-like extensions are not decorated with periodical swellings.

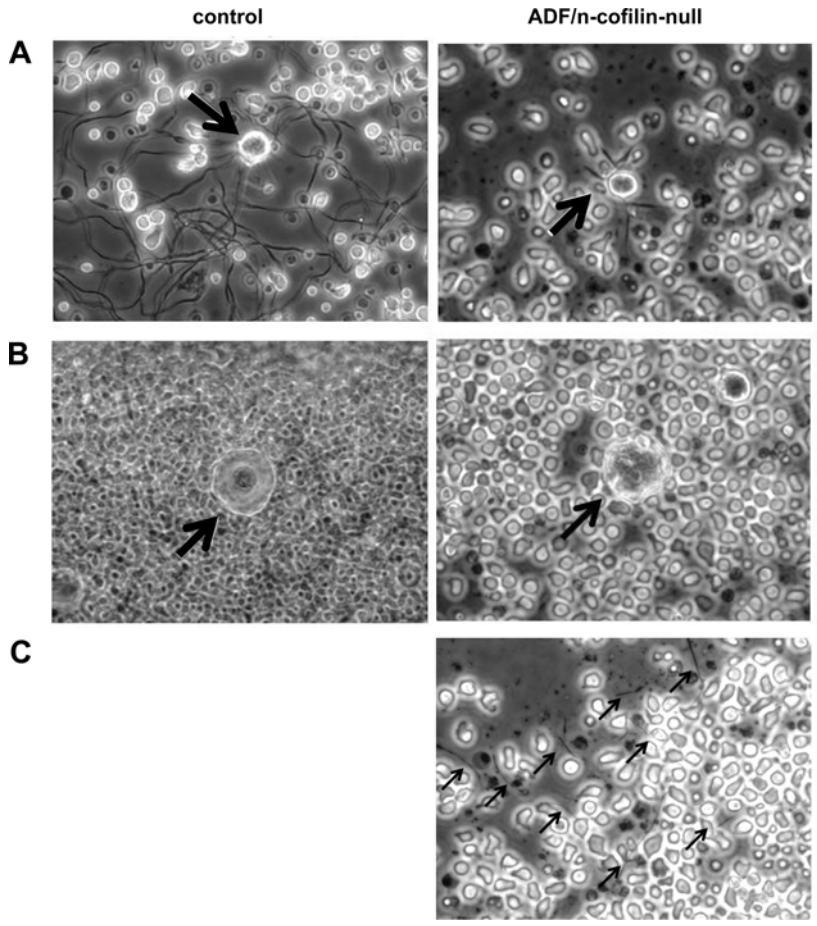

Fig. 26: Altered morphology of MKs and extension in ADF/cofilin-null bone marrow explants.
Bone marrow explants were cultured in a chamber and images were recorded after 6 hours. Proplatelet-like extensions **(A)** and morphology of spherical MKs **(B)** were compared and analyzed. **(C)** Single extensions of ADF/cofilin-null MKs found in the chamber.

C.1.4. Platelet and MK analysis of cofilin- and ADF/cofilin-deficient mice using the Mx-Cre system

Before 2007 when the mouse line was generated carrying the Cre recombinase under the PF4 promoter[125], the *Mx-Cre* mouse was the commonly accepted mouse line to study conditional gene deletion in the hematopoietic system. In contrast to the PF4-Cre system, the expression of the Cre recombinase can be induced in the Mx-Cre system by type I interferon in the adult state of a mouse. The knock-out efficacy in the hematopoietic system is extremely efficient, however, it is not specific for the hematopoietic system as it also effects other cell types including liver cells, endothelial cells and the bone marrow[126]. For these studies, Cre induction was achieved by injecting 200 µg Poly-I/Poly-C per mouse on day 0 and day 2.

Platelet counts in cofilin-null, but not control mice were dramatically reduced five days after Cre induction (Fig. 27A). Mice deficient in both ADF and cofilin showed an even stronger decrease in platelet counts at this time point. No differences in hematocrits were observed on day 5 (not shown), whereas marked differences were determined on day 9 (control: 43.5 ± 2.2%, cofilin-null: 29.7 ± 7.1%, ADF/cofilin-null: 19.7 ± 1.5%). All double-deficient mice died within ten days after Poly-I/Poly-C injection. Megakaryocytes of the mutant mice were analyzed to understand the dramatic decrease of the platelet count. MK counts were determined in spleen (Fig. 27B) and bone marrow (Fig. 27C) in control and mutant mice at different time points after Cre induction. Although the spleen structure was unaltered, the number of MKs in both spleen and bone marrow of cofilin-null mice was profoundly reduced (to 30 and 60% of control) on day 5 and further decreased on day 9 (to 13 and 17% of control) and 12 (both to 6% of control). At the later time points, a progressive destruction of bone marrow structure and reduction in bone marrow cellularity became evident in cofilin-null mice. In double-deficient mice, the reduction in MK numbers was even more severe as was the destruction of the bone marrow architecture. The results obtained by using the Mx-Cre system show that cofilin is the more important isoform for maintaining the bone marrow architecture and consequently for MK survival. However, ADF also contributes to this process as the double-mutant mice show a stronger phenotype.

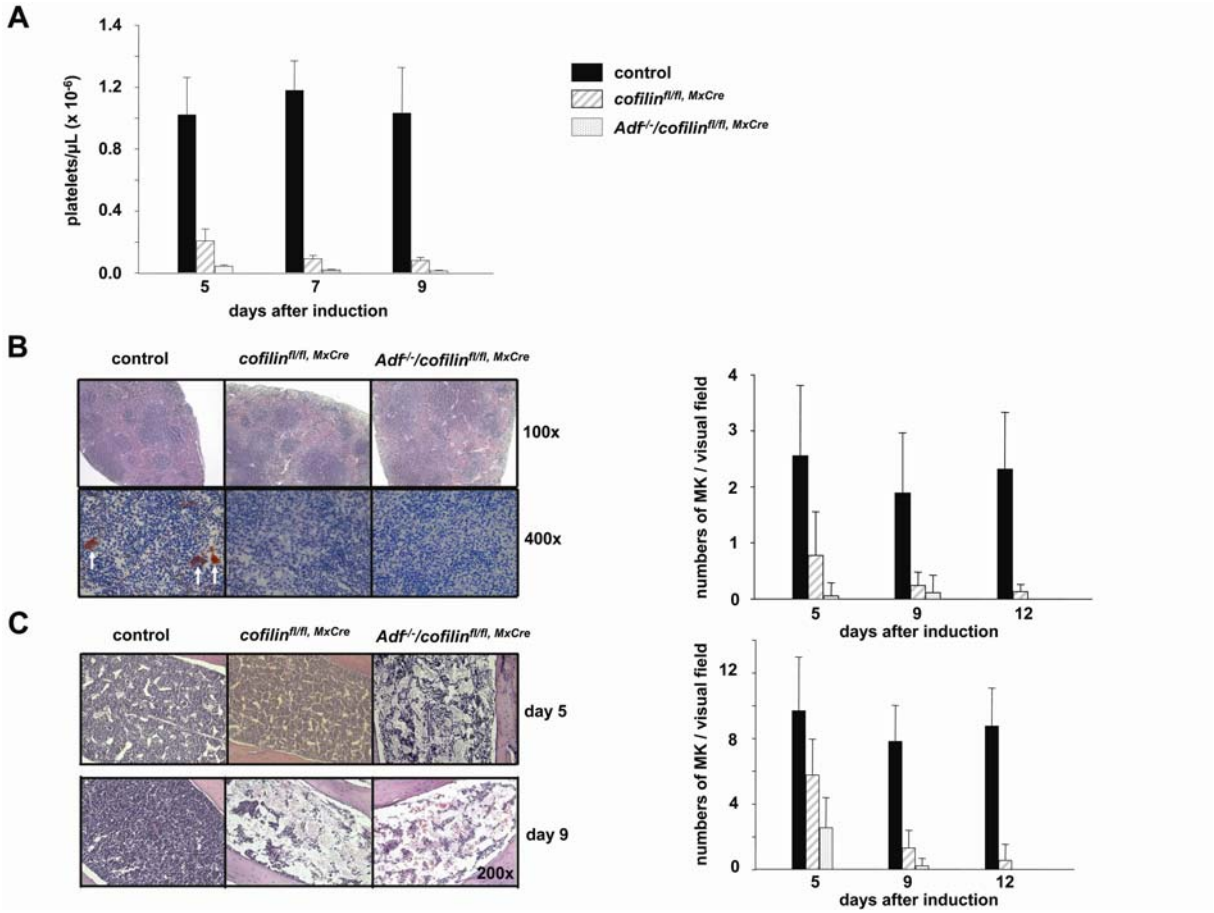

Fig. 27: Reduced platelet and MK counts in mutant mice.
(A) Platelet count was determined by flow cytometry. Results are mean ± SD (*n* = 4 mice; representative of three individual experiments). **(B)** Analysis of 5 µm splenic sections on day 9. Paraffin-embedded (upper panel) and Cryo sections (lower panel) were stained with hematoxylin/eosin and anti-GPIb-HRP/hematoxylin. Numbers of MKs per visual field (328 x 246 µm) were determined. **(C)** Analysis of 5 µm bone marrow sections. Paraffin-embedded sections were stained with hematoxylin/eosin. Numbers of MKs per visual field (328 x 246 µm) were determined.

C.2. Regulation of GPVI by ADAM metalloproteinases

In the second part of the dissertation, mechanisms underlying the regulation of the platelet receptor glycoprotein VI (GPVI) were studied. For this, a *Gp6* knock-out and an *Adam10* conditional knock-out mouse were generated. In addition to ADAM10 mice, low TACE (ADAM17) mice were used to identify the GPVI sheddase.

C.2.1. GPVI down-regulation in murine platelets through metalloproteinase-dependent shedding

GPVI mediates platelet activation which leads to firm adhesion and aggregation on subendothelial collagen. As mentioned in the introduction, GPVI can be down-regulated from the platelet surface in mice *in vivo* making this receptor a promising target for anti-thrombotic therapy. The mechanisms of down-regulation and the relevance of these observations for humans are not fully explored. To study this in more detail, genetically modified mouse lines were generated to investigate GPVI regulation.

C.2.2. Construction of targeting vectors for the generation of *Gp6* transgenic mice

The successful construction of the targeting vectors for the generation of *Gp6* transgenic mice was performed before and described in detail in the Master thesis “Targeting vectors for the generation of human GPVI transgenic mice” (Markus Bender, February 2006). Therefore, the chapters C.2.1.1. – C.2.1.6. briefly summarize the main results of the thesis.

C.2.2.1. Identification of the mouse *Gp6* gene

For identification of the mouse *Gp6* gene, a mouse genomic library was screened which represents most of mouse genes as ligated DNA fragments into BAC (bacterial artificial chromosome) vectors.

Primers were designed against the exon 2 and 3 region of the *Gp6* gene. This region was amplified, tested by Southern blot and used as an internal probe for screening the mouse library. After hybridizing the BAC filters with the radioactively labeled internal probe, five positive clones were identified and purchased. Genomic DNA from the delivered BAC clones was isolated and used as a template for the control

PCR (Fig. 28). RP22 - 365P17 and RP22 - 455P10 BAC clones (lane 2 and 4) contained the genomic region of mouse *Gp6.*

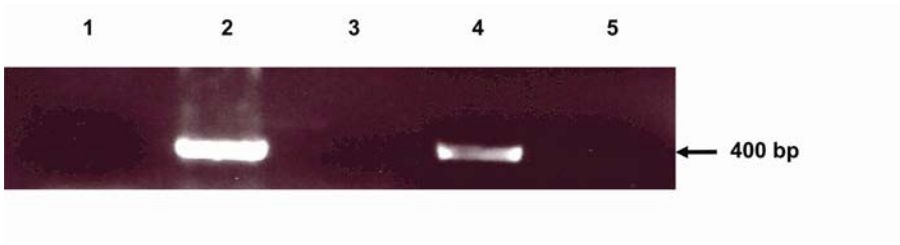

Number of BAC clones
1) RP22 - 340C14
2) RP22 - 365P17
3) RP22 - 338L17
4) RP22 - 455P10
5) RP22 - 364C5

Fig. 28: Identification of the mouse *Gp6* gene using PCR-based strategy.
Exon 2, intron 2 and exon 3 were amplified by exon 2 forward and exon 3 reverse primers. The size of the PCR products is indicated with an arrow. Lane 2 and 4 are positive.

In order to confirm the PCR results, RP22 - 365P17 clone was digested with different restriction endonucleases, fragments were size-separated, blotted onto a nitrocellulose membrane and hybridized with the internal probe. After Southern blotting, expected DNA fragments were labeled (Fig. 29). This correct BAC clone was used as a PCR template to amplify the homologous arms for the generation of the targeting vector.

A

Enzyme	Expected size
*Eco*RI	4125 bp
*Bam*HI	2940 bp
*Hind*III	8389 bp

B

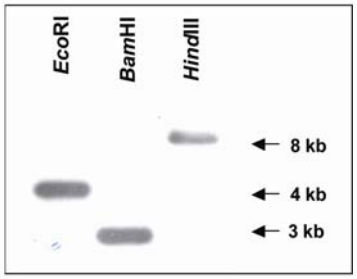

Fig. 29: Southern hybridization of a *Gp6* positive BAC clone.
(A) The mouse *Gp6* DNA sequence was virtually digested with *Eco*RI, *Bam*HI, *Hind*III. According to NCBI sequencing data, the expected sizes of DNA fragments are indicated. **(B)** Analysis of BAC clone with Southern hybridization is shown. RP22–365P17 BAC clone was digested with *Eco*RI, *Bam*HI and *Hind*III enzymes. Sizes of radioactively labeled genomic fragments are indicated with arrows.

C.2.2.2. Targeting strategy for the generation of *GP6* knock-out and knock-in mice

The strategies for the generation of *Gp6* knock-out and *GP6* knock-in mice are schematically presented in Fig. 30. The signal peptide of mouse GPVI is encoded by exons 1 and 2. The GPVI amino acid sequence of different species was aligned (not

shown) demonstrating that the signal peptide sequences strongly vary between the species. Therefore, the mouse signal peptide was preserved for the knock-in constructs. Exon 2 and intron 2 were partially deleted and a marker and a neomycin resistance cassette were inserted and fused to exon 3 in all cases. Upstream of the IRES (internal ribosome entry site) element in the knock-out vector a multiple cloning site was created which allowed to insert wild-type or mutated human *GP6* cDNA easily. The human *GP6* cDNA without the coding region of the signal peptide was fused to exon 2 in frame. This strategy makes it possible to express a chimeric GPVI protein which contains the mouse signal peptide of GPVI and the human GPVI receptor.

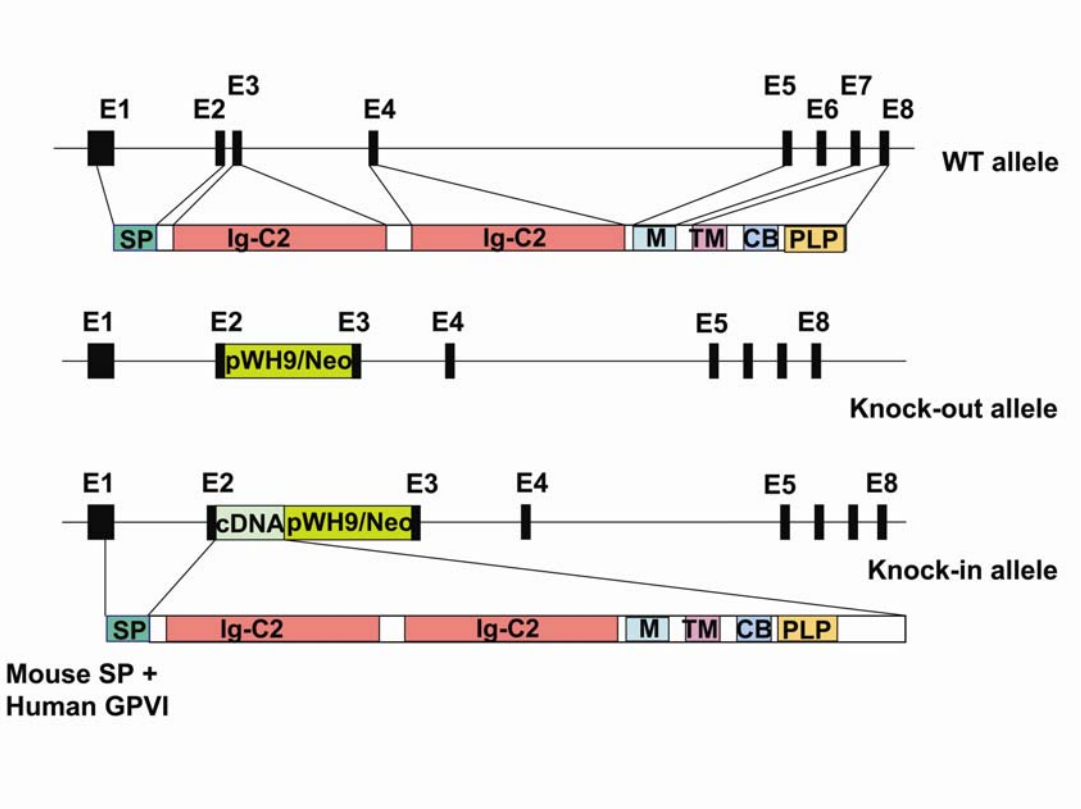

Fig. 30: Targeting strategy of the mouse *Gp6* gene; generation of *GP6* knock-out and knock-in mice. The gene structure of mouse *Gp6* is displayed. Exons (E1 to E8) are indicated as black boxes. Introns are labeled with a line. Domain structures and motifs are labeled according to the coded exons (SP: signal peptide; Ig-C2: immunoglobulin-like domain; M: mucin-rich region; TM: transmembrane domain; CB: calmodulin binding site; PLP: poly-L-proline-rich sequence). Schematic structure of the knock-out GPVI allele is shown. The pWH9 (IRES+lacZ) and neomycin resistance cassette (PGK promoter+*neo* gene) are labeled. The schematic structure of the knock-in *GP6* allele is displayed. Fusion of the human *GP6* cDNA to exon 2 is shown. The signal peptide is encoded by exon 1 and a part of exon 2, other domains and motifs are encoded by the human *GP6* cDNA.

C.2.2.3. Amplification of the homologous arms for the targeting vector

The 5´ arm of *Gp6* contains exon 1, intron 1 and a part of exon 2. The size of the 5´ arm is 3.2 kb. After subcloning, a new *Hind*III restriction enzyme site in intron 1 was

generated by using site-directed mutagenesis. This newly generated *Hind*III site in intron 1 was crucial for the identification of homologue recombinant clones. An extract of the sequencing results concerning the generation of the new *Hind*III site in intron 1 is shown (Fig. 31).

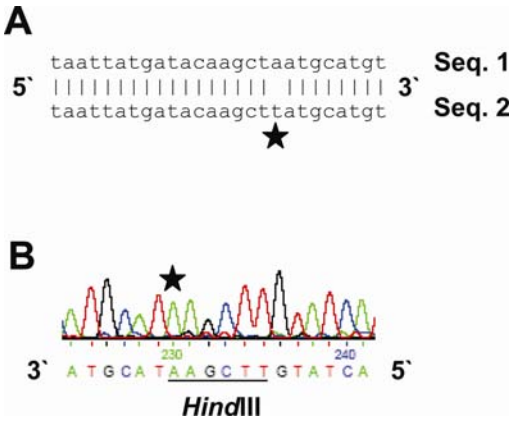

Fig. 31: Part of the *Gp6* 5` arm containing the new *Hind*III site.
(A) The upper line (Seq.1) shows an extract of the mouse *Gp6* sequence. The lower line (Seq. 2) is an extract of the sequencing result. Identical nucleotides are indicated with bars. The star marks the mutation for generation of a *Hind*III site. Reverse sequence is displayed. **(B)** An extract of the sequencing data is shown. The asterisk indicates the mutation for the generation of a *Hind*III site.

The 3´ arm with a length of about 4.1 kb was amplified with exon 3 forward and exon 4 reverse primers using the *Gp6*-specific genomic BAC clone as a template.

C.2.2.4. Amplification of the human *GP6* cDNA

To generate *GP6* knock-in mice, the human *GP6* cDNA was ligated into a cloning vector. Therefore, based on EST sequencing data (NCBI), three EST clones were purchased bearing the human *GP6* cDNA (see Table 2).

RPZD clone ID
IMAGp958M21997Q2
IMAGp958K07197Q2
HU3_p983F041002D2

Table 2: EST clones bearing the human *GP6* cDNA.

The human *GP6* cDNA was amplified from the translation initiation site until stop codon. This human cDNA served as a template for the following PCR. For generation of a mouse/human GPVI chimeric receptor, first the human signal peptide in the cDNA was deleted. For this, a primer combination was used which amplified the coding region of human *GP6*. The length of the PCR product was 1 kb.

C.2.2.5. Mutation of calmodulin, CRP and collagen binding sites on human *GP6*

In addition, three different human *GP6* cDNAs were generated which contained mutated important binding sites according to the following publications: (1) Lecut C. *et al.* identified the most important amino acid residues which are involved in collagen binding. *In vitro* studies revealed that valine 34 and leucine 36 are crucial for the interaction between GPVI and collagen. Moreover, a mutation of glycine 30 caused a stronger defect for binding to collagen[135]. (2) Smethurst *et al.* demonstrated *in vitro* that the mutation from lysine 59 to a glutamic acid on a human monomeric recombinant peptide resulted in a reduced binding to CRP (collagen-related peptide)[136]. (3) The interaction between GPVI and calmodulin was examined by Andrews *et al.* using a GPVI-related synthetic peptide (His269-Pro287). This peptide contained a calmodulin recognition site[63]. Based on the amino acid alignment with other calmodulin binding proteins, three amino acids were conserved in the motif of calmodulin binding sites. Therefore, the amino acids R271A, K273E and R280A were mutated in human GPVI which seemed to be crucial for calmodulin and GPVI interaction. Site-directed mutagenesis was performed using the subcloned wild-type human cDNA. Table 3 shows the references and the mutated amino acids.

Binding sites on human GPVI	Mutated amino acids	References
Collagen	G30A, V34A, L36A	135
CRP	K59E	136
Calmodulin	R271A, K273E, R280A	63

Table 3: Mutated binding sites on human GPVI.

Fig. 32 shows an extract from the sequencing results and the alignment of the mutated cDNAs compared with the wild-type sequence, based on nucleotide and amino acid level.

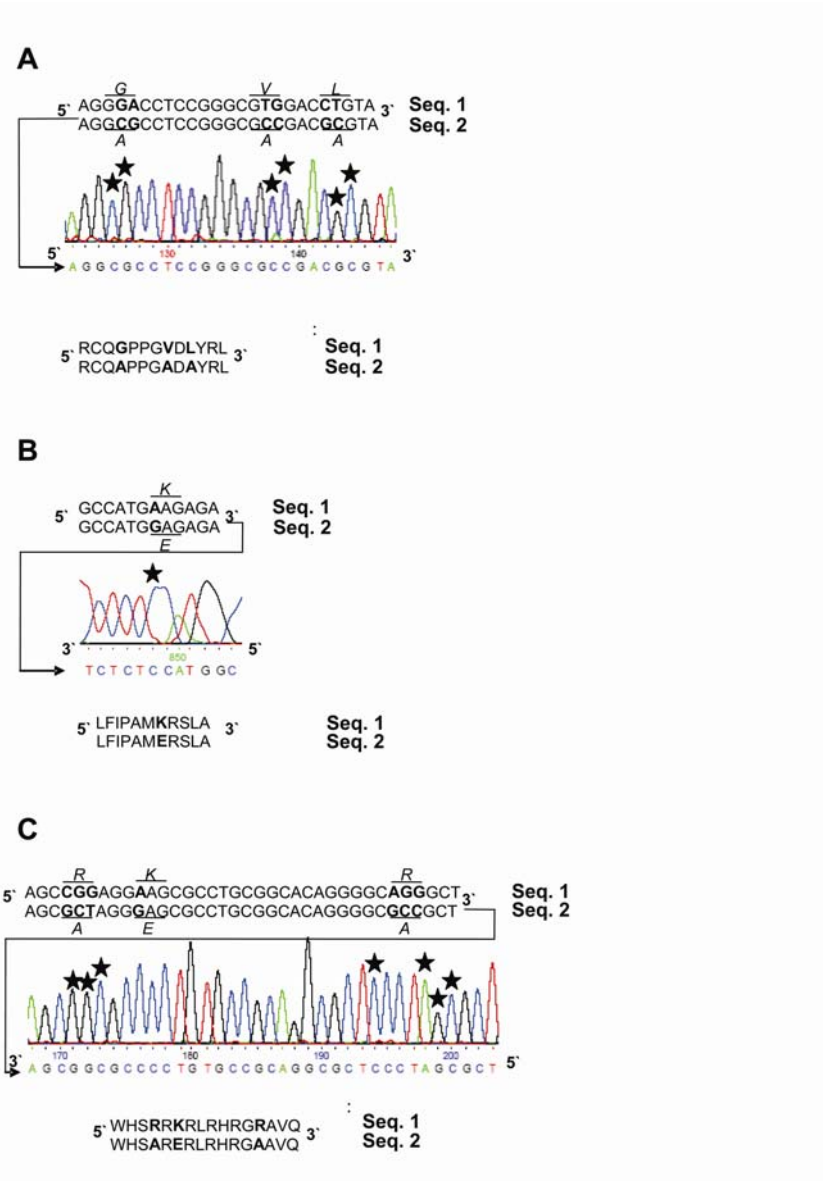

Fig. 32: Sequencing results of mutated human *GP6*.
Nucleotide and amino acid alignment of human wild-type (Seq. 1) and mutated (Seq. 2) GPVI are shown. Mutated codon triplets are labeled with a horizontal line. The corresponding amino acid is shown (italicized). An extract from the sequencing results of each mutated human *GP6* is also depicted. A reverse sequence (3´→5´) is displayed in the case of CRP and calmodulin. **(A)** mutation of the collagen binding site, **(B)** mutation of the CRP binding site, **(C)** mutation of the calmodulin binding site.

C.2.2.6. Cloning of the knock-out and knock-in vectors

A pWH9 plasmid construct was used for the generation of the final targeting vector. This construct contains an IRES element, a *lacZ* gene with a polyadenylation signal, a PGK promoter and a neomycin resistance gene.

Scheme:

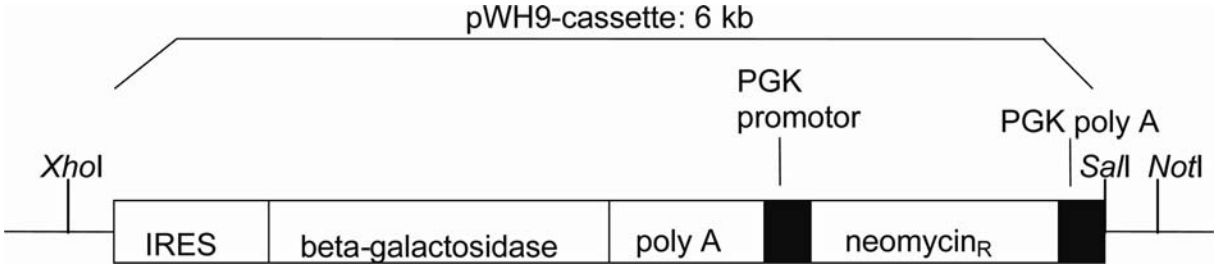

The targeting knock-out vector was sequenced to confirm that the vector contains both flanking sites (not shown). Moreover, different enzymatic digestions of the plasmids were performed (Fig. 33 and 34). The band pattern matched the expected band sizes. The correct ligation point in the knock-in vectors between exon 2 and the human cDNAs was confirmed by sequencing (not shown). It was proven that no frame shift mutation or ligation errors had occured.

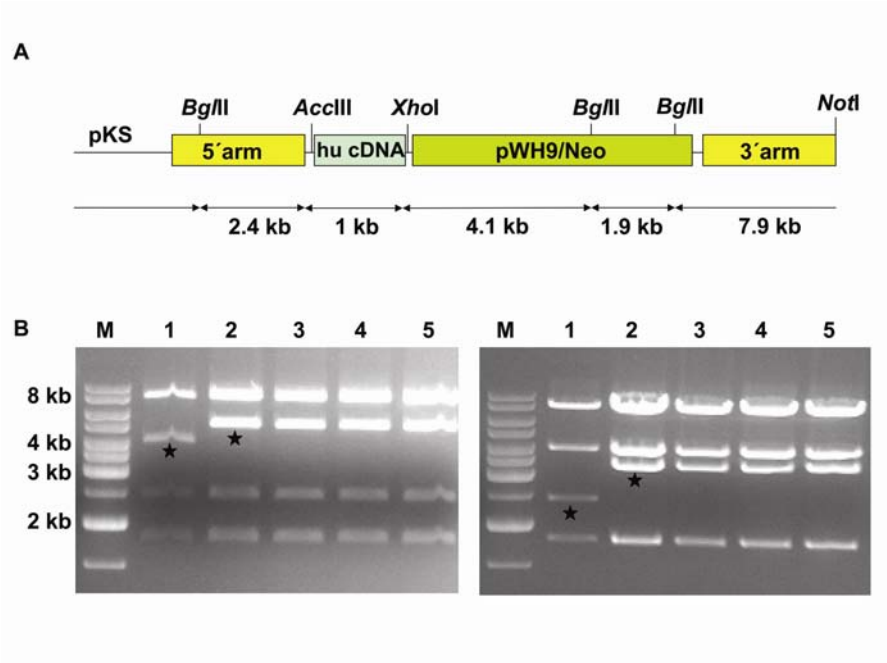

Fig. 33: Digestion of the final vector.
(A) Lengths of the fragments as indicated refer to the distance between enzyme sites. Enzyme sites used for digestion are indicated. The final vector consists of 17.3 kb. **(B)** *Acc*III/*Bgl*II (left picture) and *Xho*I/*Bgl*II (right picture) digested samples were separated on an agarose gel. 1 = knock-out final construct; 2 = human wild-type cDNA in final vector; 3 = human cDNA with mutated collagen binding site in final vector; 4 = human cDNA with mutated CRP binding site in final vector; 5 = human cDNA with mutated calmodulin binding site in final vector. M: marker. The 1kb band shift (= human cDNA) is labeled with asterisks.

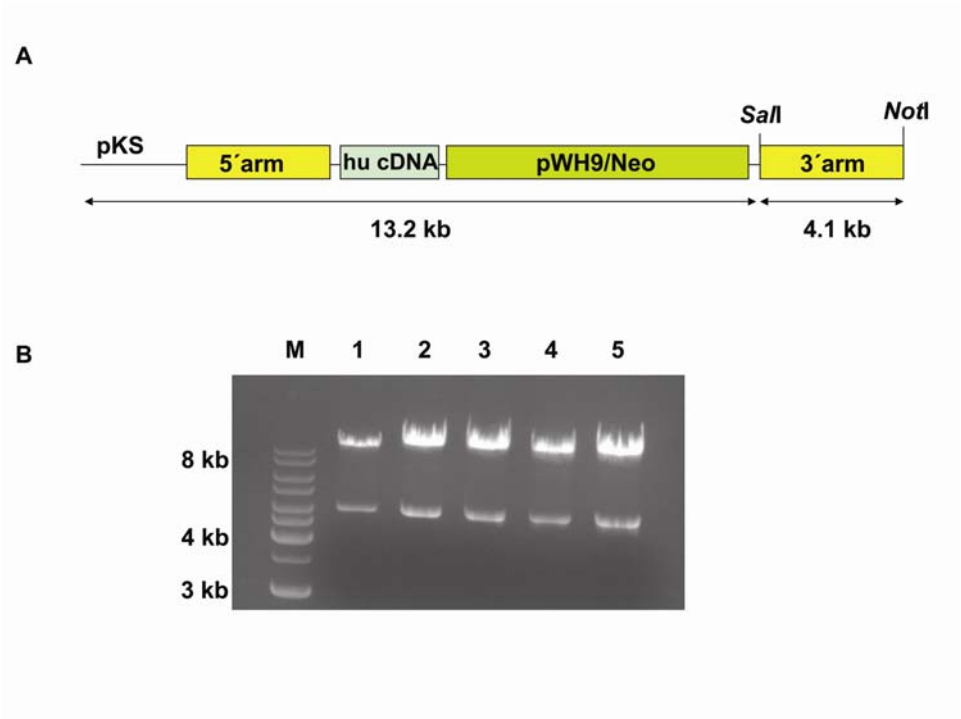

Fig. 34: Digestion of the final vector.
(A) Lengths of the fragments as indicated refer to the distance between enzyme sites. Enzyme sites used for digestion are indicated. **(B)** The final vector consists of 17.3 kb. *Not*I and *Sal*I digested samples were size-separated on an agarose gel. 1 = knock-out final construct; 2 = wild-type cDNA in final vector; 3= human cDNA with mutated collagen binding site in final vector; 4 = human cDNA with mutated CRP binding site in final vector; 5 = human cDNA with mutated calmodulin binding site in final vector. M: marker.

To have the opportunity to enhance the efficiency of the selection process after electroporation of the constructs into stem cells, a second selection marker, a thymidine kinase cassette, was inserted into the final vectors. This ligation step was proven by sequencing (not shown) and digestions (Fig. 35). To have a unique *Sal*I site for linearization, one *Sal*I site upstream of the 3´ arm was deleted.

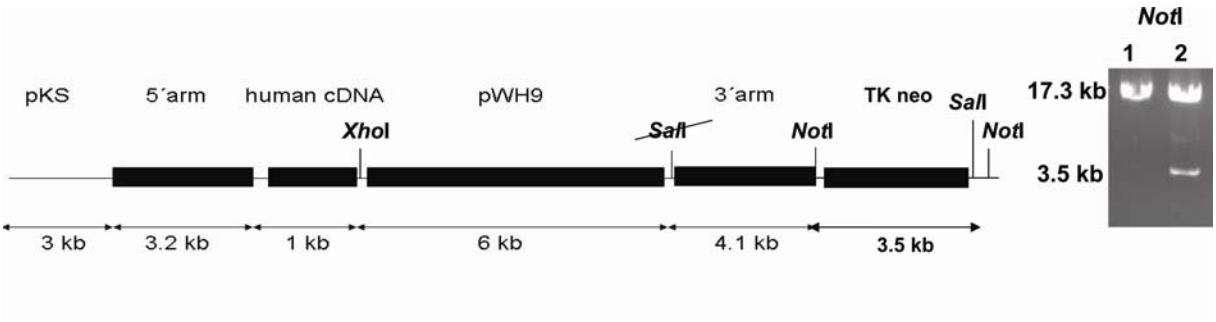

Fig. 35: Digestion of the final vector with the thymidine kinase (TK neo) cassette.
Exemplarily the *Gp6* knock-out vector without (1) and with (2) thymidine kinase cassette was digested with *Not*I.

In the end, five constructs were successfully generated: *Gp6* knock-out, human *GP6* cDNA knock-in, human *GP6* cDNA knock-in with collagen binding site mutation (G30A, V34A, L36A), human *GP6* cDNA knock-in with CRP binding site mutation (K59E) and human *GP6* cDNA knock-in with calmodulin binding site mutation (R271A, K273E, R280A).

C.2.3. Electroporation of the targeting vectors into ES cells and analysis of selected ES clones

An external probe (565 bp, forward primer: 5´-CTT TAC CTA CTG AGC TAG GG-3´; reverse primer: 5´-CAA GTG TGA GGA AAT GTC AT-3´) was used that recognizes a sequence upstream of exon 1. The scheme of a virtual *Hind*III digested *Gp6* locus shows that the wild-type allele (8.4 kb) and the knock-out / knock-in alleles (7.3 kb) can be distinguished by using this external probe (Fig. 36A).

To test whether the generated vectors can target the *GP6* locus via homologous recombination, the *Gp6* knock-out and the human wild-type *GP6* knock-in vector were electroporated into ES cells. Before electroporation, the targeting vectors were linearized with the *Sal*I enzyme. The isolated DNA of neomycin-resistant stem cells was digested with concentrated *Hind*III enzyme, size-fractionated in an agarose gel, transferred onto a nitrocellulose membrane and hybridized with the radioactively labeled external probe. The X-ray film was exposed to the Southern blot membranes and visualized bands of different ES clones were analyzed (Fig. 36B+C).

From each electroporation 384 stem cell clones were analyzed. In both cases one positive clone was obtained. The cells were recultured, tested again for successful homologous recombination and finally injected into blastocysts. The three mutated human *GP6* knock-in vectors will be electroporated in near future when the expression rate of the human GPVI protein in the *Gp6* knock-out background has been determined and is sufficient for analysis.

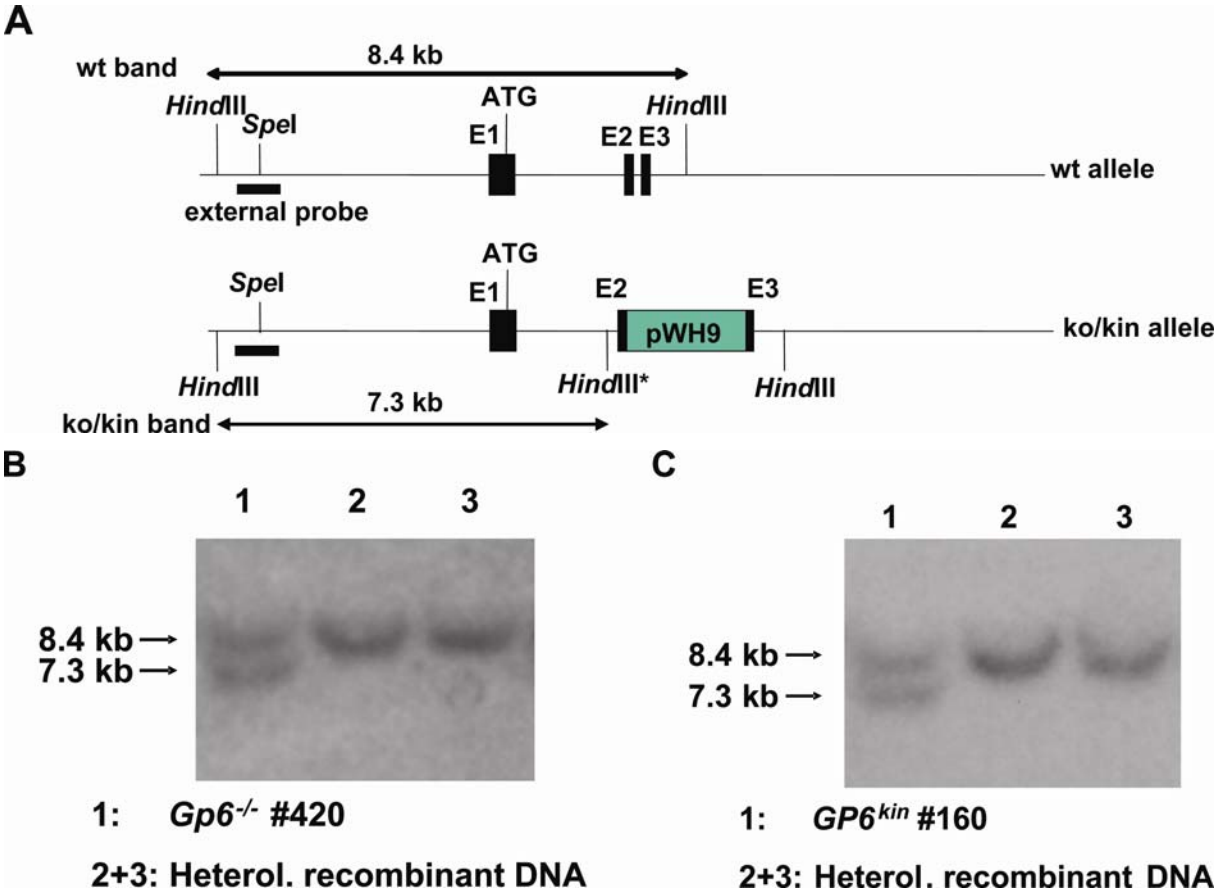

Fig. 36: Analysis of neomycin-resistant clones.
(A) The scheme shows detection of wild-type and mutant (*Gp6* knock-out / human *GP6* knock-in) bands. The external probe (black horizontal bar) recognizes a sequence upstream of exon 1. The exons are represented by black vertical bars. The wild-type band between two *Hind*III sites is about 8.4 kb. A new *Hind*III is introduced by integrating the targeting construct. The mutant band is about 7.3 kb. **(B)** *Hind*III digested DNA from ES cell after electroporation of the *Gp6* knock-out vector. **(C)** *Hind*III digested DNA from ES cell after electroporation of the human wild-type *GP6* knock-in vector.

C.2.4. *Gp6* chimeric mice

The following *Gp6* chimeric mice were obtained:

Gp6 (knock-out):

Gender	Chimerism
male	3x100%, 1x70%, 1x50%, 1x40%
female	2x100%, 1x60%

GP6 (knock-in):

Gender	Chimerism
male	2x50%, 2x40%, 1x30%, 1x20%
female	-

These mice were crossed with female C57BL/6J mice to determine germline transmission.

For the human *GP6* knock-in chimeric mice no germline transmission was obtained. Electroporation of this vector was repeated and resulted again in one positive stem cell clone which was injected into blastocysts. Soon the first chimeric offsprings are being expected.

In contrast, germline transmission was achieved for *Gp6* knock-out chimeric mice that confirms that the *GP6* multivector system is principally working.

C.2.5. Analysis of *Gp6* knock-out mice

To test the genotype after crossing heterozygous *Gp6* mice, a Southern blot (Fig. 37A) was performed that revealed that *Gp6* knock-out mice were obtained and resulted in a Mendelian ratio (not shown) excluding embryonic lethality. The absence of the protein was shown by Western blot (Fig. 37B) and flow cytometric analysis (Fig. 37C). As expected, expression of other prominent platelet surface proteins was not altered (Fig. 37D). In addition, platelet count (Fig. 37E) and platelet size (Fig. 37F) of GPVI-deficient mice were similar to wild-type controls.

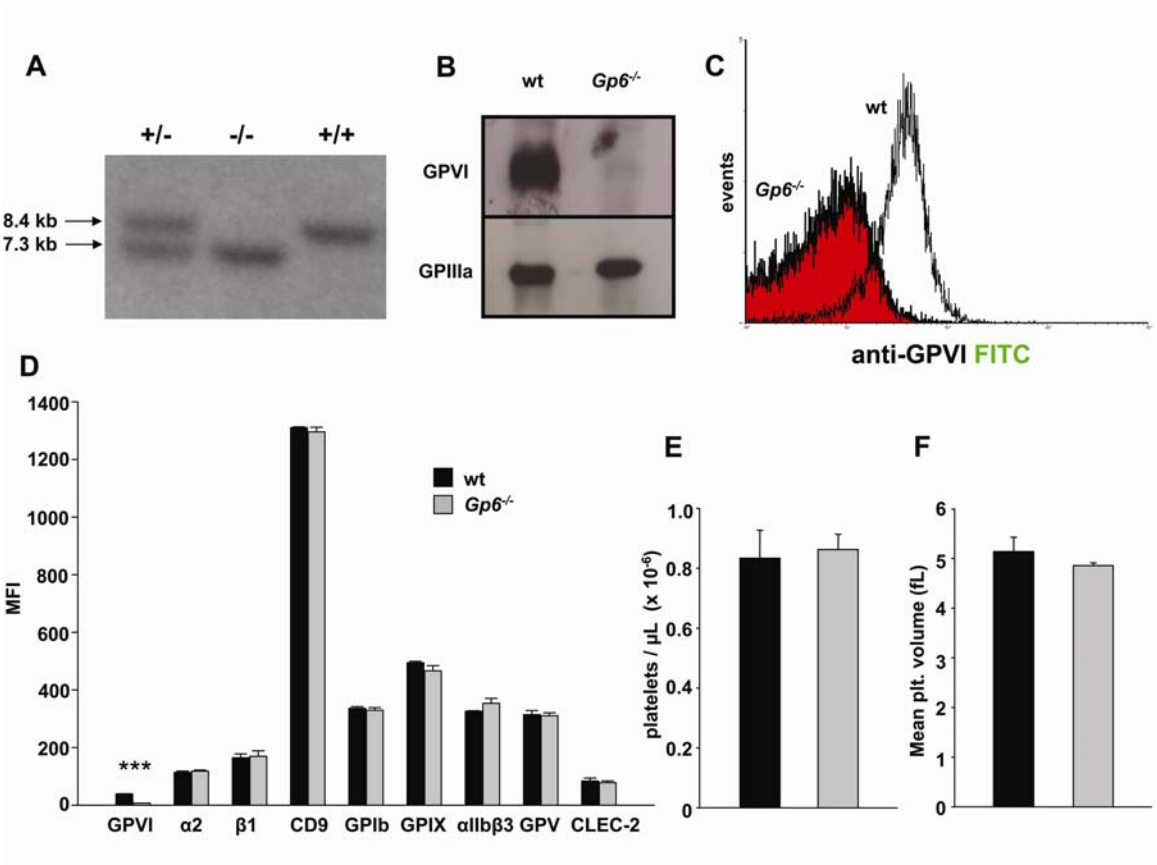

Fig. 37: Analysis of basal parameters of *Gp6*$^{-/-}$ platelets.
(A) Southern blot from tail DNA of wild-type (+/+), heterozygous (+/-) and homozygous (-/-) mice. **(B)** Western blot under non-reducing conditions with JAQ1 antibody conjugated with HRP from platelet lysates of wild-type and knock-out mice. **(C+D)** Flow cytometric analysis of glycoprotein expression. Platelets were stained with the indicated fluorophore-labeled antibodies for 15 minutes and directly analyzed. Results are mean ± SD (*n* = 6 mice per group). ***, *P* < 0.001. **(E)** Platelet count and **(F)** platelet size were determined in a Sysmex cell counter. Results are mean ± SD (*n* = 6 mice per group).

To study the functional consequences of the *Gp6* knock-out, platelet activation studies were performed. The specific GPVI-related activation defect was confirmed by flow cytometric analysis of activated integrin αIIbβ3 using the JON/A-PE antibody (Fig. 38A), and of degranulation-dependent P-selectin surface exposure (Fig. 38B) upon activation with several agonists. Loss of GPVI impaired ITAM-coupled GPVI-specific agonists (CRP, convulxin)-induced integrin activation and degranulation, whereas G protein–coupled agonists and rhodocytin, a ligand of the ITAM-coupled receptor CLEC-2, induced normal activation of GPVI-deficient platelets. *Ex vivo* aggregation studies underlined these results (Fig. 38C). Even at high concentrations of GPVI agonists like collagen, CRP and convulxin neither shape change nor aggregation of platelets occurred. However, *Gp6*$^{-/-}$ platelets aggregated normally in response to G protein-coupled agonists (thrombin, thromboxane analogue U46619).

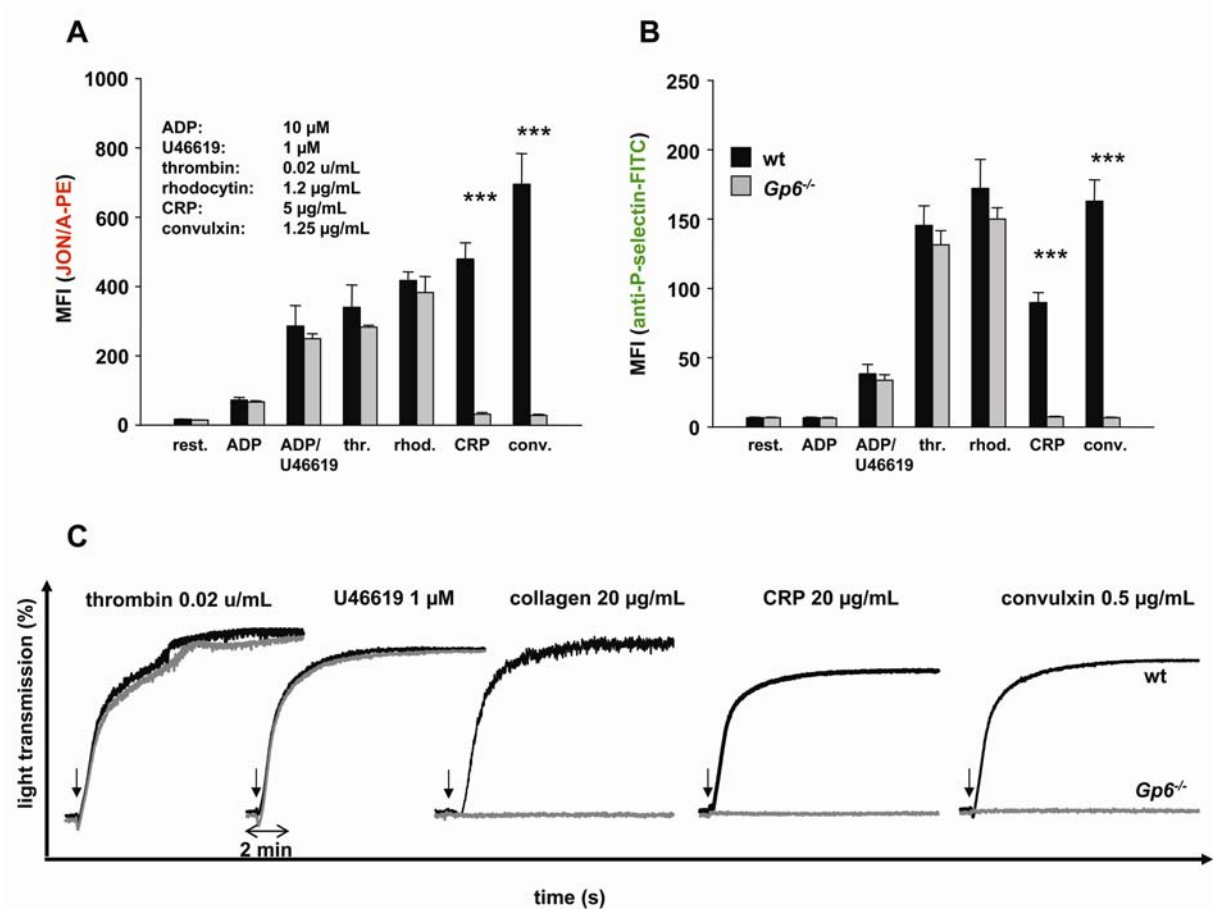

Fig. 38: Defective platelet activation and aggregation of *Gp6*$^{-/-}$ platelets.
Flow cytometric analysis of integrin αIIbβ3 activation (binding of JON/A-PE) **(A)** and degranulation-dependent P-selectin exposure **(B)**. Washed blood was incubated with the indicated agonists for 15 minutes and analyzed on a FACSCalibur. Results are mean ± SD (*n* = 6 mice per group). ***, *P* < 0.001. **(C)** Impaired aggregation of *Gp6*$^{-/-}$ platelets (gray lines) in response to collagen, CRP and convulxin but not to thrombin and U46619 a thromboxane analogue (recording time = 10 min). wt = black lines.

To investigate the role of GPVI in hemostasis and thrombus formation, mice were subjected to different models that serve as a rule for measuring the function in physiological hemostasis and pathological thrombosis. To test a role of GPVI in normal hemostasis, mice were used in a tail bleeding time assay. Here, the tip of a tail was cut and bleeding was determined to have ceased when no blood drop was observed on a filter paper. *Gp6* knock-out mice only displayed a mild bleeding phenotype demonstrating that GPVI-deficiency has no major impact on hemostasis (Fig. 39A). In sharp contrast, *ex vivo* whole blood perfusion (shear rate: 1,000 s^{-1}) over a collagen-coated matrix revealed an essential role in thrombus formation since no thrombi were formed in GPVI-deficient samples (surface coverage: wt: 37.4 ± 5.6%; *Gp6*$^{-/-}$: 5.2 ± 0.6%; Fig. 39B). This supports previous findings with antibody-

induced GPVI-deficient platelets that GPVI is the major collagen platelet-activating receptor. Surprisingly, single platelet adhesion to collagen fibers was observed in contrast to JAQ1-treated mice where no platelet adhesion was found at all[7]. The reason for this discrepancy is under investigation. Next, *Gp6* knock-out mice were challenged in two *in vivo* arterial injury models. In the first model, the abdominal aorta was mechanically injured and blood flow was measured until occlusion of the vessel occurred. The experiment showed that *Gp6* knock-out mice are completely protected against thrombotic occlusion of the vessel since blood flow was maintained throughout the observation period (Fig. 39C). Furthermore, these mice were also protected in a second model, in which $FeCl_3$ was applied on mesenteric arterioles and platelet adhesion and thrombus formation were monitored by *in vivo* fluorescence microscopy (Fig. 39D). Whereas initial platelet adhesion was unaltered in GPVI-deficient mice (Fig. 39D, left), formed thrombi were not stable and embolized which resulted in no vessel occlusion (Fig. 39D, right). This establishes GPVI as an important player in the formation of pathological thrombi, irrespective of the type of injury and size of the vessel.

Basic analyses of *Gp6*$^{-/-}$ mice showed the expected *Gp6* knock-out phenotype. These mice will serve as controls for the planned *GP6* knock-in mice and will be a valuable tool for many other projects. By means of the next section, it should be demonstrated how *Gp6* knock-out mice are going to be used in other projects.

Fig. 39: GPVI deficiency has no impact on bleeding times but on pathological thrombus formation. **(A)** A 1 mm segment of the tail tip was cut with a scalpel and bleeding was determined to have ceased when no blood drop was observed on the filter paper. **(B)** Whole blood in buffer (Tyrode`s with calcium) was perfused over 0.2 mg/mL collagen in a flow chamber with a shear rate of 1,000 s^{-1}. Representative pictures were taken (40x magnification). Mean surface coverage was measured with Metamorph. n = 8 mice; ***, $P < 0.001$. **(C)** The abdominal aorta was mechanically injured using forceps, and blood flow was monitored for 30 min or until complete vessel occlusion occurred. Left: time to occlusion; Right: representative experiment. **(D)** Mesenteric arterioles were treated with 20% $FeCl_3$, adhesion and thrombus formation of fluorescently labeled platelets were monitored by *in vivo* fluorescence microscopy. Representative images (lower panel) and statistical evaluation of the time to first appearance of a thrombus (upper left) and to occlusion (upper right) are depicted. Asterisk indicates complete occlusion of the vessel.

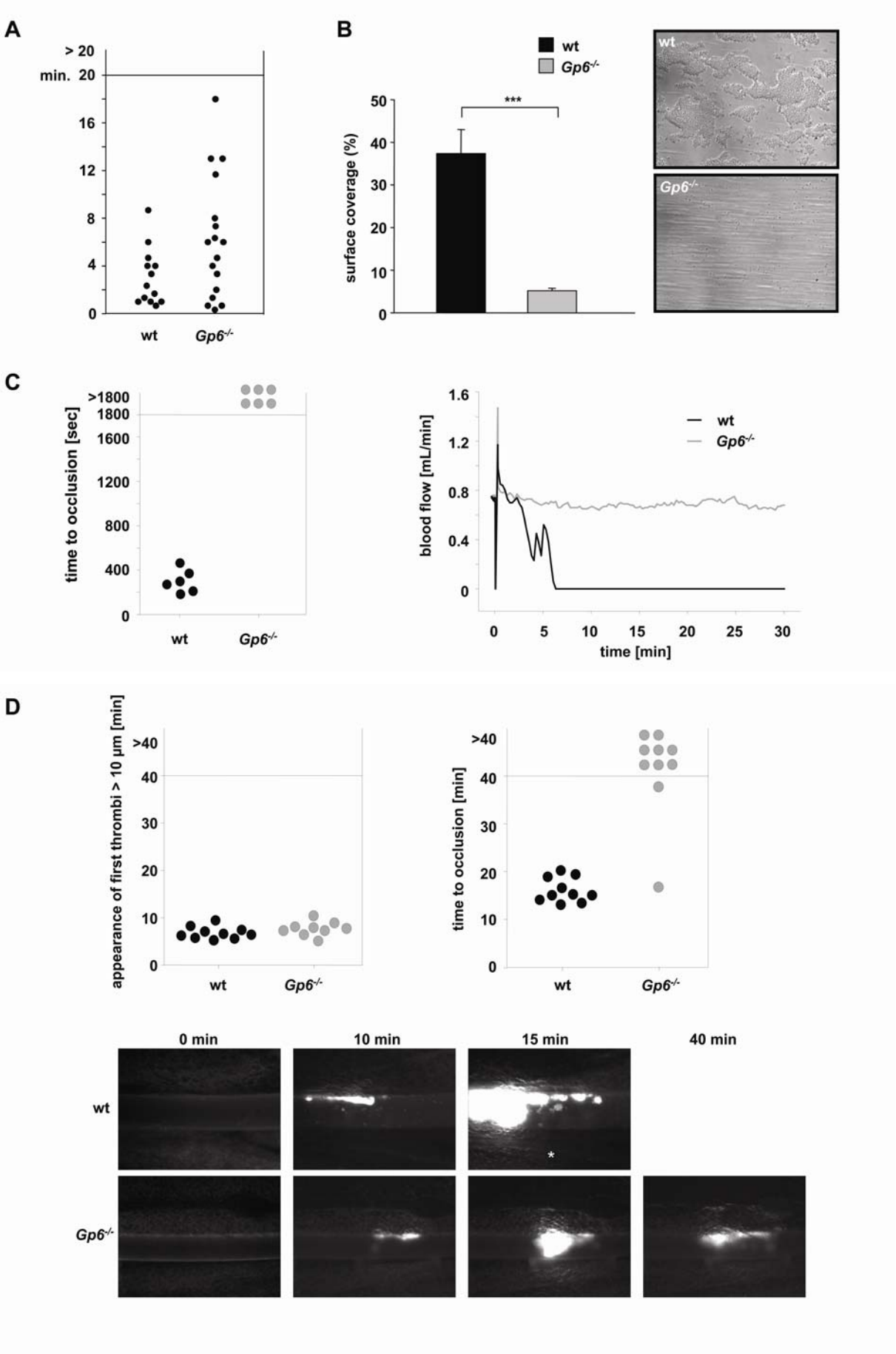
A
> 20
min. 20
16
12
8
4
0
wt
Gp6-/-
B
wt
Gp6-/-
***
surface coverage (%)
50
40
30
20
10
0
wt
Gp6-/-
C
time to occlusion [sec]
>1800
1800
1600
1200
800
400
0
wt
Gp6-/-
blood flow [mL/min]
1.6
1.2
0.8
0.4
0
wt
Gp6-/-
0
5
10
15
20
25
30
time [min]
D
appearance of first thrombi > 10 µm [min]
>40
40
30
20
10
0
wt
Gp6-/-
time to occlusion [min]
>40
40
30
20
10
0
wt
Gp6-/-
0 min
10 min
15 min
40 min
wt
Gp6-/-
*

C.2.6. Analysis of *Gp6* knock-out/CLEC-2 depleted mice

Besides GPVI, mouse platelets express a second ITAM-coupled receptor named CLEC-2 (C-type lectin-like receptor 2). CLEC-2 is a recently identified platelet-activating receptor. Rhodocytin, a snake venom toxin purified from the venom of *Calloselasma rhodostoma*, was demonstrated to be a ligand for CLEC-2, which induces potent platelet activation[137]. The physiological ligand of CLEC-2 has remained elusive. May *et al.* very recently showed that, similar to GPVI depletion achieved by treatment of mice with JAQ1, CLEC-2 can be depleted from the platelet surface by INU1 treatment resulting in CLEC-2-deficient mice. These mice showed defective aggregate formation *in vitro* and *in vivo*, variable and increased bleeding times and profound protection against arterial thrombus formation suggesting that down-regulation of the receptor could be of therapeutical importance[130].

Together with Frauke May, *Gp6*$^{-/-}$ mice, in which the CLEC-2 receptor was additionally depleted, were analyzed to determine the effect of a double knock-out-like phenotype.

To test the functional consequences of the absence of both ITAM-coupled receptors in platelets, *Gp6* knock-out mice were injected with 200 µg INU1 and after five days the double-deficient mice were analyzed.

Flow cytometric analysis confirmed the absence of both surface proteins, whereas the expression of other analyzed receptors was not affected (Fig. 40A). After transient thrombocytopenia induced by INU1 injection, the platelet count returned to normal with platelets only slightly increased in platelet size at day five (Fig. 40B+C). Platelet activation analysis by flow cytometry revealed an additive activation defect (Fig. 40D+E). Only ITAM-coupled receptor agonist-induced activation pathways were impaired (e.g. rhodocytin, CRP and convulxin), whereas G protein-coupled agonist pathways were unaffected (e.g. thrombin, thromboxane A2 and ADP) demonstrating that the absence of GPVI and CLEC-2 resulted in the expected phenotype without affecting other pathways.

To test the effect of GPVI/CLEC-2-deficiency on hemostasis, mice were subjected to the tail bleeding time assay. Hemostasis was dramatically impaired in GPVI/CLEC-2-deficient mice. Whereas *Gp6* knock-out mice have a mild and CLEC-2 depleted mice a variable and increased bleeding phenotype, double-deficient mice were not able to arrest bleeding in the 20 minutes observation period suggesting an additive function of both receptors in hemostasis (Fig. 41A).

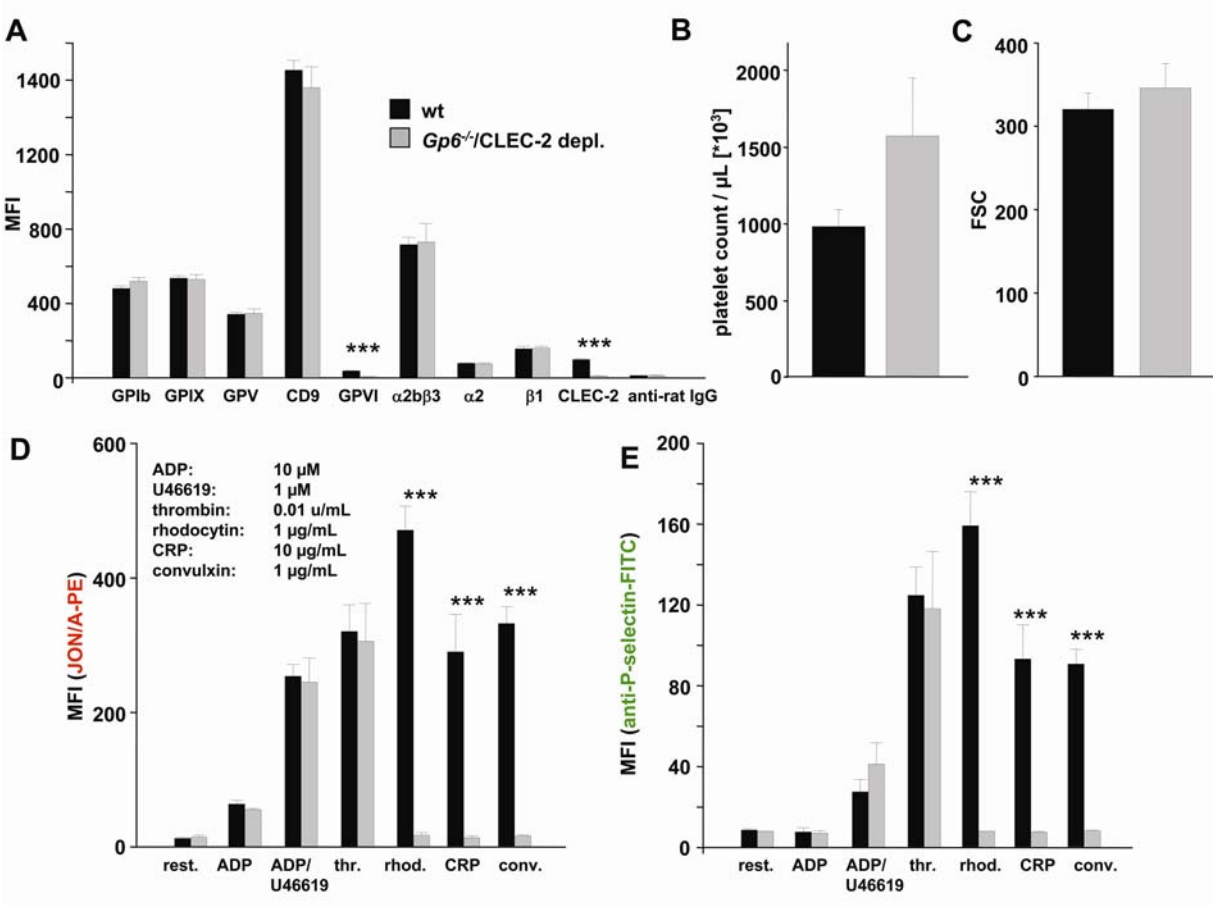

Fig. 40: Additive platelet activation defect in GPVI/CLEC-2-deficient mice.
(A) Flow cytometric analysis of glycoprotein expression. Platelets were stained with the indicated fluorophore-labeled antibodies for 15 minutes and directly analyzed. Results are mean ± SD (*n* = 6 mice per group). ***, P < 0.001. **(B+C)** Platelet count and size was determined by flow cytometry. Results are mean ± SD (*n* = 9 mice per group). **(D+E)** Flow cytometric analysis of integrin αIIbβ3 activation (binding of JON/A-PE; **(D)**) and degranulation-dependent P-selectin exposure **(E)**. Washed blood was incubated with the indicated agonists for 15 minutes and analyzed on a FACSCalibur. Results are mean ± SD (*n* = 6 mice per group). ***, *P* < 0.001.

Next, double-deficient mice were analyzed in the whole blood perfusion system. Here, the flow chamber experiments again showed a lack of thrombus formation resembling the *Gp6* knock-out phenotype (surface coverage: wt 41.3 ± 3.2%, double-deficient: 1.5 ± 0.8%; Fig. 41B). Interestingly, no platelet adhesion on collagen fibers was observed similar to results obtained with the anti-GPVI JAQ1 antibody treated mice[7]. Whether this is due to antibody injection (JAQ1 or INU1) is still under investigation.

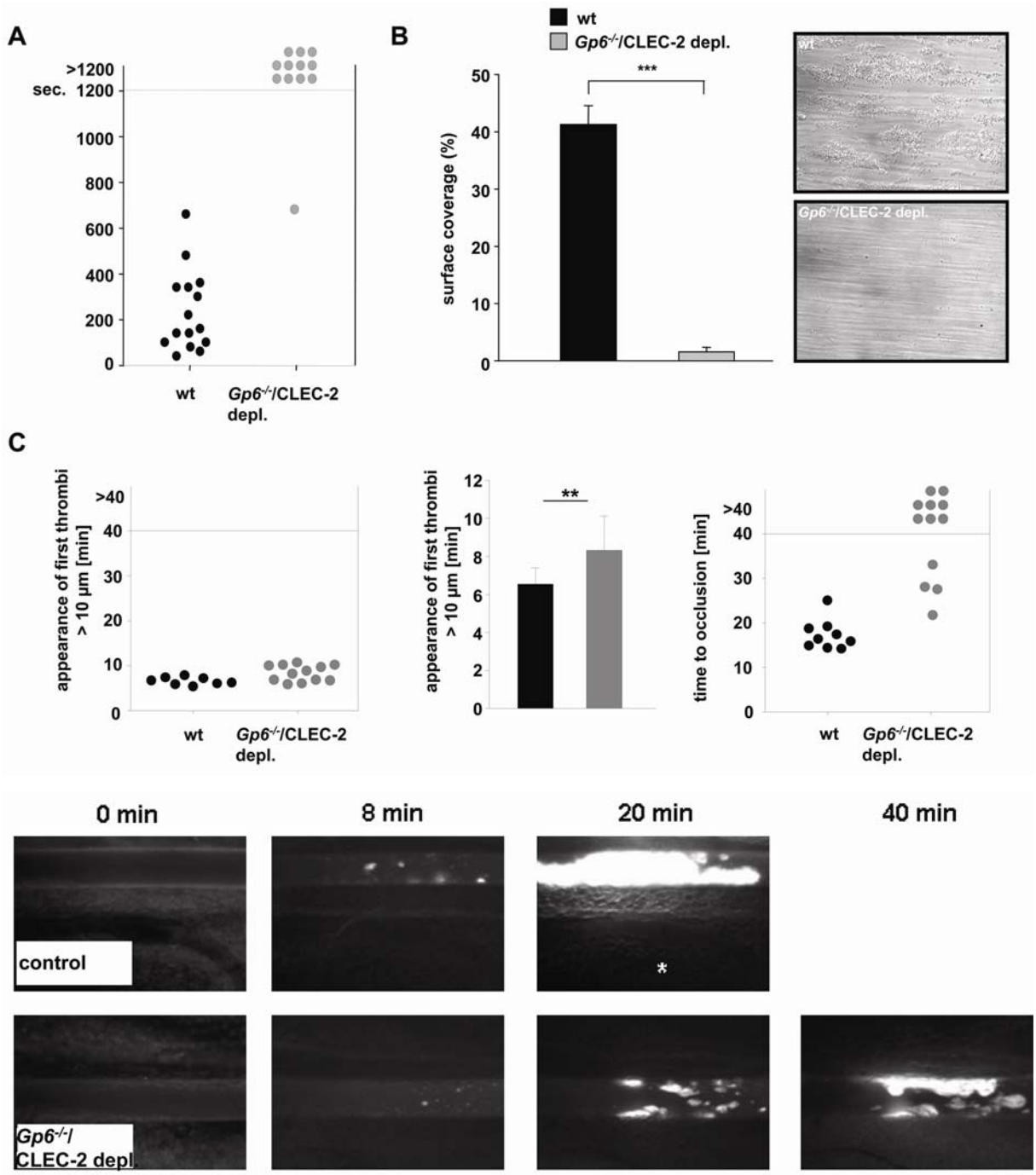

Fig. 41: Defective hemostasis and thrombus formation in GPVI/CLEC-2-deficient mice.
(A) A 1 mm segment of the tail tip was cut with a scalpel and bleeding was determined as ceased when no blood drop was observed on a whatman paper. Bleeding longer than 20 minutes was stopped manually. **(B)** Whole blood in buffer (Tyrode`s with calcium) was perfused over 0.2 mg/mL collagen in a flow chamber with a shear rate of 1,000 s^{-1}. Representative pictures were taken (40x magnification). Mean surface coverage was measured with the Metamorph software. *n* = 8 mice; ***, *P* < 0.001. **(C)** Mesenteric arterioles were treated with 20% $FeCl_3$, and appearance of first thrombi > 10 µm (upper panel: left and middle) and time to vessel occlusion (upper panel: right) were monitored by *in vivo* fluorescence microscopy and analyzed. Representative images are shown (lower panel). Asterisk indicates complete occlusion of the vessel.

Finally, mice were challenged in the *in vivo* $FeCl_3$ arterial thrombosis model. Here, in addition to a lack of vessel occlusion, a significant delay in the onset of thrombus formation was observed as compared to wild-type controls (Fig. 41C).
In an ongoing study, mice depleted in GPVI and CLEC-2 after antibody injection of JAQ1 and INU1, respectively, are being analyzed. Preliminary data revealed that both receptors can be down-regulated at the same time and the obtained results are similar to those of the *Gp6* knock-out/CLEC-2 depleted mice (not shown).

C.2.7. Construction of a targeting vector for the generation of conditional *Adam10* knock-out mice

Deficiency in ADAM10 is embryonic lethal as shown by Hartmann *et al.*[101]. Therefore, a conditional approach (loxP) was used to specifically delete *Adam10* in various tissues upon mating with different Cre-transgenic mice.

C.2.7.1. Identification of the mouse *Adam10* gene

To generate a targeting construct for conditional knock-out mice, a RPCI-22 mouse bacterial artificial chromosome (BAC) library was screened which represents the genome of the SV129 mouse strain. Using a radioactively labeled exon 2 DNA fragment as an *Adam10* gene specific probe, BAC clones possibly containing the *Adam10* region were identified. BAC clones were verified by PCR using exon 2 specific primers and by physical mapping via Southern blotting (not shown). The BAC clone RP22-299D1 was identified containing the *Adam10* gene and used for amplification of the homologous arms.

C.2.7.2. Targeting strategy for the generation of conditional (loxP) *Adam10* knock-out mice

Figure 42 depicts the strategy to target the *Adam10* gene. Exon 2 is flanked by loxP sites to induce a site-specific deletion of *Adam10* after recombination of the loxP sites mediated by a Cre recombinase. Deletion of exon 2 results in a frame shift mutation. A neomycin cassette flanked by FRT sites is inserted upstream of exon 2 which leads to a constitutive knock-out of *Adam10*. The neomycin cassette can be removed after recombination with a FLP recombinase.

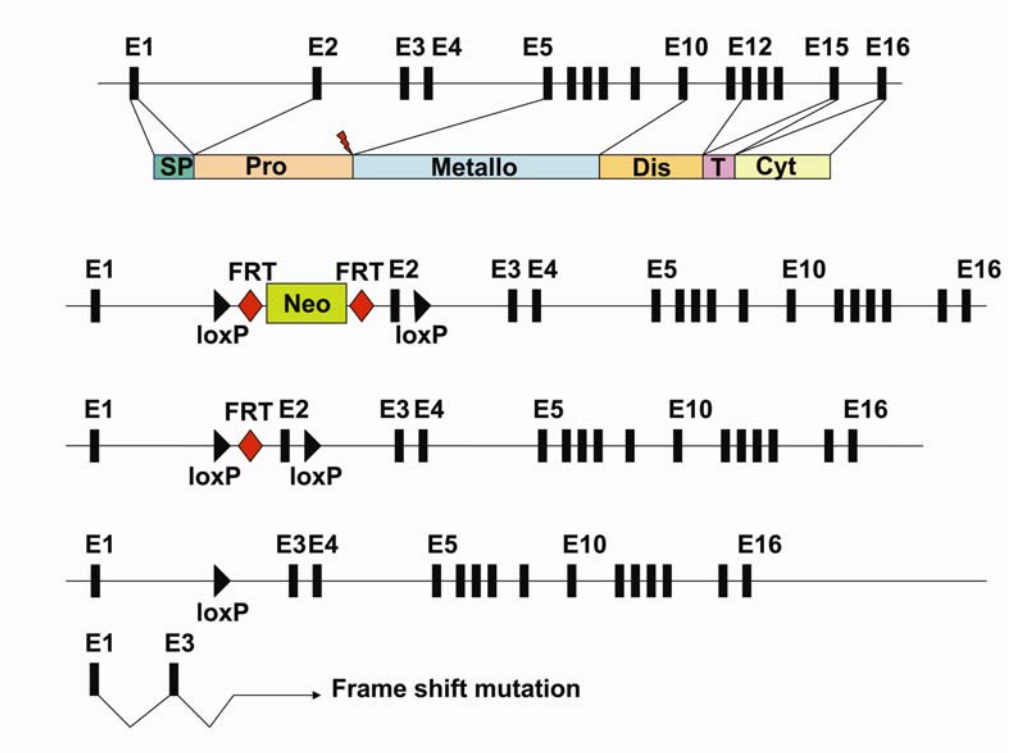

Fig. 42: Targeting strategy of the mouse *Adam10* gene.
The gene structure of mouse *Adam10* is displayed. Exons (E1 to E16) are indicated as black boxes. Introns are labeled with a line. Domain structures and motifs are labeled according to the coded exons (SP: signal peptide; Pro: prodomain; Metallo: metalloprotease domain; Dis: disintegrin domain; T: transmembrane domain; Cyt: cytoplasmic domain). The FLP recombinase mediates the recombination of the FRT sites (red) and consequently to a deletion of the neomycin cassette (green box). The Cre recombinase mediates a recombination of the loxP sites (black triangle) and thus, exon 2 is removed. The consequence is a frame shift mutation downstream of exon 3.

C.2.7.3. Amplification and subcloning of the homologous arms

The 5´ arm of the *Adam10* construct containing a part of intron 1 was amplified with the primers 5´-AAAGCGGCCGCGTCTGGATGTCTCTCAATC-3´ (forward) and 5´-AAAGCGGCCGCATATGGCGATGCATGCCTTT-3´ (reverse) resulting in a 4 kb product. The primers were designed to introduce enzyme sites (Forward primer: *Not*I and reverse primer: *Not*I). This fragment was ligated via blunt-end ligation into a pKS vector. In order to confirm successful cloning, the 5´ arm in the pKS vector was digested with different enzymes and loaded on an agarose gel (Fig. 43). The expected size of DNA fragments was confirmed. Additionally, the 5´ arm was sequenced and no mutations were observed (data not shown).

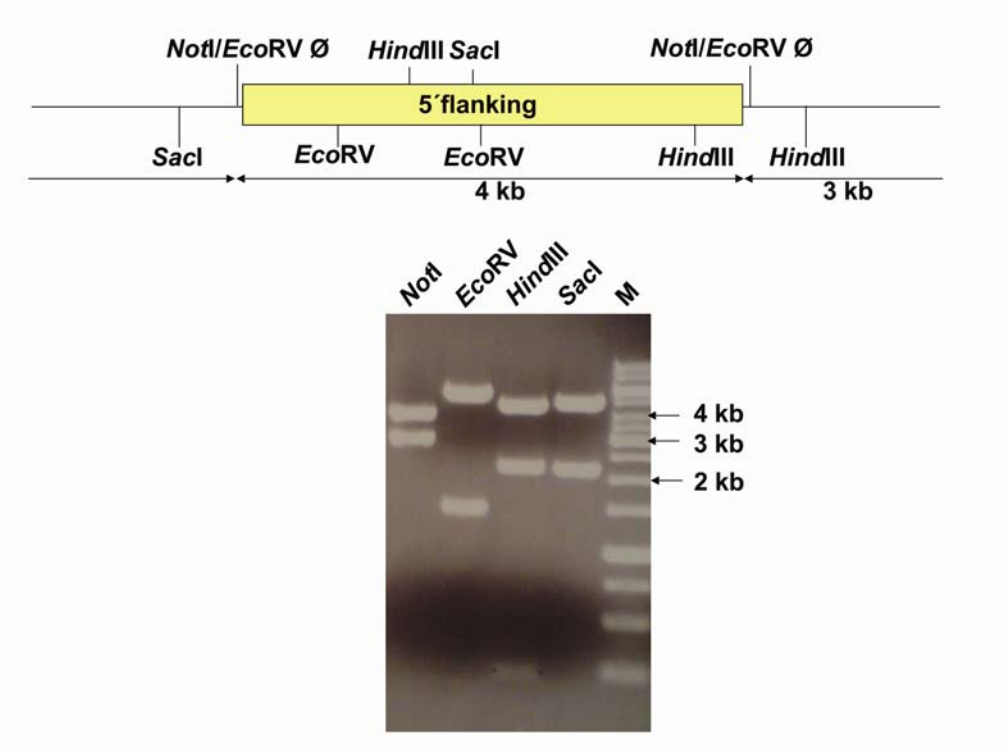

Fig. 43: Digestion of the subcloned 5´ arm in the pKS vector.
Upper panel: The 5` arm and the vector are represented by the yellow bar and the thin horizontal line, respectively. The insert and the vector consist of 7 kb. Enzyme sites used for digestion are indicated. The *Eco*RV site was deleted (Ø). **Lower panel:** The digested samples were separated on an agarose gel and compared with the expected band sizes.

The 3´ arm with a length of about 2.3 kb was amplified with the primers 5´-AAACTCGAGAGATAAGACATACTTTATTT-3´ (forward) and 5´-AAAGTCGACTTCTTACATAGCTTCATCAC-3´ (reverse). These primers were also designed to introduce enzyme sites (Forward primer: *Xho*I and reverse primer: *Sal*I). The introduction of the consensus sequences of *Xho*I and *Sal*I enzymes at the ends of the 3´ arm was crucial for the ligation of the 3´ arm into the targeting vector. Again, this fragment was ligated via blunt-end ligation into a pKS vector. Restriction endonucleases (*Xho*I, *Sal*I, *Bam*HI and *Eco*RI) were chosen to digest the subcloned 3´ arm (Fig. 44). Again, the product was sequenced confirming the amplification of the *Adam10* product (not shown).

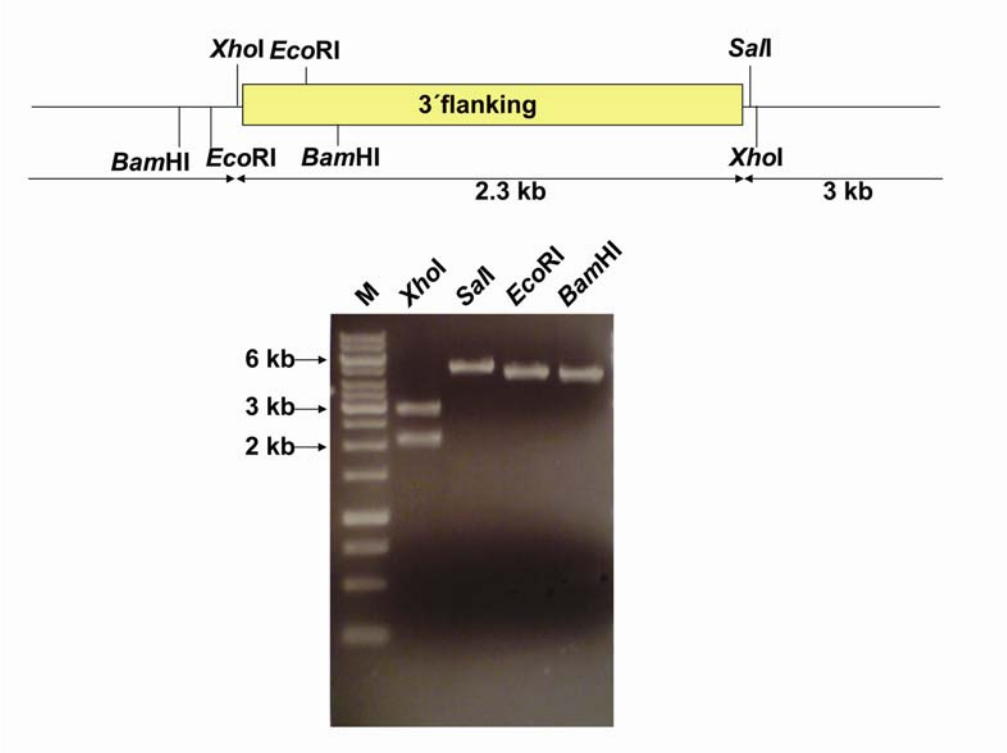

Fig. 44: Cloning of the 3´ arm into the pKS vector.
Upper panel: The 3` arm and the vector are represented by the yellow bar and the thin horizontal line, respectively. The insert and the vector consist of 5.3 kb. Enzymes sites used for digestion are indicated. **Lower panel:** The digested samples were separated on an agarose gel and the band sizes were compared with the predicted band sizes.

C.2.7.4. Amplification and subcloning of *Adam10* exon 2

Exon 2 with flanking intron sequences was amplified with the primers 5´-AAAGGATCCCTCGAGTGTCACTCTTACAACAATAAG-3´ (forward) and 5´-AAAGGATCCGGCTCCTCACATTTTCTA-3´ (reverse) resulting in a product of approximately 700 bp. The introduction of the consensus sequences of *Bam*HI and *Xho*I in the forward primer and a *Bam*HI enzyme site in the reverse primer were useful for the following ligation steps. This sequence was inserted into a pKS vector containing a loxP site. To confirm successful cloning, different enzymes were chosen for digestion of the vector (Fig. 45).

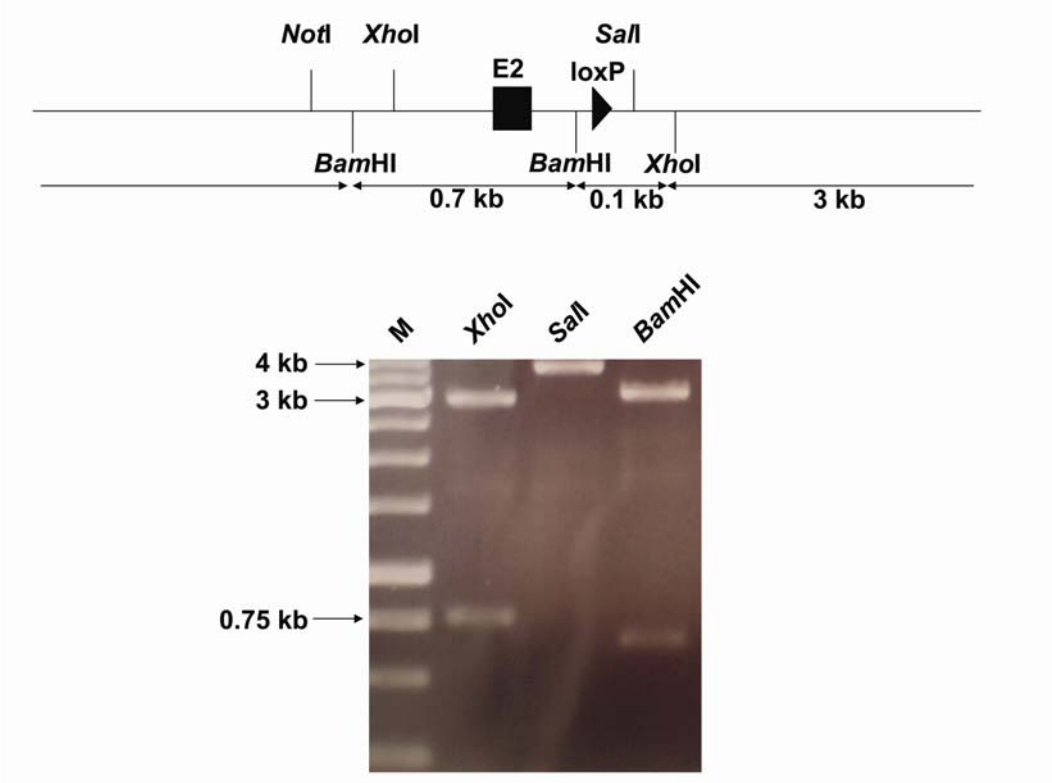

Fig. 45: Cloning of exon 2 into the pKS vector.
Upper panel: Scheme of the vector. Enzymes sites used for digestion are indicated. **Lower panel:** The digested samples were separated on an agarose gel and the band sizes were compared with the predicted band sizes.

C.2.7.5. Cloning of the final *Adam10* targeting vector

A vector containing a neomycin cassette and FRT sites was used to construct the final targeting vector. Therefore, following ligation steps were performed: first, exon 2 was ligated into the final vector, then, the subcloned 3´ arm was inserted, followed by cloning the 5´ arm into the final vector. Finally, a thymidine kinase cassette was inserted downstream of the 3´ arm to use this optionally as a second selection marker during selection of the embryonic stem cells. Fig. 46 displays the final *Adam10* targeting vector that was used for electroporation. In addition to sequencing (not shown), different enzymes were used to confirm successful cloning.

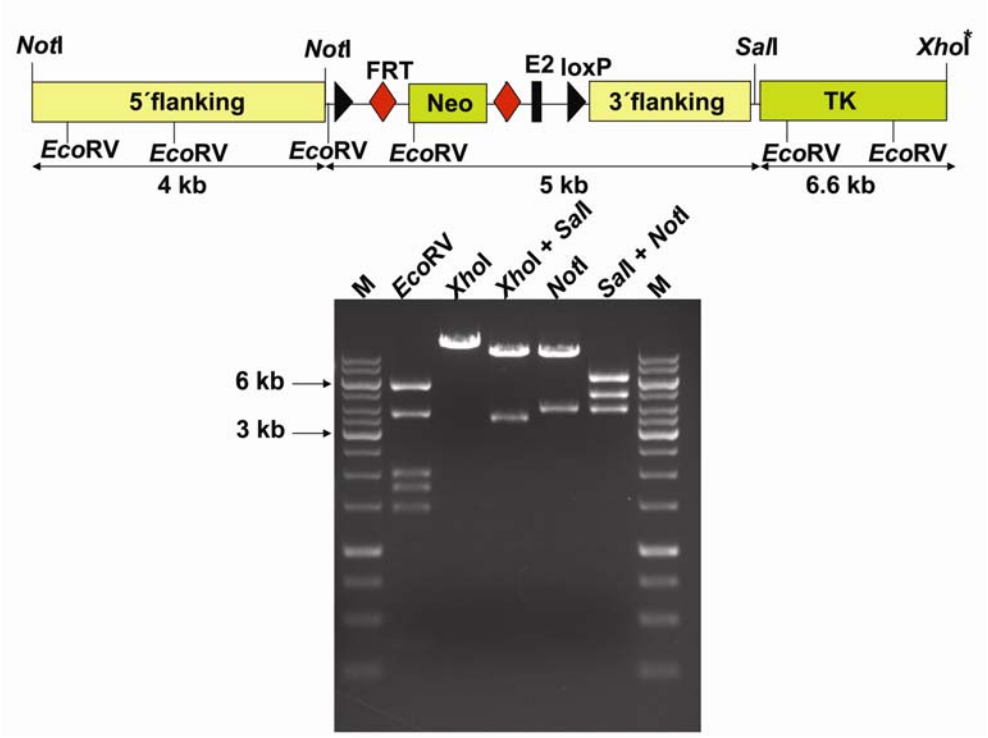

Fig. 46: Final targeting *Adam10* vector.
Upper panel: Scheme of the final vector. Enzymes used for digestion are indicated. **Lower panel:** The digested samples were separated on an agarose gel and the band sizes were compared with the predicted band sizes.

C.2.8. Electroporation of the *Adam10* targeting vector into ES cells and analysis of selected ES cell clones

An external probe (generated by PCR using the primers: 5´-CAGTGATTGGATTATGGCT-3´ (forward); 5´-CCCTTGATTTCCACAGCTGG-3´ (reverse); 2 kb length) was used that recognizes a sequence in intron 1. Fig. 47 depicts that the external probe recognizes for the wt allele a 13.5 kb band, whereas a band of 9.5 kb is detected for the floxed allele after digestion with *Pst*I.

The final vector was linearized with the *Xho*I enzyme and electroporated into the SV 129/R1 ES cells. Isolated DNA of neomycin resistant stem cells was digested with concentrated *Pst*I enzyme and size-fractionated on an agarose gel. Subsequently, the DNA was transferred onto a nitrocellulose membrane and hybridized with the radioactively labeled external probe. The X-ray film was exposed to the Southern blot membranes and visualized bands of the obtained ES clones were analyzed (Fig. 47). In total 384 picked stem cell clones were analyzed. One positive clone with the number 228 was obtained after *Pst*I digestion. The positive stem cell clone was

recultured, tested for Mycoplasm contamination by PCR and injected into C57BL/6 blastocysts.

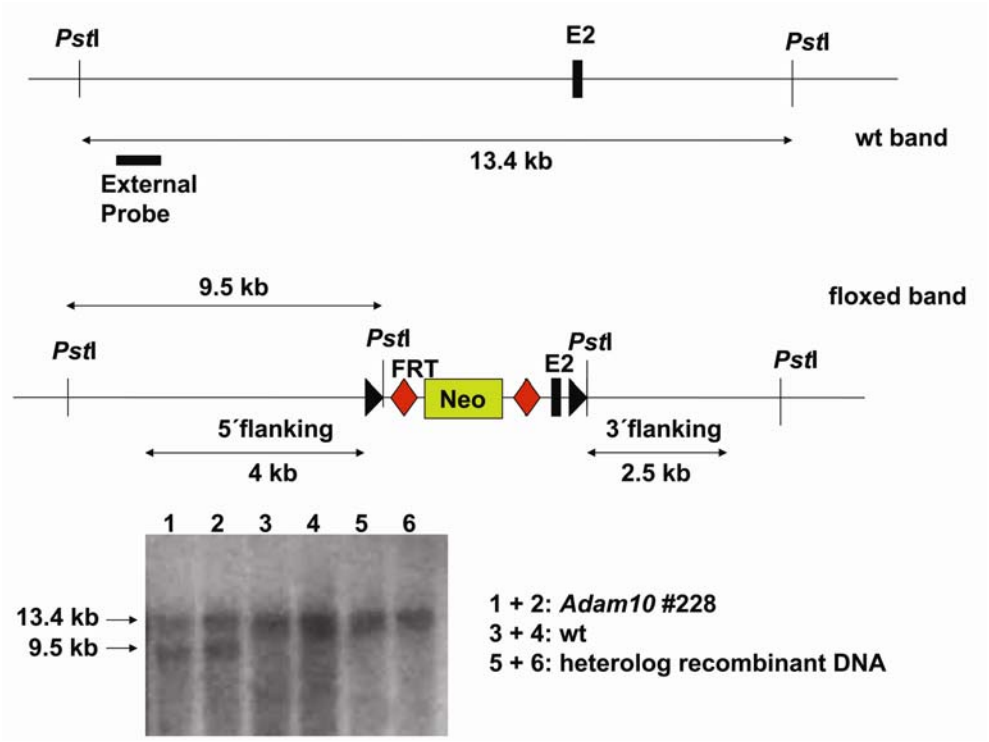

Fig. 47: Analysis of neomycin-resistant stem cell clones.
The scheme (upper panel) depicts detection of wild-type and floxed alleles. The external probe (black horizontal bar) recognizes a sequence upstream of exon 2. Exon 2 is represented as a black vertical bar. The wild-type band between two *Pst*I sites is about 13.4 kb, whereas the floxed band recognized by the external probe is about 9.5 kb. In the lower panel, stem cell DNA was digested with *Pst*I and labeled with the external probe. The positive stem cell clone showed the expected band sizes.

C.2.9. *Adam10* chimeric mice

The following *Adam10* chimeric mice were obtained:

Adam10 chimeric mice:

Gender	Chimerism
male	100%, 100%, 75%, 60%, 30%
female	-

These highly chimeric mice were crossed with female C57BL/6J mice to achieve germline transmission.

C.2.10. Megakaryocyte/platelet-specific ADAM10 deficiency has no impact on platelet production

Germline transmission was obtained as crossing of chimeric mice with C57BL/6 mice resulted in birth of *Adam10*$^{wt/fl}$ mice. To test the genotype after crossing of heterozygous mice, Southern blotting (Fig. 48A) was performed revealing that wild-type, heterozygous and homozygous mice were obtained in a Mendelian ratio (not shown). To study the effect of ADAM10 deficiency on megakaryocytes and platelets, *Adam10*$^{fl/fl}$ mice were crossed with mice carrying the Cre recombinase under the platelet factor 4 (PF4) promoter. Thus, ADAM10 deficiency is restricted to megakaryocytes and platelets. To obtain *Adam10*$^{fl/fl,\ PF4\text{-}Cre}$ (referred to as ADAM10-deficient) mice, a crossing over had to occur as both genes, *Adam10* and *PF4-Cre*, are located on the same chromosome (chromosome 9). After ADAM10-deficient mice were obtained, the absence of the protein was shown by Western blot analysis (Fig. 48B) of platelet lysates. Platelet count of ADAM10-deficient mice was similar to control mice (Fig. 48C). In addition, the expression of prominent platelet surface proteins was not altered (Fig. 48D). This demonstrates that ADAM10 is dispensable for normal platelet production and it does not seem to be a constitutive sheddase of platelet surface receptors.

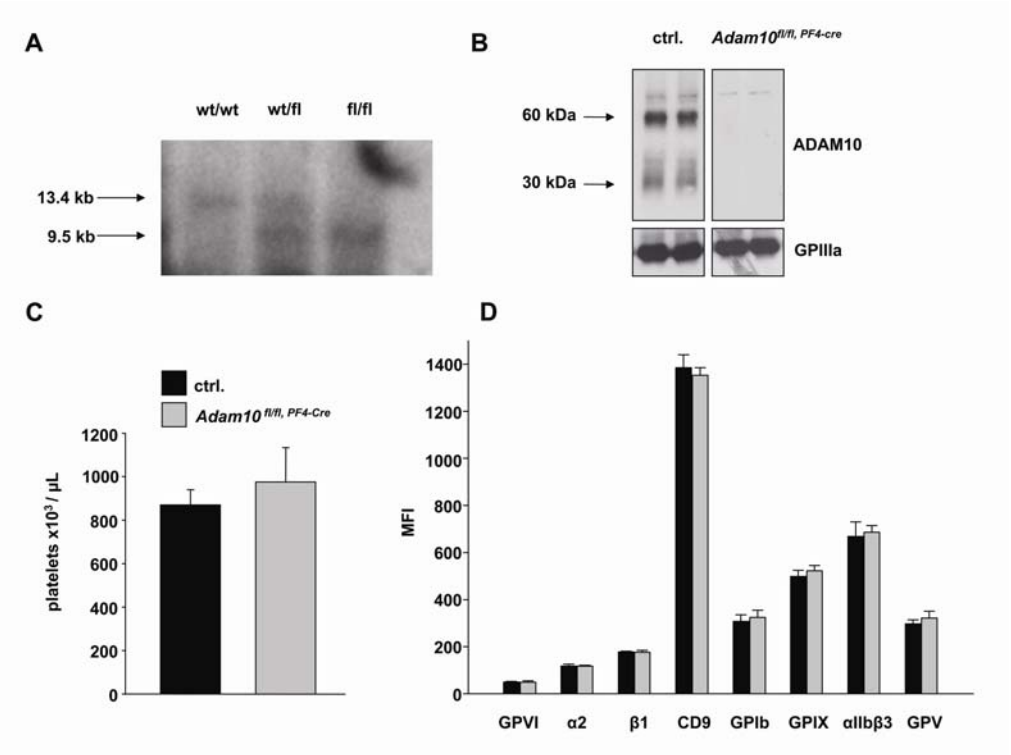

Fig. 48: Analysis of basal platelet parameters of *Adam10*$^{fl/fl,\ PF4\text{-}Cre}$ mice.
(A) Southern blot from tail DNA of wild-type (wt/wt), heterozygous (wt/fl) and homozygous (fl/fl) mice. **(B)** Western blot of platelet lysates from control and *Adam10*$^{fl/fl,\ PF4\text{-}Cre}$ mice. **(C+D)** Flow cytometric

analysis of platelet count and glycoprotein expression. Platelets were stained with the indicated fluorophore-labeled antibodies for 15 minutes and analyzed directly. Results are mean ± SD (*n* = 4 mice per group, representative for 3 individual experiments).

C.2.11. Low TACE mice show increased GPIb expression on platelets

Adam17 knock-out mice die between day 17.5 of embryonic development or perinatally[104;107]. Chalaris *et al.* (unpublished) used a different approach named EXITS (exon induced translational stop) to analyze ADAM17-deficient mice. With this, a new exon within the *Adam17* gene was introduced which starts with an in-frame translational stop codon. This strategy enables the investigators to study ADAM17 function in adult mice (referred to as low TACE (*Adam17*$^{ex/ex}$) mice)). As the data are unpublished, no details about the phenotype of the low TACE mice will be reported in this thesis. In collaboration, these mice were used for studying the role of TACE in regulation of platelet surface receptors. Bone marrow of low TACE mice was transferred to lethally irradiated recipient C57BL/6 mice. Bone marrow chimeric mice were used for all experiments performed in this project.

To determine whether low TACE mice are useful to study platelet receptor regulation, the GPIb expression level on platelets was measured. It was described that TACE is a constitutive sheddase of GPIb that can be used as a marker for platelet aging[120]. The GPIb expression rate was markedly increased on platelets of low TACE, but not of control and ADAM10-deficient mice (Fig. 49A+48D). These results were confirmed by measuring GPIb levels in the plasma of control and mutant mice. Here, the level of cleaved GPIb (glycocalicin) was decreased in plasma of low TACE mice as measured by ELISA (Fig. 49B) and Western blot (Fig. 49C). These results again underline the role of TACE in constitutive shedding of the platelet receptor GPIb and demonstrate that the low TACE mice are useful to study platelet receptor regulation.

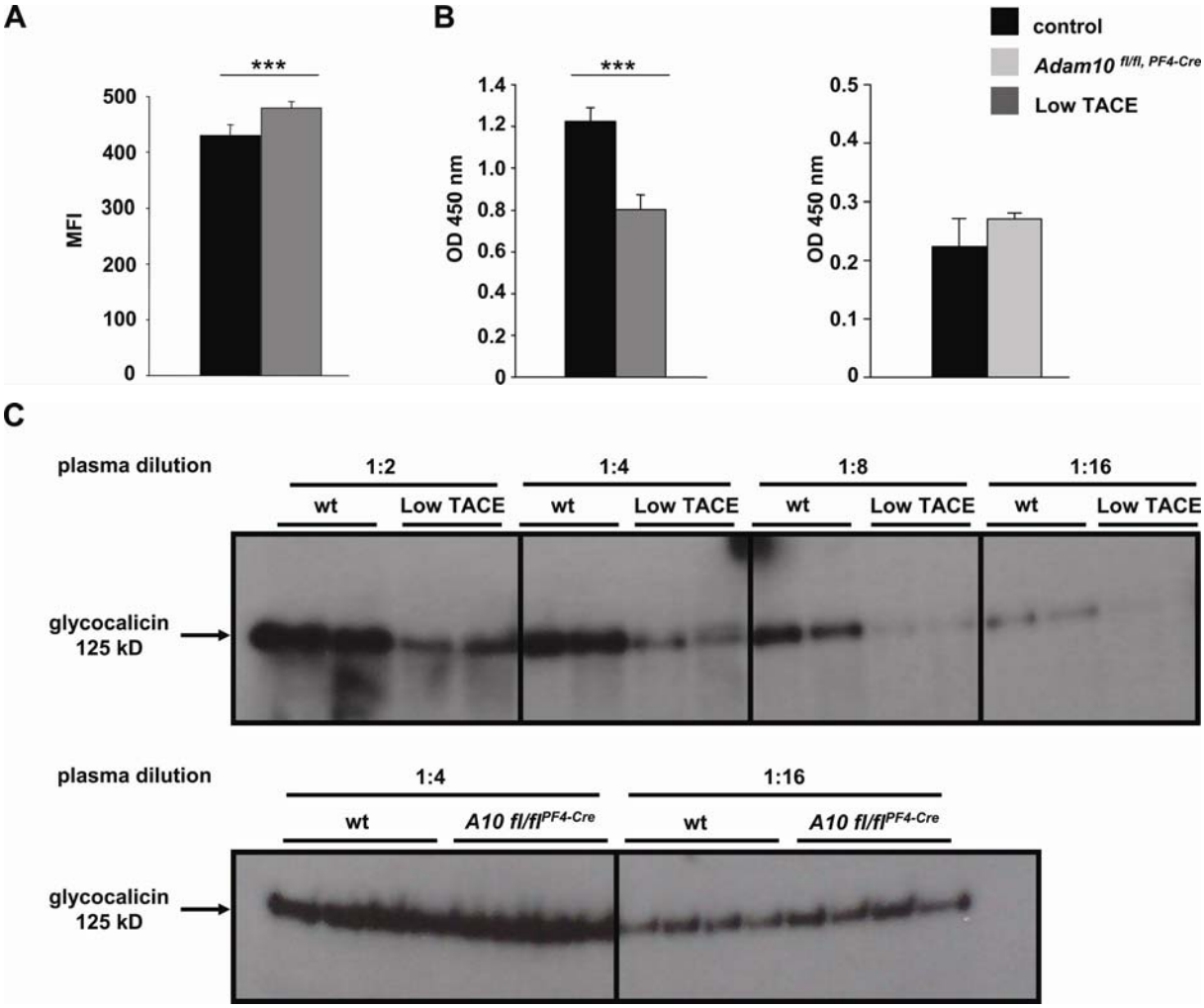

Fig. 49: TACE, but not ADAM10, constitutively cleaves platelet GPIb.
(A) Flow cytometric analysis of GPIb expression. Platelets were stained with a fluorophore-labeled antibody recognizing GPIb for 15 minutes and directly analyzed. Results are mean ± SD (*n* = 12 mice per group). **(B)** GPIb levels in plasma were determined by ELISA as described in Materials and Methods. Results are mean ± SD (*n* = 4 mice per group, representative for two individual experiments). **(C)** Western blot from plasma of wild-type and mutant mice. Plasma dilution is indicated. ***, $P < 0.001$.

C.2.12. GPVI is differentially regulated by ADAM10 and ADAM17 *in vitro*

In contrast to GPIb, the sheddase of GPVI has remained elusive. Two possible candidates are currently under discussion in the literature, namely the metalloproteinases ADAM10 and 17. Therefore, shedding of GPVI was investigated in ADAM10-deficient and low TACE mice.

For this, platelets were incubated with different shedding-inducing reagents and glycoprotein expression was measured by flow cytometry. Treatment of platelets with the calmodulin-inhibitor W7, and the protease-activating agent NEM, revealed that GPIb is exclusively cleaved by TACE, whereas GPV is down-regulated in both

mutant mice suggesting both metalloproteinases to be involved in GPV shedding (Fig. 50). The expression rate of GPVI was either unaltered upon W7 incubation or only slightly decreased upon NEM treatment, respectively, in ADAM10-deficient mice. These results show that ADAM10 is the sheddase of GPVI *in vitro* after incubation with W7 or NEM.

However, treatment with CCCP, a substance that leads to damage of mitochondria, revealed that under these conditions, TACE, but not ADAM10, is the sheddase for GPIb, GPV and surprisingly for GPVI (Fig. 50).

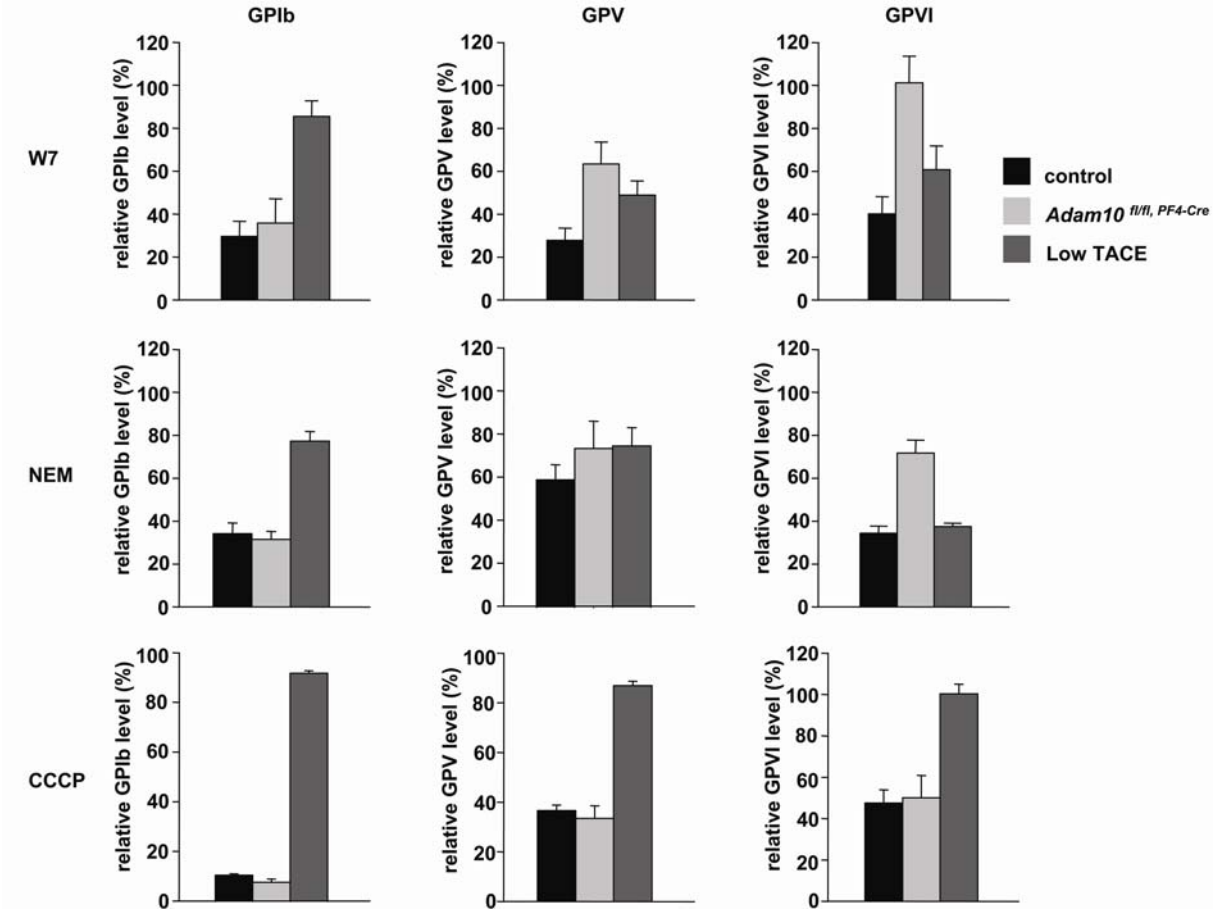

Fig. 50: Studies in flow cytometry: GPVI is differentially regulated *in vitro*.
Platelets were treated with the indicated reagents (W7: 150 µM, 1h at 37°C; NEM: 2 mM, 20 min at 37°C; CCCP: 100 µM, 1h at 37°C), stained with a fluorophore-labeled antibody recognizing the indicated glycoprotein for 15 minutes and directly analyzed. Results are mean ± SD (*n* = 4 mice per group, representative for 2 individual experiments).

The results of GPVI shedding were confirmed by detection of cleaved GPVI in an ELISA system (Fig. 51). Again, ADAM10 was able to proteolytically cleave GPVI upon incubation with W7, whereas CCCP-induced shedding of GPVI was mediated by TACE (ADAM17). These data demonstrate that GPVI can be cleaved by ADAM10

or TACE *in vitro* depending on the shedding-inducing reagent and most likely on different metalloprotease-activating pathways.

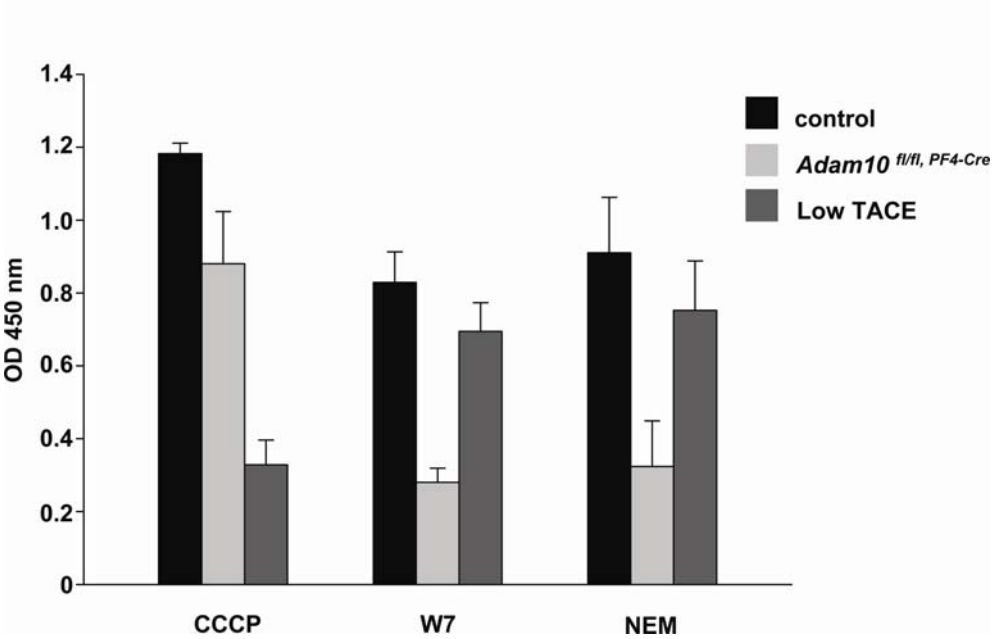

Fig. 51: ELISA: GPVI is differentially regulated *in vitro*.
Platelets were treated with CCCP (100 µM) or W7 (150 µM) for 1 h at 37°C or NEM (2 mM) for 20 min at 37°C and cleaved GPVI was detected in an ELISA system.

C.2.13. GPVI is cleaved *in vivo* in ADAM10-deficient and low TACE mice

To study GPVI regulation *in vivo*, biotinylated anti-GPVI antibody JAQ1 (100 µg), described to induce shedding of the receptor *in vivo*[82;85], was injected into control and mutant mice. After 30 minutes and 3 hours, platelet count, GPVI expression and cleaved GPVI levels in plasma were measured in both control and mutant mice. Interestingly, in control and mutant mice GPVI was down-regulated from the platelet surface (Fig. 52B) and thrombocytopenia (Fig. 52A) was observed in all analyzed mouse strains. In addition, preliminary data showed that similar levels of cleaved GPVI in plasma were detected in control and mutant mice (Fig. 52C).

In summary, upon anti-GPVI JAQ1 antibody injection GPVI is cleaved in both mutant mouse lines suggesting that neither ADAM10 nor TACE alone is the exclusive sheddase of GPVI *in vivo*. Either ADAM10 and TACE are able to cleave GPVI and can compensate each other or another metalloproteinase is exclusively or in addition responsible for GPVI shedding *in vivo*.

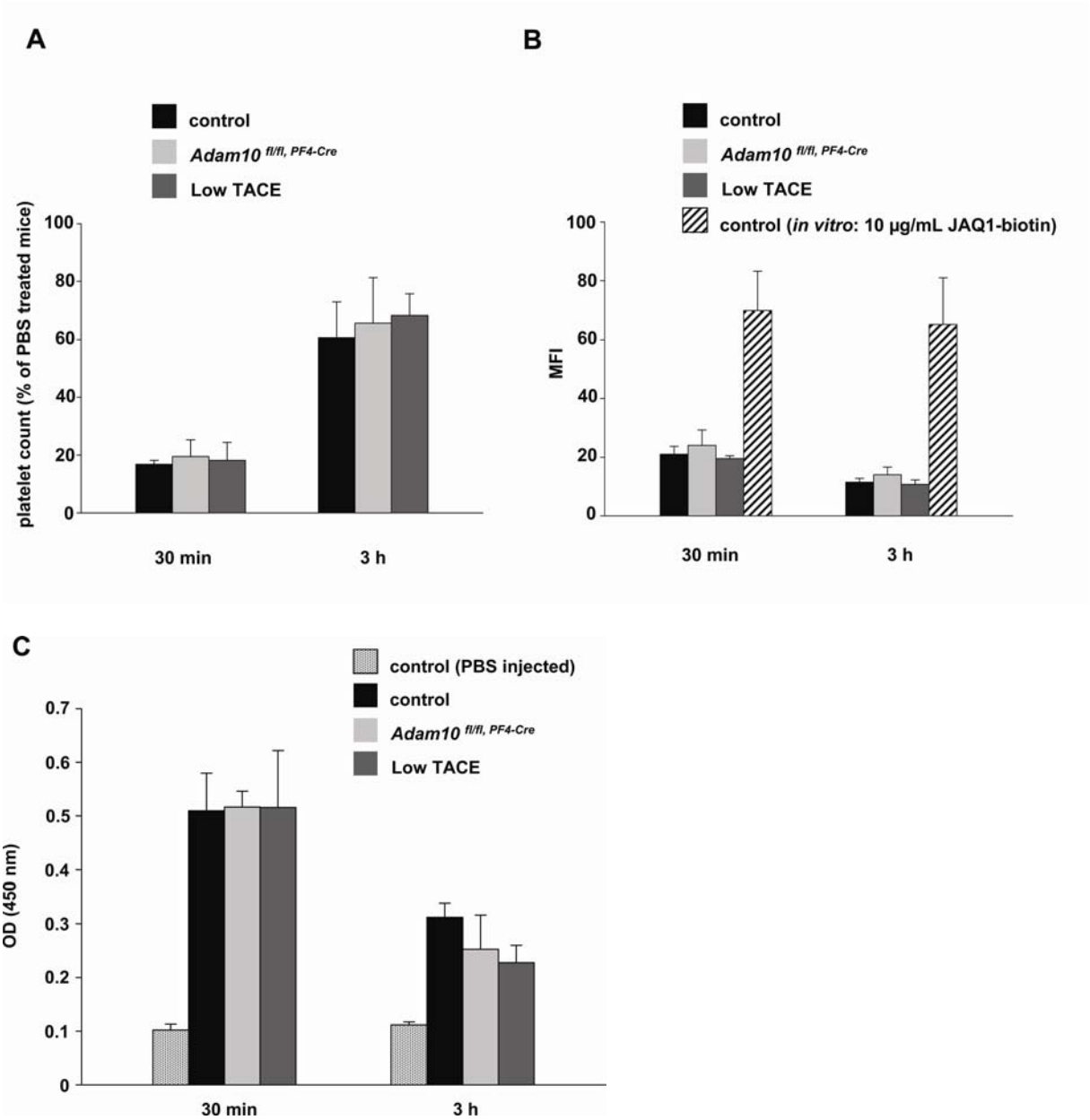

Fig. 52: GPVI is cleaved in ADAM10-deficient and low TACE mice *in vivo*.
Control and mutant mice were injected i.v. with 100 µg of biotinylated anti-GPVI (JAQ1) antibody. Flow cytometric analysis of platelet count **(A)** and GPVI expression **(B)** (indirectly: streptavidin-FITC) was performed. Platelets were stained with the fluorophore-labeled antibodies for 15 minutes and directly analyzed. Results are mean ± SD (*n* = 4 mice per group, representative for 3 individual experiments). As a positive control in **(B)**, wild-type platelets from untreated mice were incubated with 10 µg/mL JAQ1-biotin and stained with streptavidin-FITC. **(C)** Mice were injected with 100 µg biotinylated-JAQ1 and plasma was collected at the indicated time points. GPVI levels in plasma were determined by ELISA as described in Materials and Methods. Results are mean ± SD (*n* = 4 mice per group).

D. Discussion

D.1. ADF/cofilin-null mice have a severe defect in platelet formation

In this thesis, it was shown that ADF/cofilin-dependent actin turnover plays a fundamental role in the terminal step of platelet production.

It is well established that sliding of microtubules is the primary force for elaboration of proplatelets with the help of dynein that appears to be the motor protein of this event[16;138]. However, the role of actin turnover in proplatelet formation is less well defined. Until today, only *in vitro* studies have been performed using cytochalasin, a fungal metabolite which is able to inhibit actin assembly, resulting in defects in proplatelet branching leading to reduced complexity and rolling of proplatelets[138]. Here, megakaryocytes deficient in ADF and cofilin displayed a significant reduction in proplatelet formation *in vitro* (Fig. 25A) and *ex vivo* (Fig. 25D), and actin accumulation within the megakaryocyte (Fig. 25B+C). Surprisingly, some MKs were able to produce proplatelets. Confocal microscopy (Fig. 25C) revealed that these proplatelets lacked the beaded appearance typically found in control MKs. Some extensions were devoid of actin supporting observations that actin is particularly enriched in swellings[138]. In general, proplatelets of double-deficient MKs appeared to be less complex and shorter. This was also found in the bone marrow explant model in which the few formed extensions of ADF/cofilin-deficient MKs appeared thinner and, interestingly, were found detached in the bottom of the incubation chamber after the observation period (Fig. 26C). This indicates that proplatelets without swellings are less stable. Together, these results demonstrate that actin turnover is important for proplatelet formation, but extensions can be formed without appropriate actin turnover by microtubules sliding, but then proplatelets are malformed.

In ADF/cofilin-null mice the number of MKs in spleen and bone marrow (Fig. 21B+23A) were elevated despite normal plasma TPO levels (Fig. 22), excluding a possible TPO-driven feedback mechanism due to the low platelet counts. This observation was also made in other mice (*Stim1*$^{Sax/+}$ *and Wdr1*$^{rd/rd}$) with low platelet counts, elevated MK numbers and unaltered TPO levels[132;139]. Furthermore, measurement of bone marrow MK ploidy revealed comparable results between wild-type and mutant mice demonstrating that MK endomitosis was not affected by ADF/cofilin-deficiency (Fig. 24).

Ultrastructural analysis of mature wild-type MKs showed that the cytoplasm contains a characteristic demarcation membrane system (DMS). Schulze *et al.* demonstrated that the DMS is the source for proplatelet membranes and that DMS development is strongly dependent on actin[140]. Therefore, ADF/cofilin-null MKs were analyzed in transmission electron microscopy (Fig. 23B). Bone marrow MKs of double-deficient mice revealed an absence of the DMS. Only underdeveloped remnants of the DMS were observed in the cytoplasm. Again, actin-rich structures were found in the cytoplasm of the MKs (Fig. 23B) but also in the cortical zone (not shown). This finding was confirmed by immunolocalization using an anti-actin antibody (Fig. 23C). The strikingly abnormal morphologies in the bone marrow MKs were not only restricted to the development of the DMS since granules were represented only sparsely and granule distribution was highly disordered. Taken together, this is in agreement with investigations on mice having a mutation in the *Wdr1* gene, a cofilin interaction partner. The MKs of mutant *Wdr1* mice also displayed a strong defect in DMS development and granule distribution[139]. This confirms that ADF/cofilin-dependent actin turnover is crucial for the development of the DMS *in vivo* a prerequisite for normal platelet formation.

Platelet counts of ADF/cofilin-null mice were profoundly reduced to less than 5% of control mice (Fig. 19A). This striking observation was surprising since other mice lacking prominent proteins involved in the structure of the cytoskeleton or in MK maturation showed a milder reduction (15% of control in *GATA-1 Δneo Δ HS* mice[141], approximately 40% of control in *β1-tubulin*$^{-/-}$ mice[142]). Although the platelet count was markedly reduced, ADF/cofilin-null mice were viable and did not suffer from internal bleedings (not shown). The residual platelets displayed a heterogeneous population ranging from microparticle- to proplatelet-like platelets containing aggregates of actin (Fig. 19B+C). These platelets were not able to fulfill normal platelet function as they were unable to spread on immobilized fibrinogen (Fig. 19D) and to assemble F-actin (Fig. 20). Taken together, these data provide new important insights into the process of platelet formation. This may be clinically significant as detailed information on the mechanisms of platelet production is essential to develop new strategies to treat thrombocytopenic patients.

D.2. ADF and cofilin are functionally redundant: a role for cofilin in platelet sizing

Despite the severe defects caused by the *Adf* mutation in *corn1* mice[52], defects in megakaryocyte maturation, platelet formation or changes in platelet count and size in *Adf*$^{-/-}$ mice (Fig. 12A+C) were not observed suggesting that cofilin completely compensated the lack of ADF function. In contrast, conditional deletion of *cofilin* in megakaryocytes and platelets yielded a moderately reduced platelet count (Fig. 12A) and markedly increased platelet size with a change from a discoid to a spherical shape (Fig. 12B+C). In line with this, Junt *et al.* described that protrusions from MKs extended into the microvessels and that platelet-particles exceeding the size of a normal platelet were released into the blood stream through shear forces as revealed by multiphoton intravital microscopy[18]. This supports previous reports suggesting that the finalization of platelet-sizing occurs in the circulation[143]. The markedly increased platelet size and altered shape strongly suggest that cofilin plays a pivotal role in the finalization of platelet size and shape after release from proplatelets into the circulation. Several studies established a critical role for actin filament dynamics and cofilin in mitosis and cytokinesis. The activity of the cofilin phosphatase Slingshot-1 in HeLa cells was decreased in the early stage of mitosis but increased in the telophase and cytokinesis. Moreover, expression of inactive Slingshot-1 resulted in formation of multinuclear cells[144]. The same group also observed multinuclear cell formation by ectopic expression of the cofilin kinase LIMK1[145]. Similar results with defects in cytokinesis and misshaped structures were obtained by mutations of the ADF/cofilin homologue twinstar in *Drosophila* and suppressed expression of the *Caenorhabditis elegans* homologue UNC-60A, respectively[45;146]. These results demonstrated a role for cofilin in mitosis and cytokinesis. However, further studies will be required to address the important question of how cofilin regulates platelet size and shape mechanistically.

In addition, cofilin-deficient platelets were delayed in spreading on immobilized fibrinogen but principally able to form lamellipodia with normal cytoskeletal rearrangement as shown after 60 minutes in scanning electron and STED microscopy (Fig. 18). This is in line with results from studies investigating phosphorylation events in human platelets from healthy volunteers and patients with Glanzmann thrombasthenia. In addition, this was also observed in studies using blockers of αIIbβ3 integrin[44]. They suggested that cofilin is essential for actin turnover

mediated by outside-in signaling through the αIIbβ3 integrin. Here, it is also concluded that cofilin, but not ADF, is the central mediator of actin dynamics upon outside-in signaling, since *Adf*$^{-/-}$ platelets were able to spread with similar kinetics as control platelets. However, initial agonist-induced actin rearrangement does not seem to be affected in cofilin-null platelets (Fig. 15C). This function is generally supposed to be gelsolin-dependent[147].

D.3. Conditional deletion of *cofilin* using the Mx-Cre system leads to destruction of the bone marrow

In the present study, the recently established *PF4-Cre* mouse line was used to delete *cofilin* conditionally in megakaryocytes and platelets[125]. Before the PF4-Cre system was available, the interferon-inducible *Mx-Cre* mouse line was generally used to conditionally delete genes supposed to be important for platelet function and to avoid embryonic lethality in constitutive knock-out mice. However, the Mx-Cre system is not specific for megakaryocytes and platelets as it also affects other tissues including other cells of the hematopoietic system[126]. Here, after induction of the *cofilin* knock-out by injection of Poly-I/Poly-C, mice were analyzed at day 5. In both mouse lines, *cofilin*$^{fl/fl,\ Mx\text{-}Cre}$ *and Adf*$^{-/-}$*/cofilin*$^{fl/fl,\ Mx\text{-}Cre}$, a progressive destruction of the bone marrow structure and a reduction in bone marrow cellularity was observed (Fig. 27C). As a consequence, the numbers of MKs and platelets were dramatically decreased (Fig. 27), accompanied by a strong reduction in the hematocrit. All double-deficient mice died within ten days after Poly-I/Poly-C injection. Together, this demonstrates that the PF4-Cre system is a more appropriate tool to analyze megakaryocyte and platelet function as the Mx-Cre system may lead to overinterpretation of the phenotype.

In summary, using the *PF4-Cre* mice it was demonstrated that ADF/cofilin-mediated actin turnover is of central importance in the terminal step of platelet formation and moreover, cofilin is a key regulator of platelet size and shape.

D.4. The activating platelet collagen receptor GPVI is a promising anti-thrombotic target

Over the last years many laboratories have intensively studied the role of GPVI in platelets. GPVI, the activating platelet collagen receptor, was placed in a central position in the steps of platelet tethering, activation, firm adhesion and aggregation[8].

These results led to a revision of the long-standing concept that GPIa/IIa would be the major collagen receptor[148;149]. Although these investigations revealed detailed information on GPVI function in platelets, there is still considerable conflicting literature about the receptor. Many studies demonstrated that GPVI deficiency only results in a minor effect on tail bleeding times and in a protection against thrombus formation in various thrombosis models[61;82;90;91]. Consequently, GPVI is believed to be an appropriate target for the development of new and safe anti-thrombotic agents. Two major issues about GPVI are on the one hand the role of GPVI in thrombus formation in different arterial thrombosis models and on the other hand the role of GPVI in primary adhesion to collagen. Recently, Mangin P. *et al.* challenged GPVI/FcRγ-deficient mice in three distinct arterial thrombosis models and could not observe a defect in arterial thrombus formation after deep vascular injury. However, the authors demonstrated that inhibition of thrombin produces a much greater defect in thrombus formation in GPVI/FcRγ-deficient mice as compared to controls. In contrast, thrombus growth was reduced in GPVI/FcRγ-deficient mice after mild vascular injury[150]. Although it is known that for instance the $FeCl_3$-induced thrombosis model is a mainly thrombin-driven model, nevertheless, the results are in contrast to other reports as mentioned above.

To date, two research groups have reported studies on *Gp6* knock-out mice by using different strategies to delete the *Gp6* gene. For deletion of the *Gp6* gene, Kato *et al.*[90] inserted a neo-cassette into exon 1, whereas Lockyer *et al.*[91] chose a different strategy and deleted part of exon 2 to half of exon 3 by replacing this region with a neo-cassette. Similar phenotypic observations were made by both groups. However, interestingly, investigations regarding the precise role of GPVI in the primary adhesion process resulted in different observations. The results of Kato *et al.* did not support any participation of GPVI in the initial platelet adhesion process[90], which disagrees with results of other groups. There, platelets of GPVI-depleted mice failed to adhere to the injured vessel wall, demonstrating a role of GPVI in this process[7;84]. This disagreement is possibly related to the different approaches to produce GPVI-deficient mice. But contrary to Kato *et al.*, Lockyer *et al.* suggested a role of GPVI in primary platelet adhesion. Platelets without GPVI on their surface completely lacked primary adhesion and subsequent thrombus formation[91].

Thus, it is noteworthy that examinations and results about GPVI are still in the focus of interest. To address this issues about the role of GPVI in the process of initial platelet attachment and arterial thrombus formation, an own strategy was designed for the generation of *Gp6* knock-out mice (Fig. 30). A neomycin-cassette was inserted between exon 2 and exon 3 of *Gp6*, thereby removing intron 2. Consequently, platelets of these mice can not express GPVI on their surface. At first, it was confirmed that the protein is absent in platelets (Fig. 37B-D) and that platelets are not activated upon incubation with GPVI-specific agonists like CRP or convulxin (Fig. 38). As expected, *Gp6* knock-out mice displayed a minor increase in bleeding times (Fig. 39A) and GPVI-deficient platelets were not able to form thrombi on a collagen coated surface (Fig. 39B). Surprisingly, single GPVI-deficient platelets adhered to collagen fibers. Regarding the conflicting literature as mentioned above, it is difficult to interpret these results. Either differences in the technical performance or different strategies in the generation of the mutant mice are the reason for the different results. Alternatively, *Gp6* knock-out platelets are able to compensate the lack of GPVI regarding the defect in primary adhesion in contrast to GPVI-depleted platelets. Further studies are necessary to address this issue. *In vivo* studies revealed that GPVI is important for thrombus formation as shown in the aorta thrombosis model and also in the $FeCl_3$-induced thrombosis model (Fig. 39C+D). These results support previous findings that GPVI may serve as an appropriate target for the development of anti-thrombotic drugs.

This newly generated mouse line will serve as control for future investigations and to address GPVI-related questions. GPVI and CLEC-2 are ITAM-coupled receptors in platelets that can be down-regulated by antibody injection into mice. This makes both receptors interesting as therapeutical targets. To understand the effect in mice upon removal of both ITAM-coupled receptors, *Gp6* knock-out mice were injected with the INU1 antibody to induce CLEC-2 deficiency. It could be shown that single deficiency in GPVI or CLEC-2 leads only to a mild (Fig. 39A) or variable and increased bleeding phenotype[130], respectively. However, lack of both ITAM-coupled receptors resulted in a severe bleeding phenotype (Fig. 41A). Similar results were obtained by depleting GPVI and CLEC-2 at the same time by antibody-treatment with JAQ1 and INU1 (data not shown).

D.5. Generation of human *GP6* knock-in mice: a tool to investigate differences between mouse and human GPVI

Mouse and human GPVI share 64.4% and 67.3% identity at protein and nucleotide level, respectively[55]. Especially the cytoplasmic tail of the protein varies between human and mouse. The C-terminal region is 24 amino acids longer in human than in mouse[62]. This raised the question whether there are different regulation mechanisms of human GPVI compared to mouse GPVI. For that reason, the construction of a knock-in vector was performed based on the knock-out vector that was used as a "multifunctional vector". With this vector only minor alteration in the cloning strategy was necessary to generate a new targeting vector. The human *GP6* wild-type cDNA was inserted in-frame downstream of exon 2 of the 5´ flanking region (Fig. 30). As a consequence, platelets of these knock-in mice should express human GPVI at an appropriate level on their surface. This approach could provide new information about regulation and signaling of human GPVI *in vivo*. In addition, as mentioned above, GPVI is suggested to be a major target for the development of novel anti-thrombotic drugs. This model might be suitable for designing and testing new pharmaceuticals directed against human GPVI. Furthermore, it is interesting to know whether this technique will work to generate mice expressing the human protein at a similar level as the wild-type protein. So far, chimeric mice were obtained that did not produce offsprings with germline transmission. The chimerism of these mice was comparably low indicating that not the targeting strategy was responsible for the lack of germline transmission but rather the quality of the stem cell clone was not sufficient. This is also supported by the observation that most of the chimeric mice were infertile. A new positive stem cell clone was recently injected into blastocysts and the birth of the first offsprings is going to be expected soon (Fig. 36C).

In addition, it was decided to mutate important binding sites on human GPVI (Fig. 32). It was suggested that two different collagen binding sites exist on mouse GPVI[73;151]. Smethurst *et al.* described the identification of the binding site of CRP on human GPVI. Binding studies with CRP and immunoglobulin-like ectodomains of human GPVI expressed in insect cells demonstrated that the exchange of the human lysine through a murine glutamic acid at position 59 on the human monomeric recombinant peptide significantly reduced binding to CRP[136]. Later, Lecut *et al.* reported on the identification of residues in the first Ig-like domain on human GPVI that are involved in binding to collagen. Recombinant soluble human GPVI-Fc

mutants were generated and their binding to collagen was examined. The results revealed that the triple mutation of G30A, V34A, and L36A yielded full inhibition of binding to collagen[135]. It was decided to introduce the same mutations in the human *GP6* wild-type cDNA, to test the platelet response to collagen and CRP of the mutant mice *in vivo*. This approach will be interesting to address the hypothesis of two distinct collagen binding sites. Finally, one additional vector was constructed with a mutated calmodulin binding site. Andrews *et al.* identified the calmodulin recognition site on a GPVI-related synthetic peptide His269-Pro287[63]. Based on an alignment of several calmodulin binding sites, the three most conserved amino acids were selected for mutation namely R271A, K273E and R280A. It was shown that calmodulin is involved in regulation of GPVI. If the association between GPVI and calmodulin, which constitutively binds the cytoplasmic tail of GPVI, is blocked, GPVI is shed from the platelet surface by a metalloproteinase-mediated mechanism *in vitro*[64]. It will be interesting to investigate this regulation mechanism *in vivo*. In summary, four vectors were successfully constructed for the generation of human *GP6* knock-in mice, namely human wild-type *GP6* knock-in, human *GP6* knock-in with mutated collagen binding site, human *GP6* knock-in with mutated CRP binding site and human *GP6* knock-in with mutated calmodulin binding site. The vectors with the mutated human cDNA will be electroporated when the first human wild-type knock-in mice will have been analyzed and have shown sufficient human GPVI protein expression in platelets.

D.6. GPVI is differently regulated by the metalloproteinases ADAM10 and ADAM17

Previously, it was demonstrated that GPVI can be down-regulated from the platelet surface by injection of the anti-GPVI antibody JAQ1 into mice. It was shown that this event occurrs through two different pathways: internalization and ectodomain shedding[82;85;89]. However, the GPVI sheddase has not been identified. Two possible candidate metalloproteinases are suspected to be the GPVI sheddase: ADAM10 and ADAM17. Bergmeier *et al.* showed that GPVI is down-regulated in murine platelets by a metalloproteinase-dependent mechanism. The authors suggested a different metalloproteinase to be involved in GPVI shedding as in GPIb shedding since thrombin or CRP treatment of platelets led to GPIb, but not GPVI proteolysis[89]. Upon this, subsequent publications either speculated[152] or suggested[123] ADAM10 to be

responsible for GPVI shedding. Here, megakaryocyte/platelet-specific (PF4-Cre) *Adam10* knock-out mice were generated to address the function of ADAM10 in the shedding of GPVI (Fig. 48A). In addition, low TACE (ADAM17) mice with approximately 10% residual activity were analyzed. Enhanced GPIb surface expression and reduced GPIb levels in plasma of low TACE mice indicated, as expected, that TACE is the constitutive sheddase of GPIb and that these mice are useful for platelet studies (Fig. 49). To investigate the role of ADAM10 and ADAM17 in GPVI shedding, platelets were treated with different shedding-inducing reagents and glycoprotein expression was measured in FACS. Using the calmodulin-inhibitor W7 and the metalloproteinase-activating substance NEM, it was revealed that ADAM10, but not ADAM17, is the sheddase of GPVI under these conditions (Fig. 50). This result was also confirmed by an ELISA system in which cleaved GPVI of ADAM10-deficient platelets was significantly reduced (Fig. 51). This is in line with the findings of Gardiner *et al.* who showed in their cleavage studies on GPVI-based synthetic peptides that ADAM10 is the GPVI sheddase using W7 and NEM as shedding-inducing reagents[123]. In previous studies, CCCP was also used to induce mitochondrial damage which leads to subsequent shedding of platelet receptors. As expected, TACE was responsible for shedding of GPIb and GPV (Fig. 50). However surprisingly, TACE was also identified to be the sheddase of GPVI after platelet treatment with CCCP (Fig. 50+51). This is the first demonstration that GPVI can be down-regulated by two different metalloproteinases, ADAM10 and ADAM17, under different experimental conditions. However, the mechanistic basis for two different pathways/metalloproteinases cleaving the GPVI receptor remains elusive. In some cases it was already shown that a substrate is cleaved by more than one sheddase such as CX3CL-1 and the IL-6 receptor and that these proteins are processed by both metalloproteinases, ADAM10 and ADAM17[116-118]. However, the use of reagents like W7, NEM and CCCP does possibly not reflect the *in vivo* situation as obtained by injection of the anti-GPVI antibody JAQ1. Therefore, ADAM10-deficient and low TACE mice were injected with the antibody and GPVI expression was determined in flow cytometry. Interestingly, preliminary results revealed that GPVI is down-regulated from the platelet surface and transient thrombocytopenia occurs in both ADAM10-deficient and low TACE mice (Fig. 52). However, further studies have to be performed to confirm this result. One reason for the down-regulation of GPVI could be that another metalloproteinase either exclusively or in addition is responsible for

GPVI shedding *in vivo*. One candidate could be ADAM9 because it is widely expressed, highly conserved between species and is a catalytically active metalloprotease. Mice lacking ADAM9 have, in contrast to ADAM10- or ADAM17-deficient mice, no abnormalities in development and adult life. The authors suggest that ADAM9 could have a potential function in shedding of receptors[153]. Another more likely reason could be that both proteins, ADAM10 and ADAM17, are able to cleave GPVI *in vivo* and that lack of one metalloproteinase is compensated by the other. To address this, mating of both mouse strains to obtain double-deficient mice is in process. However, first matings revealed that mice lacking both proteins come to birth very rarely. This is in line with statistics from unpublished data demonstrating that birth of low TACE mice does not follow the Mendelian ratio (Chalaris *et al.*, unpublished). This problem seems to be even more severe when crossing the mice to double-deficiency (data not shown). Once double-deficient mice come to birth, bone marrow of these mice will be transferred to lethally irradiated recipient C57BL/6 mice to increase the number of mice available for analysis. Analysis of these mice might help to answer the question as to whether exclusively ADAM10 and ADAM17 are the sheddases for GPVI or whether another metalloproteinase is involved in this process.

Furthermore, both mouse lines will be analyzed to address the role of ADAM10 and ADAM17 in thrombus formation *in vitro* and *in vivo*.

D.7. Concluding remarks

The work presented here shows studies on the regulation of the platelet cytoskeleton and on the activating platelet collagen receptor GPVI in genetically modified mice. In addition, two knock-out mice were generated to understand the mechanisms underlying the cellular regulation of GPVI.
The major findings are:

Function of ADF and n-cofilin in platelets:

- ADF is dispensable for platelet production and function
- n-cofilin is critically involved in platelet sizing and integrin outside-in signaling
- ADF and n-cofilin are functionally redundant

- ADF/n-cofilin-dependent actin turnover is essential for platelet formation

Deficiency and regulation of GPVI in platelets:

- Mice deficient in GPVI display a mild bleeding phenotype and are protected from thrombotic events
- CLEC-2 depleted *Gp6* knock-out mice display a severe bleeding phenotype
- ADAM10 and ADAM17 are able to cleave GPVI, depending on the shedding-inducing signaling pathway
- Shedding of GPVI *in vivo* is either mediated by both metalloproteinases (ADAM10 and ADAM17) or an additional metalloproteinase is involved in GPVI ectodomain shedding

D.8. Outlook

The process of platelet formation *in vivo* is still only poorly understood. Further studies on platelets deficient in n-cofilin will provide deeper insights into the mechanisms of platelet size and shape determination. The *in vivo* visualization of the platelet formation process by multiphoton intravital microscopy in cofilin-deficient mice will reveal interesting information to better understand this process.

This study could not provide the information which metalloproteinase is the *in vivo* sheddase of GPVI. Analysis of conditional *Adam10* knock-out and low TACE mice revealed that neither ADAM10 nor ADAM17 alone is the *in vivo* GPVI sheddase. To understand whether both metalloproteinases are responsible for GPVI cleavage or another metalloproteinase is also involved, double-deficient mice will be analyzed in the near future.

E. References

1. Ruggeri ZM. Platelets in atherothrombosis. Nat.Med. 2002;8:1227-1234.

2. Lusis AJ. Atherosclerosis. Nature 2000;407:233-241.

3. Varga-Szabo D, Pleines I, Nieswandt B. Cell adhesion mechanisms in platelets. Arterioscler.Thromb.Vasc.Biol. 2008;28:403-412.

4. Penz S, Reininger AJ, Brandl R et al. Human atheromatous plaques stimulate thrombus formation by activating platelet glycoprotein VI. FASEB J. 2005;19:898-909.

5. Moroi M, Jung SM, Nomura S et al. Analysis of the involvement of the von Willebrand factor-glycoprotein Ib interaction in platelet adhesion to a collagen-coated surface under flow conditions. Blood 1997;90:4413-4424.

6. Ruggeri ZM. Von Willebrand factor, platelets and endothelial cell interactions. J.Thromb.Haemost. 2003;1:1335-1342.

7. Nieswandt B, Brakebusch C, Bergmeier W et al. Glycoprotein VI but not alpha2beta1 integrin is essential for platelet interaction with collagen. EMBO J. 2001;20:2120-2130.

8. Nieswandt B, Watson SP. Platelet-collagen interaction: is GPVI the central receptor? Blood 2003;102:449-461.

9. Clemetson KJ. Platelet activation: signal transduction via membrane receptors. Thromb.Haemost. 1995;74:111-116.

10. Jung SM, Moroi M. Platelets interact with soluble and insoluble collagens through characteristically different reactions. J.Biol.Chem. 1998;273:14827-14837.

11. Kaushansky K, Drachman JG. The molecular and cellular biology of thrombopoietin: the primary regulator of platelet production. Oncogene 2002;21:3359-3367.

12. Patel SR, Hartwig JH, Italiano JE, Jr. The biogenesis of platelets from megakaryocyte proplatelets. J.Clin.Invest 2005;115:3348-3354.

13. Geddis AE, Fox NE, Tkachenko E, Kaushansky K. Endomitotic megakaryocytes that form a bipolar spindle exhibit cleavage furrow ingression followed by furrow regression. Cell Cycle 2007;6:455-460.

14. Nagata Y, Muro Y, Todokoro K. Thrombopoietin-induced polyploidization of bone marrow megakaryocytes is due to a unique regulatory mechanism in late mitosis. J.Cell Biol. 1997;139:449-457.

15. Vitrat N, Cohen-Solal K, Pique C et al. Endomitosis of human megakaryocytes are due to abortive mitosis. Blood 1998;91:3711-3723.

16. Battinelli EM, Hartwig JH, Italiano JE, Jr. Delivering new insight into the biology of megakaryopoiesis and thrombopoiesis. Curr.Opin.Hematol. 2007;14:419-426.

17. Hartwig J, Italiano J, Jr. The birth of the platelet. J.Thromb.Haemost. 2003;1:1580-1586.

18. Junt T, Schulze H, Chen Z et al. Dynamic visualization of thrombopoiesis within bone marrow. Science 2007;317:1767-1770.

19. Kunishima S, Saito H. Congenital macrothrombocytopenias. Blood Rev. 2006;20:111-121.

20. Nurden AT. Qualitative disorders of platelets and megakaryocytes. J.Thromb.Haemost. 2005;3:1773-1782.

21. Bamburg JR. Proteins of the ADF/cofilin family: essential regulators of actin dynamics. Annu.Rev.Cell Dev.Biol. 1999;15:185-230.

22. Maciver SK, Hussey PJ. The ADF/cofilin family: actin-remodeling proteins. Genome Biol. 2002;3:reviews3007.

23. Bamburg JR, Bray D. Distribution and cellular localization of actin depolymerizing factor. J.Cell Biol. 1987;105:2817-2825.

24. Dos Remedios CG, Chhabra D, Kekic M et al. Actin binding proteins: regulation of cytoskeletal microfilaments. Physiol Rev. 2003;83:433-473.

25. Vartiainen MK, Mustonen T, Mattila PK et al. The three mouse actin-depolymerizing factor/cofilins evolved to fulfill cell-type-specific requirements for actin dynamics. Mol.Biol.Cell 2002;13:183-194.

26. Theriot JA, Mitchison TJ. Actin microfilament dynamics in locomoting cells. Nature 1991;352:126-131.

27. Wang YL. Exchange of actin subunits at the leading edge of living fibroblasts: possible role of treadmilling. J.Cell Biol. 1985;101:597-602.

28. Zigmond SH. Recent quantitative studies of actin filament turnover during cell locomotion. Cell Motil.Cytoskeleton 1993;25:309-316.

29. Ono S. Mechanism of depolymerization and severing of actin filaments and its significance in cytoskeletal dynamics. Int.Rev.Cytol. 2007;258:1-82.

30. Ayscough KR. In vivo functions of actin-binding proteins. Curr.Opin.Cell Biol. 1998;10:102-111.

31. Moon A, Drubin DG. The ADF/cofilin proteins: stimulus-responsive modulators of actin dynamics. Mol.Biol.Cell 1995;6:1423-1431.

32. Welch MD, Mallavarapu A, Rosenblatt J, Mitchison TJ. Actin dynamics in vivo. Curr.Opin.Cell Biol. 1997;9:54-61.

33. Carlier MF, Laurent V, Santolini J et al. Actin depolymerizing factor (ADF/cofilin) enhances the rate of filament turnover: implication in actin-based motility. J.Cell Biol. 1997;136:1307-1322.

34. Maciver SK. How ADF/cofilin depolymerizes actin filaments. Curr.Opin.Cell Biol. 1998;10:140-144.

35. Bamburg JR, McGough A, Ono S. Putting a new twist on actin: ADF/cofilins modulate actin dynamics. Trends Cell Biol. 1999;9:364-370.

36. Maciver SK, Zot HG, Pollard TD. Characterization of actin filament severing by actophorin from Acanthamoeba castellanii. J.Cell Biol. 1991;115:1611-1620.

37. McGough A, Pope B, Chiu W, Weeds A. Cofilin changes the twist of F-actin: implications for actin filament dynamics and cellular function. J.Cell Biol. 1997;138:771-781.

38. Abe H, Obinata T, Minamide LS, Bamburg JR. Xenopus laevis actin-depolymerizing factor/cofilin: a phosphorylation-regulated protein essential for development. J.Cell Biol. 1996;132:871-885.

39. Arber S, Barbayannis FA, Hanser H et al. Regulation of actin dynamics through phosphorylation of cofilin by LIM-kinase. Nature 1998;393:805-809.

40. Gohla A, Birkenfeld J, Bokoch GM. Chronophin, a novel HAD-type serine protein phosphatase, regulates cofilin-dependent actin dynamics. Nat.Cell Biol. 2005;7:21-29.

41. Maekawa M, Ishizaki T, Boku S et al. Signaling from Rho to the actin cytoskeleton through protein kinases ROCK and LIM-kinase. Science 1999;285:895-898.

42. Niwa R, Nagata-Ohashi K, Takeichi M, Mizuno K, Uemura T. Control of actin reorganization by Slingshot, a family of phosphatases that dephosphorylate ADF/cofilin. Cell 2002;108:233-246.

43. Toshima J, Toshima JY, Amano T et al. Cofilin phosphorylation by protein kinase testicular protein kinase 1 and its role in integrin-mediated actin reorganization and focal adhesion formation. Mol.Biol.Cell 2001;12:1131-1145.

44. Falet H, Chang G, Brohard-Bohn B, Rendu F, Hartwig JH. Integrin alpha(IIb)beta3 signals lead cofilin to accelerate platelet actin dynamics. Am.J.Physiol Cell Physiol 2005;289:C819-C825.

45. Gunsalus KC, Bonaccorsi S, Williams E et al. Mutations in twinstar, a Drosophila gene encoding a cofilin/ADF homologue, result in defects in centrosome migration and cytokinesis. J.Cell Biol. 1995;131:1243-1259.

46. Iida K, Moriyama K, Matsumoto S et al. Isolation of a yeast essential gene, COF1, that encodes a homologue of mammalian cofilin, a low-M(r) actin-binding and depolymerizing protein. Gene 1993;124:115-120.

47. Moon AL, Janmey PA, Louie KA, Drubin DG. Cofilin is an essential component of the yeast cortical cytoskeleton. J.Cell Biol. 1993;120:421-435.

48. McKim KS, Matheson C, Marra MA, Wakarchuk MF, Baillie DL. The Caenorhabditis elegans unc-60 gene encodes proteins homologous to a family of actin-binding proteins. Mol.Gen.Genet. 1994;242:346-357.

49. Ono S, Benian GM. Two Caenorhabditis elegans actin depolymerizing factor/cofilin proteins, encoded by the unc-60 gene, differentially regulate actin filament dynamics. J.Biol.Chem. 1998;273:3778-3783.

50. Gurniak CB, Perlas E, Witke W. The actin depolymerizing factor n-cofilin is essential for neural tube morphogenesis and neural crest cell migration. Dev.Biol. 2005;278:231-241.

51. Bellenchi GC, Gurniak CB, Perlas E et al. N-cofilin is associated with neuronal migration disorders and cell cycle control in the cerebral cortex. Genes Dev. 2007;21:2347-2357.

52. Ikeda S, Cunningham LA, Boggess D et al. Aberrant actin cytoskeleton leads to accelerated proliferation of corneal epithelial cells in mice deficient for destrin (actin depolymerizing factor). Hum.Mol.Genet. 2003;12:1029-1037.

53. Ezumi Y, Uchiyama T, Takayama H. Molecular cloning, genomic structure, chromosomal localization, and alternative splice forms of the platelet collagen receptor glycoprotein VI. Biochem.Biophys.Res.Commun. 2000;277:27-36.

54. Clemetson JM, Polgar J, Magnenat E, Wells TN, Clemetson KJ. The platelet collagen receptor glycoprotein VI is a member of the immunoglobulin superfamily closely related to FcalphaR and the natural killer receptors. J.Biol.Chem. 1999;274:29019-29024.

55. Jandrot-Perrus M, Busfield S, Lagrue AH et al. Cloning, characterization, and functional studies of human and mouse glycoprotein VI: a platelet-specific collagen receptor from the immunoglobulin superfamily. Blood 2000;96:1798-1807.

56. Berlanga O, Bobe R, Becker M et al. Expression of the collagen receptor glycoprotein VI during megakaryocyte differentiation. Blood 2000;96:2740-2745.

57. Moroi M, Jung SM. Platelet glycoprotein VI: its structure and function. Thromb.Res. 2004;114:221-233.

58. Zheng YM, Liu C, Chen H et al. Expression of the platelet receptor GPVI confers signaling via the Fc receptor gamma -chain in response to the snake venom convulxin but not to collagen. J.Biol.Chem. 2001;276:12999-13006.

59. Berlanga O, Tulasne D, Bori T et al. The Fc receptor gamma-chain is necessary and sufficient to initiate signalling through glycoprotein VI in transfected cells by the snake C-type lectin, convulxin. Eur.J.Biochem. 2002;269:2951-2960.

60. Gibbins JM, Okuma M, Farndale R, Barnes M, Watson SP. Glycoprotein VI is the collagen receptor in platelets which underlies tyrosine phosphorylation of the Fc receptor gamma-chain. FEBS Lett. 1997;413:255-259.

61. Nieswandt B, Bergmeier W, Schulte V et al. Expression and function of the mouse collagen receptor glycoprotein VI is strictly dependent on its association with the FcRgamma chain. J.Biol.Chem. 2000;275:23998-24002.

62. Bori-Sanz T, Inoue KS, Berndt MC, Watson SP, Tulasne D. Delineation of the region in the glycoprotein VI tail required for association with the Fc receptor gamma-chain. J.Biol.Chem. 2003;278:35914-35922.

63. Andrews RK, Suzuki-Inoue K, Shen Y et al. Interaction of calmodulin with the cytoplasmic domain of platelet glycoprotein VI. Blood 2002;99:4219-4221.

64. Gardiner EE, Arthur JF, Kahn ML, Berndt MC, Andrews RK. Regulation of platelet membrane levels of glycoprotein VI by a platelet-derived metalloproteinase. Blood 2004;104:3611-3617.

65. Suzuki-Inoue K, Tulasne D, Shen Y et al. Association of Fyn and Lyn with the proline-rich domain of glycoprotein VI regulates intracellular signaling. J.Biol.Chem. 2002;277:21561-21566.

66. Morton LF, Hargreaves PG, Farndale RW, Young RD, Barnes MJ. Integrin alpha 2 beta 1-independent activation of platelets by simple collagen-like peptides: collagen tertiary (triple-helical) and quaternary (polymeric) structures are sufficient alone for alpha 2 beta 1-independent platelet reactivity. Biochem.J. 1995;306 (Pt 2):337-344.

67. Jandrot-Perrus M, Lagrue AH, Okuma M, Bon C. Adhesion and activation of human platelets induced by convulxin involve glycoprotein VI and integrin alpha2beta1. J.Biol.Chem. 1997;272:27035-27041.

68. Polgar J, Clemetson JM, Kehrel BE et al. Platelet activation and signal transduction by convulxin, a C-type lectin from Crotalus durissus terrificus (tropical rattlesnake) venom via the p62/GPVI collagen receptor. J.Biol.Chem. 1997;272:13576-13583.

69. Teng CM, Ko FN, Tsai IH, Hung ML, Huang TF. Trimucytin: a collagen-like aggregating inducer isolated from Trimeresurus mucrosquamatus snake venom. Thromb.Haemost. 1993;69:286-292.

70. Asazuma N, Marshall SJ, Berlanga O et al. The snake venom toxin alboaggregin-A activates glycoprotein VI. Blood 2001;97:3989-3991.

71. Dormann D, Clemetson JM, Navdaev A, Kehrel BE, Clemetson KJ. Alboaggregin A activates platelets by a mechanism involving glycoprotein VI as well as glycoprotein Ib. Blood 2001;97:929-936.

72. Du X, Magnenat E, Wells TN, Clemetson KJ. Alboluxin, a snake C-type lectin from Trimeresurus albolabris venom is a potent platelet agonist acting via GPIb and GPVI. Thromb.Haemost. 2002;87:692-698.

73. Schulte V, Snell D, Bergmeier W et al. Evidence for two distinct epitopes within collagen for activation of murine platelets. J.Biol.Chem. 2001;276:364-368.

74. Gibbins J, Asselin J, Farndale R et al. Tyrosine phosphorylation of the Fc receptor gamma-chain in collagen-stimulated platelets. J.Biol.Chem. 1996;271:18095-18099.

75. Gibbins JM. Platelet adhesion signalling and the regulation of thrombus formation. J.Cell Sci. 2004;117:3415-3425.

76. Briddon SJ, Watson SP. Evidence for the involvement of p59fyn and p53/56lyn in collagen receptor signalling in human platelets. Biochem.J. 1999;338 (Pt 1):203-209.

77. Ezumi Y, Shindoh K, Tsuji M, Takayama H. Physical and functional association of the Src family kinases Fyn and Lyn with the collagen receptor glycoprotein VI-Fc receptor gamma chain complex on human platelets. J.Exp.Med. 1998;188:267-276.

78. Fujii C, Yanagi S, Sada K et al. Involvement of protein-tyrosine kinase p72syk in collagen-induced signal transduction in platelets. Eur.J.Biochem. 1994;226:243-248.

79. Yanaga F, Poole A, Asselin J et al. Syk interacts with tyrosine-phosphorylated proteins in human platelets activated by collagen and cross-linking of the Fc gamma-IIA receptor. Biochem.J. 1995;311 (Pt 2):471-478.

80. Zhang W, Trible RP, Samelson LE. LAT palmitoylation: its essential role in membrane microdomain targeting and tyrosine phosphorylation during T cell activation. Immunity. 1998;9:239-246.

81. Gross BS, Lee JR, Clements JL et al. Tyrosine phosphorylation of SLP-76 is downstream of Syk following stimulation of the collagen receptor in platelets. J.Biol.Chem. 1999;274:5963-5971.

82. Nieswandt B, Schulte V, Bergmeier W et al. Long-term antithrombotic protection by in vivo depletion of platelet glycoprotein VI in mice. J.Exp.Med. 2001;193:459-469.

83. Gruner S, Prostredna M, Koch M et al. Relative antithrombotic effect of soluble GPVI dimer compared with anti-GPVI antibodies in mice. Blood 2005;105:1492-1499.

84. Massberg S, Gawaz M, Gruner S et al. A crucial role of glycoprotein VI for platelet recruitment to the injured arterial wall in vivo. J.Exp.Med. 2003;197:41-49.

85. Schulte V, Rabie T, Prostredna M et al. Targeting of the collagen-binding site on glycoprotein VI is not essential for in vivo depletion of the receptor. Blood 2003;101:3948-3952.

86. Boylan B, Chen H, Rathore V et al. Anti-GPVI-associated ITP: an acquired platelet disorder caused by autoantibody-mediated clearance of the GPVI/FcRgamma-chain complex from the human platelet surface. Blood 2004;104:1350-1355.

87. Moroi M, Jung SM, Okuma M, Shinmyozu K. A patient with platelets deficient in glycoprotein VI that lack both collagen-induced aggregation and adhesion. J.Clin.Invest 1989;84:1440-1445.

88. Boylan B, Berndt MC, Kahn ML, Newman PJ. Activation-independent, antibody-mediated removal of GPVI from circulating human platelets: development of a novel NOD/SCID mouse model to evaluate the in vivo effectiveness of anti-human platelet agents. Blood 2006;108:908-914.

89. Bergmeier W, Rabie T, Strehl A et al. GPVI down-regulation in murine platelets through metalloproteinase-dependent shedding. Thromb.Haemost. 2004;91:951-958.

90. Kato K, Kanaji T, Russell S et al. The contribution of glycoprotein VI to stable platelet adhesion and thrombus formation illustrated by targeted gene deletion. Blood 2003;102:1701-1707.

91. Lockyer S, Okuyama K, Begum S et al. GPVI-deficient mice lack collagen responses and are protected against experimentally induced pulmonary thromboembolism. Thromb.Res. 2006;118:371-380.

92. Sugiyama T, Okuma M, Ushikubi F et al. A novel platelet aggregating factor found in a patient with defective collagen-induced platelet aggregation and autoimmune thrombocytopenia. Blood 1987;69:1712-1720.

93. Arthur JF, Dunkley S, Andrews RK. Platelet glycoprotein VI-related clinical defects. Br.J.Haematol. 2007;139:363-372.

94. Wolfsberg TG, Straight PD, Gerena RL et al. ADAM, a widely distributed and developmentally regulated gene family encoding membrane proteins with a disintegrin and metalloprotease domain. Dev.Biol. 1995;169:378-383.

95. Primakoff P, Myles DG. The ADAM gene family: surface proteins with adhesion and protease activity. Trends Genet. 2000;16:83-87.

96. Yamazaki K, Mizui Y, Tanaka I. Radiation hybrid mapping of human ADAM10 gene to chromosome 15. Genomics 1997;45:457-459.

97. Yamazaki K, Mizui Y, Sagane K, Tanaka I. Assignment of a disintegrin and metalloproteinase domain 10 (Adam10) gene to mouse chromosome 9. Genomics 1997;46:528-529.

98. Prinzen C, Muller U, Endres K, Fahrenholz F, Postina R. Genomic structure and functional characterization of the human ADAM10 promoter. FASEB J. 2005;19:1522-1524.

99. Pan D, Rubin GM. Kuzbanian controls proteolytic processing of Notch and mediates lateral inhibition during Drosophila and vertebrate neurogenesis. Cell 1997;90:271-280.

100. Wen C, Metzstein MM, Greenwald I. SUP-17, a Caenorhabditis elegans ADAM protein related to Drosophila KUZBANIAN, and its role in LIN-12/NOTCH signalling. Development 1997;124:4759-4767.

101. Hartmann D, De SB, Serneels L et al. The disintegrin/metalloprotease ADAM 10 is essential for Notch signalling but not for alpha-secretase activity in fibroblasts. Hum.Mol.Genet. 2002;11:2615-2624.

102. Tian L, Wu X, Chi C et al. ADAM10 is essential for proteolytic activation of Notch during thymocyte development. Int.Immunol. 2008;20:1181-1187.

103. Cerretti DP, Poindexter K, Castner BJ et al. Characterization of the cDNA and gene for mouse tumour necrosis factor alpha converting enzyme (TACE/ADAM17) and its location to mouse chromosome 12 and human chromosome 2p25. Cytokine 1999;11:541-551.

104. Black RA, Rauch CT, Kozlosky CJ et al. A metalloproteinase disintegrin that releases tumour-necrosis factor-alpha from cells. Nature 1997;385:729-733.

105. Marino MW, Dunn A, Grail D et al. Characterization of tumor necrosis factor-deficient mice. Proc.Natl.Acad.Sci.U.S.A 1997;94:8093-8098.

106. Pasparakis M, Alexopoulou L, Episkopou V, Kollias G. Immune and inflammatory responses in TNF alpha-deficient mice: a critical requirement for TNF alpha in the formation of primary B cell follicles, follicular dendritic cell networks and germinal centers, and in the maturation of the humoral immune response. J.Exp.Med. 1996;184:1397-1411.

107. Peschon JJ, Torrance DS, Stocking KL et al. TNF receptor-deficient mice reveal divergent roles for p55 and p75 in several models of inflammation. J.Immunol. 1998;160:943-952.

108. Horiuchi K, Kimura T, Miyamoto T et al. Conditional inactivation of TACE by a Sox9 promoter leads to osteoporosis and increased granulopoiesis via dysregulation of IL-17 and G-CSF. J.Immunol. 2009;182:2093-2101.

109. Blobel CP. ADAMs: key components in EGFR signalling and development. Nat.Rev.Mol.Cell Biol. 2005;6:32-43.

110. Abel S, Hundhausen C, Mentlein R et al. The transmembrane CXC-chemokine ligand 16 is induced by IFN-gamma and TNF-alpha and shed by the activity of the disintegrin-like metalloproteinase ADAM10. J.Immunol. 2004;172:6362-6372.

111. Black RA, Doedens JR, Mahimkar R et al. Substrate specificity and inducibility of TACE (tumour necrosis factor alpha-converting enzyme) revisited: the Ala-Val preference, and induced intrinsic activity. Biochem.Soc.Symp. 200339-52.

112. Gomez-Gaviro MV, Gonzalez-Alvaro I, Dominguez-Jimenez C et al. Structure-function relationship and role of tumor necrosis factor-alpha-converting enzyme in the down-regulation of L-selectin by non-steroidal anti-inflammatory drugs. J.Biol.Chem. 2002;277:38212-38221.

113. Rio C, Buxbaum JD, Peschon JJ, Corfas G. Tumor necrosis factor-alpha-converting enzyme is required for cleavage of erbB4/HER4. J.Biol.Chem. 2000;275:10379-10387.

114. Sahin U, Weskamp G, Kelly K et al. Distinct roles for ADAM10 and ADAM17 in ectodomain shedding of six EGFR ligands. J.Cell Biol. 2004;164:769-779.

115. Six E, Ndiaye D, Laabi Y et al. The Notch ligand Delta1 is sequentially cleaved by an ADAM protease and gamma-secretase. Proc.Natl.Acad.Sci.U.S.A 2003;100:7638-7643.

116. Garton KJ, Gough PJ, Blobel CP et al. Tumor necrosis factor-alpha-converting enzyme (ADAM17) mediates the cleavage and shedding of fractalkine (CX3CL1). J.Biol.Chem. 2001;276:37993-38001.

117. Hundhausen C, Misztela D, Berkhout TA et al. The disintegrin-like metalloproteinase ADAM10 is involved in constitutive cleavage of CX3CL1 (fractalkine) and regulates CX3CL1-mediated cell-cell adhesion. Blood 2003;102:1186-1195.

118. Matthews V, Schuster B, Schutze S et al. Cellular cholesterol depletion triggers shedding of the human interleukin-6 receptor by ADAM10 and ADAM17 (TACE). J.Biol.Chem. 2003;278:38829-38839.

119. Berger G, Hartwell DW, Wagner DD. P-Selectin and platelet clearance. Blood 1998;92:4446-4452.

120. Bergmeier W, Piffath CL, Cheng G et al. Tumor necrosis factor-alpha-converting enzyme (ADAM17) mediates GPIbalpha shedding from platelets in vitro and in vivo. Circ.Res. 2004;95:677-683.

121. Jin Y, Nonoyama S, Morio T et al. Characterization of soluble CD40 ligand released from human activated platelets. J.Med.Dent.Sci. 2001;48:23-27.

122. Rabie T, Strehl A, Ludwig A, Nieswandt B. Evidence for a role of ADAM17 (TACE) in the regulation of platelet glycoprotein V. J.Biol.Chem. 2005;280:14462-14468.

123. Gardiner EE, Karunakaran D, Shen Y et al. Controlled shedding of platelet glycoprotein (GP)VI and GPIb-IX-V by ADAM family metalloproteinases. J.Thromb.Haemost. 2007;5:1530-1537.

124. Nagy A, Rossant J, Nagy R, Abramow-Newerly W, Roder JC. Derivation of completely cell culture-derived mice from early-passage embryonic stem cells. Proc.Natl.Acad.Sci.U.S.A 1993;90:8424-8428.

125. Tiedt R, Schomber T, Hao-Shen H, Skoda RC. Pf4-Cre transgenic mice allow the generation of lineage-restricted gene knockouts for studying megakaryocyte and platelet function in vivo. Blood 2007;109:1503-1506.

126. Kuhn R, Schwenk F, Aguet M, Rajewsky K. Inducible gene targeting in mice. Science 1995;269:1427-1429.

127. Nieswandt B, Bergmeier W, Rackebrandt K, Gessner JE, Zirngibl H. Identification of critical antigen-specific mechanisms in the development of immune thrombocytopenic purpura in mice. Blood 2000;96:2520-2527.

128. Nieswandt B, Echtenacher B, Wachs FP et al. Acute systemic reaction and lung alterations induced by an antiplatelet integrin gpIIb/IIIa antibody in mice. Blood 1999;94:684-693.

129. Bergmeier W, Schulte V, Brockhoff G et al. Flow cytometric detection of activated mouse integrin alphaIIbbeta3 with a novel monoclonal antibody. Cytometry 2002;48:80-86.

130. May F, Hagedorn I, Pleines I et al. CLEC-2 is an essential platelet activating receptor in hemostasis and thrombosis. Blood 2009

131. Gajewski A, Krohne G. Subcellular distribution of the Xenopus p58/lamin B receptor in oocytes and eggs. J.Cell Sci. 1999;112 (Pt 15):2583-2596.

132. Grosse J, Braun A, Varga-Szabo D et al. An EF hand mutation in Stim1 causes premature platelet activation and bleeding in mice. J.Clin.Invest 2007;117:3540-3550.

133. Levin J, Levin FC, Penington DG, Metcalf D. Measurement of ploidy distribution in megakaryocyte colonies obtained from culture: with studies of the effects of thrombocytopenia. Blood 1981;57:287-297.

134. Shivdasani RA, Schulze H. Culture, expansion, and differentiation of murine megakaryocytes. Curr.Protoc.Immunol. 2005;Chapter 22:Unit.

135. Lecut C, Arocas V, Ulrichts H et al. Identification of residues within human glycoprotein VI involved in the binding to collagen: evidence for the existence of distinct binding sites. J.Biol.Chem. 2004;279:52293-52299.

136. Smethurst PA, Joutsi-Korhonen L, O'Connor MN et al. Identification of the primary collagen-binding surface on human glycoprotein VI by site-directed mutagenesis and by a blocking phage antibody. Blood 2004;103:903-911.

137. Suzuki-Inoue K, Fuller GL, Garcia A et al. A novel Syk-dependent mechanism of platelet activation by the C-type lectin receptor CLEC-2. Blood 2006;107:542-549.

138. Italiano JE, Jr., Lecine P, Shivdasani RA, Hartwig JH. Blood platelets are assembled principally at the ends of proplatelet processes produced by differentiated megakaryocytes. J.Cell Biol. 1999;147:1299-1312.

139. Kile BT, Panopoulos AD, Stirzaker RA et al. Mutations in the cofilin partner Aip1/Wdr1 cause autoinflammatory disease and macrothrombocytopenia. Blood 2007;110:2371-2380.

140. Schulze H, Korpal M, Hurov J et al. Characterization of the megakaryocyte demarcation membrane system and its role in thrombopoiesis. Blood 2006;107:3868-3875.

141. Shivdasani RA, Fujiwara Y, McDevitt MA, Orkin SH. A lineage-selective knockout establishes the critical role of transcription factor GATA-1 in megakaryocyte growth and platelet development. EMBO J. 1997;16:3965-3973.

142. Schwer HD, Lecine P, Tiwari S et al. A lineage-restricted and divergent beta-tubulin isoform is essential for the biogenesis, structure and function of blood platelets. Curr.Biol. 2001;11:579-586.

143. Behnke O, Forer A. From megakaryocytes to platelets: platelet morphogenesis takes place in the bloodstream. Eur.J.Haematol.Suppl 1998;61:3-23.

144. Kaji N, Ohashi K, Shuin M et al. Cell cycle-associated changes in Slingshot phosphatase activity and roles in cytokinesis in animal cells. J.Biol.Chem. 2003;278:33450-33455.

145. Amano T, Kaji N, Ohashi K, Mizuno K. Mitosis-specific activation of LIM motif-containing protein kinase and roles of cofilin phosphorylation and dephosphorylation in mitosis. J.Biol.Chem. 2002;277:22093-22102.

146. Ono K, Parast M, Alberico C, Benian GM, Ono S. Specific requirement for two ADF/cofilin isoforms in distinct actin-dependent processes in Caenorhabditis elegans. J.Cell Sci. 2003;116:2073-2085.

147. Witke W, Sharpe AH, Hartwig JH et al. Hemostatic, inflammatory, and fibroblast responses are blunted in mice lacking gelsolin. Cell 1995;81:41-51.

148. Kehrel B, Balleisen L, Kokott R et al. Deficiency of intact thrombospondin and membrane glycoprotein Ia in platelets with defective collagen-induced aggregation and spontaneous loss of disorder. Blood 1988;71:1074-1078.

149. Nieuwenhuis HK, Akkerman JW, Houdijk WP, Sixma JJ. Human blood platelets showing no response to collagen fail to express surface glycoprotein Ia. Nature 1985;318:470-472.

150. Mangin P, Yap CL, Nonne C et al. Thrombin overcomes the thrombosis defect associated with platelet GPVI/FcRgamma deficiency. Blood 2006;107:4346-4353.

151. Snell DC, Schulte V, Jarvis GE et al. Differential effects of reduced glycoprotein VI levels on activation of murine platelets by glycoprotein VI ligands. Biochem.J. 2002;368:293-300.

152. Aktas B, Pozgajova M, Bergmeier W et al. Aspirin induces platelet receptor shedding via ADAM17 (TACE). J.Biol.Chem. 2005;280:39716-39722.

153. Weskamp G, Cai H, Brodie TA et al. Mice lacking the metalloprotease-disintegrin MDC9 (ADAM9) have no evident major abnormalities during development or adult life. Mol.Cell Biol. 2002;22:1537-1544.

F. Appendix

Abbreviations

ADAM	A disintegrin and metalloproteinase
ADP	Adenosine diphosphate
BAC	Bacterial artificial chromosome
BM	Bone marrow
BSA	Bovine serum albumin
Calm	Calmodulin
CCCP	Carbonyl cyanide m-chlorophenylhydrazone
Ci	Curie
CIP	Calf intestine phosphatase
Coll	Collagen
CRP	Collagen-related peptide
Cvx	Convulxin
DAG	Diacylglycerol
DAPI	4'-6-Diamidino-2-phenylindole
DMEM	Dulbecco's Modified Eagle's Medium
DMS	Demarcation membrane system
DMSO	Dimethylsulfoxide
EDTA	Ethylenediaminetetraacetic acid
ELISA	Enzyme linked immunosorbent assay
EF	Embryonic feeder cells
ES	Embryonic stem cells
EST	Expressed sequence tag
FCS	Fetal calf serum
Fig	Figure
G418	Geneticin
GA	Glutaraldehyde
GP	Glycoprotein
HEPES	N-2-Hydroxyethylpiperazine-N'-2-ethanesulfonic acid
HRP	Horseradish peroxidase
Ig	Immunoglobulin

IL	Interleukin
IP	Immunoprecipitation
IRES	Internal ribosome entry site
ITAM	Immunoreceptor tyrosine-based activation motif
i.v.	intravenously
kb	kilo base pairs
kD	kilo Dalton
LAT	Linker for activation of T-cells
LB-medium	Luria-Bertani-Medium
LIF	Leukemia inhibitory factor
NEM	N-ethylmaleimide
M	Molar
MCS	Multiple cloning site
MK	Megakaryocyte
MOPS	3-(N-morpholino) propanesulfonic acid
NCBI	National Center for Biotechnology Information
Neo	Neomycin
NP-40	Nonidet P-40
PAGE	Polyacrylamide gel electrophoresis
PBS	Phosphate buffered saline
PCR	Polymerase chain reaction
PDGF	Platelet-derived growth factor
PF4	Platelet factor 4
PFA	Paraformaldehyde
PGK	Phosphoglycerate kinase
PI	Phosphatidylinositol
PKC	Proteinkinase C
PMA	Phorbol 12-myristate 13-acetate
PLC	Phospholipase C
PRP	Platelet rich plasma
RT	Room temperature
SDS	Sodium dodecyl sulfate
Seq	Sequence

SLP-76	Src-homology 2 domain-containing leukocyte-specific phospho-protein of 76 kDa
TACE	TNFα converting enzyme
TBS	Tris buffered saline
TK	Thymidine kinase
TPO	Thrombopoietin
u	units
Vol	Volume
vWF	von Willebrand factor
WT	Wild-type

Acknowledgements

The work presented here was performed at the Rudolf Virchow Center, DFG Research Center for Experimental Biomedicine, University of Würzburg, in the group of Prof. Dr. Bernhard Nieswandt.

During the period of my PhD work (2006 - 2009), many people helped and supported me. I would like to thank the following people for their help:

- Prof. Dr. Bernhard Nieswandt for allowing me to perform my PhD work in his laboratory and for his constant support, trust, useful advice and financing my projects, participations on workshops and scientific congresses.
- all supervisors of my PhD work.
- all present and past members of the lab for their experimental support, useful discussions and pleasant atmosphere in the lab.
- all external collaborators who contributed to this work.
- all proof-readers of this thesis.
- finally I would like to thank Anita, my family and friends for their continuous support and patience.

Publications

Articles

Bender M, Eckly A, Hartwig JH, Elvers M, Gurniak C, Pleines I, Gupta S, Jeanclos E, Gohla A, Krohne G, Gachet C, Witke W, Nieswandt B**.**
“ADF/n-cofilin dependent actin turnover is essential for platelet formation.”
(in preparation)

Bender M, Stegner D, Hofmann S, Chalaris A, Braun A, Rose-John S, Nieswandt B**.**
“Glycoprotein VI (GPVI) down-regulation is differentially regulated by ADAM10 and ADAM17.”
(in preparation)

Pleines I, Eckly A, Elvers M, Hagedorn I, Eilautou S, **Bender M**, Wu X, Lanza F, Gachet C, Brakebusch C, Nieswandt B.
“Increased granule secretion and accelerated thrombus formation in mice lacking Cdc42 in platelets.” [in revision]

May F, Hagedorn I, Pleines I, **Bender M**, Vogtle T, Eble J, Elvers M, Nieswandt B.
„CLEC-2 is an essential platelet activating receptor in hemostasis and thrombosis.“
Blood 2009, Jul 29. [Epub ahead of print]

Braun A, Varga-Szabo D, Kleinschnitz C, Pleines I, **Bender M**, Austinat M, Bösl M, Stoll G, Nieswandt B.
„Orai1 (CRACM1) is the platelet SOC channel and essential for pathological thrombus formation.“
Blood 2009 Feb 26;113(9):2056-63.

Varga-Szabo D, Braun A, Kleinschnitz C, **Bender M**, Pleines I, Pham M, Renné T, Stoll G, Nieswandt B.
„The calcium sensor STIM1 is an essential mediator of arterial thrombosis and ischemic brain infarction.“
J Exp Med 2008 Jul 7;205(7):1583-91.

Varga-Szabo D, Authi KS, Braun A, **Bender M**, Ambily A, Hassock SR, Gudermann T, Dietrich A, Nieswandt B.
„Store-operated Ca(2+) entry in platelets occurs independently of transient receptor potential (TRP) C1."
Pflugers Arch 2008 Nov;457(2):377-87.

Rabie T, Varga-Szabo D, **Bender M**, Pozgaj R, Lanza F, Saito T, Watson SP, Nieswandt B.
„Diverging signaling events control the pathway of GPVI down-regulation *in vivo*."
Blood 2007 Jul 15;110(2):529-35.

International oral presentations

"ADF/cofilin-dependent actin turnover is essential for platelet formation"
XXIInd European Platelet Meeting, October 2007, Wittenberg, Germany

"*In vivo* regulation of GPVI by metalloproteinases"
4th International Symposium, GSLS, Würzburg, Germany

"ADF/cofilin-dependent actin turnover is essential for platelet formation"
The International Society on Thrombosis and Haemostasis XXIInd Congress, July 2009, Boston, USA

International poster presentation

"Cofilin, but not ADF, is essential for platelet formation *in vivo*"
The International Society on Thrombosis and Haemostasis XXIst Congress, July 2007, Geneva, Switzerland

International award

Young Investigator Award
The International Society on Thrombosis and Haemostasis XXIInd Congress, July 2009, Boston, USA

Affidavit
(*Eidesstattliche Erklärung*)

I hereby declare that my thesis entitled “Studies on platelet cytoskeletal dynamics and receptor regulation in genetically modified mice” is the result of my own work. I did not receive any help or support from commercial consultants. All sources and / or materials applied are listed and specified in the thesis.

Furthermore, I verify that this thesis has not yet been submitted as part of another examination process neither in identical nor in similar form.

Würzburg ……

Date Signature